

An Investigation of Asymptotic Equations for the Resonant Interaction of Sound and Entropy Waves and Their Long-Time Behavior

By

Yifeng Chen
DISSERTATION

Submitted in partial satisfaction of the requirements for the degree of

DOCTOR OF PHILOSOPHY

in

APPLIED MATHEMATICS

in the

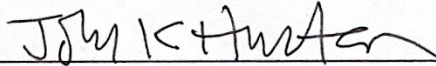
OFFICE OF GRADUATE STUDIES

of the

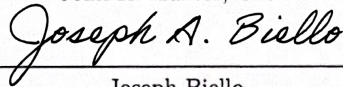
UNIVERSITY OF CALIFORNIA

DAVIS

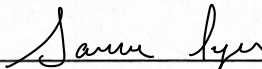
Approved:



John K. Hunter, Chair



Joseph Biello



Sameer Iyer

Committee in Charge

2024

Contents

Abstract	v
Acknowledgments	vi
Chapter 1. Introduction	1
1.1. Gas Dynamics	1
1.2. The Majda-Rosales-Schonbek System for Entropy-Sound Wave Interaction	3
1.3. Motivation for Extended Lifespan	5
1.4. The DQS Equation	6
1.5. Outline	7
Part 1.	9
Chapter 2. The Burgers-Hilbert Equation	10
2.1. Proving Local Existence with Method of Energy Estimates	11
2.2. Normal Form Transformation	12
2.3. NFT on Burgers-Hilbert	14
2.4. Modified Energy method	14
2.5. Time Resonance	15
2.6. Normal Form Flow	19
2.7. Reduced NFT	20
Chapter 3. The Majda-Rosales-Schonbek System	23
3.1. Background	23
3.2. Smooth Solution Lifespan	26
3.3. Naive NFT	26
3.4. Modified Energy	27
3.5. Time Resonance	28

3.6. Normal Form Flow	29
3.7. Reduced NFT	30
Chapter 4. Numerical Results for the MRS System	33
4.1. Numerical Scheme	33
4.2. Shock	33
4.3. Shock with Zero Boundary Value	37
4.4. Lifespan	37
Part 2.	41
Chapter 5. The Degenerate Quasi-linear Schrodinger Equation	42
5.1. Derivation	42
5.2. Basic Properties	44
5.3. Special Exact Solutions of the DQS Equation	45
5.4. Solutions with Cube Root Singularity	48
5.5. Modulation System	50
5.6. Energy Estimates	53
5.7. Weighted Energy Estimates	54
5.8. Ill-posedness in H^s	56
5.9. Well-posedness Result	57
Chapter 6. Numerical Results for the DQS Equation	66
6.1. Motivation for Front Propagating Solutions of the DQS Equation	66
6.2. Previous Numerical experiment	67
6.3. Numerical Method	67
6.4. Front Expansion	70
6.5. Dispersive Shocks	75
6.6. Comparison with the MRS numerical solution	78
Chapter 7. Conclusion	82
Appendix A. DQS Numerical Scheme Code	84

Appendix B. Alternate WENO Scheme Code	89
Appendix C. Movie Links	92
Bibliography	93

Abstract

The Majda-Rosales-Schonbek (MRS) system, obtained through an asymptotic expansion of the non-isentropic compressible Euler equations in one space dimension, describes resonant interactions of small amplitude, spatially periodic sound waves with a small amplitude entropy wave. In particular, we are interested in when a small-amplitude smooth solution develops singularities. Previous work has shown that for small initial data of order ϵ , the solution will remain smooth for time $O(\frac{\log \epsilon}{\epsilon})$. However, numerical simulations suggest the lifespan of small initial data can be extended to $O(\frac{1}{\epsilon^2})$. In this paper, we will explore multiple approaches that are often used to prove extended lifespans of quadratically quasilinear PDEs, which usually corresponds to an $O(\frac{1}{\epsilon})$ lifespan of small smooth solutions.

An asymptotic expansion of the MRS system produces a Degenerate Quasilinear Schrodinger (DQS) equation, which formally describes the behavior of small solutions of the MRS system on order $O(\frac{1}{\epsilon^2})$ timescale. The degeneracy of the equation makes it very difficult to obtain well-posedness results. In fact, previous work by Jeong and Oh has shown the DQS equation is ill-posed in H^s for sufficiently large s . However, we will show that the equation is well-posed in a highly restricted function space of compactly supported solutions with sufficient endpoint decay.

Numerical simulations of the DQS equation appear to confirm that it does provide a good asymptotic description of the behavior of the MRS solutions on timescale $O(\frac{1}{\epsilon^2})$. In addition, we study the possible existence of compactly supported solutions through numerical simulations. The numerical results of a front spreading solution seem to suggest that, in the absence of dissipation, a compactly supported initial pulse forms oscillations that spread to $\pm\infty$ once a singularity occurs, and therefore, does not stay compact for later time.

Acknowledgments

I would like to express my deepest gratitude to those who have supported me throughout the journey of completing this thesis.

First and foremost, I extend my heartfelt appreciation to my advisor, Prof. John Hunter. Your invaluable guidance, patience, and expertise have been crucial to the successful completion of this work. Your insightful feedback and constant encouragement have significantly shaped this research, and I am profoundly grateful for your support and mentorship.

I also want to thank my parents, Fei Chen, and Bei Zhang, for your unwavering support and belief in me. Your sacrifices and love have been the foundation of my academic pursuits. This achievement would not have been possible without your constant encouragement, and I owe much of my success to your unfailing support.

To my girlfriend, Rachel Guo, thank you for your endless patience, understanding, and emotional support. Your love and encouragement have been my anchor throughout this challenging process. I am also thankful to the faculty members of the Department of Mathematics at UC Davis for their insightful feedback and guidance. Special thanks to Prof. Sameer Iyer for his valuable input and support.

Lastly, I would like to acknowledge my fellow students and friends who have made this journey memorable. Your camaraderie, discussions, and support have been incredibly motivating. I am grateful for the countless hours spent together in study groups, and your collective encouragement has been invaluable.

Thank you to everyone who has contributed to this journey, directly or indirectly. Your support and encouragement have been greatly appreciated.

CHAPTER 1

Introduction

1.1. Gas Dynamics

The compressible Euler equations are one of the most widely known systems of nonlinear PDEs describing gas dynamics. The Euler equations were first published in 1757 (see [6] for history of the Euler equations). However, considerable gaps in knowledge still exist in many aspects of the equations. In particular, we are interested in the behavior of spatially periodic solutions. The compressible Euler equations in one space dimension are given by

$$(1.1) \quad \begin{aligned} \rho_t + (\rho u)_x &= 0 \\ (\rho u)_t + (\rho u^2 + p)_x &= 0 \\ E_t + (u(E + p))_x &= 0. \end{aligned}$$

Assume we are working with a polytropic ideal gas, for which

$$e = (\gamma - 1)^{-1} \frac{p}{\rho} \quad \text{where } \gamma \text{ is the ratio of specific heats,}$$

and energy E is given by

$$E = \rho \left(e + \frac{1}{2} u^2 \right).$$

From thermodynamic relations (see [53]), we can get the entropy relation

$$p = \kappa \rho^\gamma e^{S/c_v},$$

where S is the entropy, c_v is the speed of sound, and κ is a constant.

Then, we can write the system in ρ, u, p

$$(1.2) \quad \begin{bmatrix} \rho \\ u \\ p \end{bmatrix}_t + \begin{bmatrix} u & \rho & 0 \\ 0 & u & \frac{1}{\rho} \\ 0 & \gamma p & u \end{bmatrix} \begin{bmatrix} \rho \\ u \\ p \end{bmatrix}_x = 0.$$

If the flow is isentropic, which means the entropy is a constant, the last equation of (1.1) can be dropped and the first two equations become a closed system [53]. The isentropic Euler equations are

$$(1.3) \quad \begin{aligned} \rho_t + (\rho u)_x &= 0 \\ (\rho u)_t + (\rho u^2 + p)_x &= 0. \end{aligned}$$

The non-isentropic Euler equations (1.1) and the isentropic Euler equations (1.3) are two of the most important systems of hyperbolic conservation laws

$$(1.4) \quad \mathbf{u}_t + f(\mathbf{u})_x = 0$$

where $\mathbf{u} = \mathbf{u}(x, t) \in \mathbb{R}^n$ and $x \in \mathbb{R}^m$.

There has been much work on shock formation of hyperbolic systems. It is established that we cannot obtain global existence of smooth solutions for hyperbolic systems with genuine non-linearity. Lax first proved the result for 2×2 strictly hyperbolic systems ([31]). It was then extended to $n \times n$ hyperbolic systems by John in [11], and improved by Liu in [34] to allow linearly degenerate characteristic fields. Here, genuinely non-linear and linearly degenerate characteristic fields are defined in the sense of [31] and [34] respectively,

$$\begin{aligned} \nabla \lambda_i(\mathbf{u}) r_i(\mathbf{u}) &\neq 0 && \text{(genuinely non-linear)} \\ \nabla \lambda_i(\mathbf{u}) r_i(\mathbf{u}) &\equiv 0 && \text{(linearly degenerate)} \end{aligned}$$

where λ_i is the i -th eigenvalue of ∇f in (1.4), and r_i is the corresponding eigenvector. Nevertheless, the non-isentropic Euler equations do not satisfy the genuinely nonlinear requirement and we cannot apply the aforementioned theory.

The behavior of smooth solutions of the non-isentropic Euler equations is a long standing problem. Recent work [51] by Temple and Young proved global existence of spatially periodic solutions. Recent works [3], [43], and [37] proved that there exist smooth solutions to the non-isentropic Euler equations which form a stable shock by constructing steep initial data that imitates a shock (see [37] for proof in 1D, and [3], [43] in multi-D). The general theory of shock formation in non-isentropic Euler is still to be understood.

Glimm first proved global existence of weak solutions with small total variation in $n \times n$ hyperbolic systems, both genuinely non-linear and linearly degenerate (see [7] [18]). This is one of the most fundamental results on hyperbolic systems. Unfortunately, the problem of existence theory on data with large variation, for example, spatially periodic solutions, for 3×3 non-isentropic Euler equations is still open.

The famous work by James Glimm and Peter Lax proved the global existence of weak solutions of 2×2 hyperbolic systems of conservation laws, provided that the initial data has sufficiently small sup-norm (see [19] [32]). Here, admissible weak solutions are taken to be those with shocks that satisfy the Rankine–Hugoniot jump condition. In addition, the Glimm-Lax theory shows if the initial data is spatially periodic, then the solution decays like $\frac{1}{t}$. However, the theory provided by Glimm and Lax only applies to 2×2 hyperbolic systems, such as the isentropic Euler equations (1.3), and does not extend to the 3×3 non-isentropic Euler equations (1.1).

We follow the approach in [35] and use the method of multiple scales to study the propagation of small amplitude high frequency solutions of non-isentropic Euler equations.

1.2. The Majda-Rosales-Schonbek System for Entropy-Sound Wave Interaction

The non-isentropic Euler equations (1.2) have three eigenvalues

$$\lambda_1 = u + c, \quad \lambda_2 = u, \quad \lambda_3 = u - c,$$

where $c = \sqrt{\frac{\gamma p}{\rho}}$ is the speed of sound. The corresponding eigenvectors \mathbf{r}_i are given by

$$\mathbf{r}_1 = \begin{bmatrix} \rho \\ \sqrt{\frac{\gamma p}{\rho}} \\ \gamma p \end{bmatrix}, \quad \mathbf{r}_2 = \begin{bmatrix} 1 \\ 0 \\ 0 \end{bmatrix}, \quad \mathbf{r}_3 = \begin{bmatrix} \rho \\ -\sqrt{\frac{\gamma p}{\rho}} \\ \gamma p \end{bmatrix}.$$

Here, λ_1, λ_3 correspond to two sound waves traveling in opposite directions with velocities $\pm c$ relative to the fluid velocity u . And λ_2 corresponds to an entropy wave that propagates with the fluid velocity.

Majda, Rosales, and Schonbek ([35]) studied the resonant interaction of small amplitude, spatially periodic sound waves with a small amplitude entropy wave. In particular, the system describes the reflection of sound waves off of a background entropy wave. We look at the perturbation around a

constant background state $\mathbf{u}_0 = [\rho_0 \ 0 \ p_0]^T$. Consider the set of phases $\varphi_1, \varphi_2, \varphi_3$

$$\varphi_1 = x - c_0 t, \quad \varphi_2 = 2x, \quad \varphi_3 = x + c_0 t,$$

where $c_0 = \sqrt{\frac{\gamma p_0}{\rho_0}}$. We then consider the perturbation $\mathbf{u} = \mathbf{u}_0 + \epsilon(\mathbf{u}_1 + \mathbf{u}_2 + \mathbf{u}_3)$ where $\mathbf{u}_i = a_i(t, \frac{\varphi_i}{\epsilon}) \mathbf{r}_i$. The perturbation does not depend on x explicitly. The calculation then shows a_2 is independent of t , therefore, the expansion has the form

$$\mathbf{u} = \begin{bmatrix} \rho_0 \\ 0 \\ p_0 \end{bmatrix} + \epsilon \left\{ a_1(t, \frac{x - c_0 t}{\epsilon}) \begin{bmatrix} \rho_0 \\ \sqrt{\frac{\gamma p_0}{\rho_0}} \\ \gamma p_0 \end{bmatrix} + a_2(\frac{2x}{\epsilon}) \begin{bmatrix} 1 \\ 0 \\ 0 \end{bmatrix} + a_3(t, \frac{x + c_0 t}{\epsilon}) \begin{bmatrix} \rho_0 \\ -\sqrt{\frac{\gamma p_0}{\rho_0}} \\ \gamma p_0 \end{bmatrix} \right\}.$$

Define $\theta = \frac{\phi_j}{\epsilon}$ and $a_j(t, \theta) = a_j(t, \frac{\phi_j}{\epsilon})$. In other words, $a_j(t, \theta)$ is evaluated at different θ value for different j . Then \mathbf{u} can also be written as

$$\mathbf{u} = \begin{bmatrix} \rho_0 \\ 0 \\ p_0 \end{bmatrix} + \epsilon \left\{ a_1(t, \theta) \begin{bmatrix} \rho_0 \\ \sqrt{\frac{\gamma p_0}{\rho_0}} \\ \gamma p_0 \end{bmatrix} + a_2(\theta) \begin{bmatrix} 1 \\ 0 \\ 0 \end{bmatrix} + a_3(t, \theta) \begin{bmatrix} \rho_0 \\ -\sqrt{\frac{\gamma p_0}{\rho_0}} \\ \gamma p_0 \end{bmatrix} \right\}$$

The asymptotic expansion then provides equations for the sound waves. After normalization and a change of notation ($u = a_1, v = a_3, x = \theta$), we get the following system

$$(1.5) \quad \begin{aligned} u_t + \left(\frac{1}{2}u^2\right)_x + \int_0^1 K(x-y)v(y,t)dy &= 0 \\ v_t + \left(\frac{1}{2}v^2\right)_x - \int_0^1 K(y-x)u(y,t)dy &= 0 \end{aligned}$$

$$\text{where } K(x) = \frac{\partial a_2}{\partial x}.$$

See [35] for details of the expansion.

Majda, Rosales, and Schonbek examined the case where $u(t, x), v(t, x)$ are 1-periodic with zero mean with respect to x , and a_2 is a spatially periodic function

$$a_2 = x - \frac{1}{2} \quad 0 < x < 1.$$

Then $K(x) = 1 - \sum_{n=-\infty}^{\infty} \delta(x - n)$ and (1.5) reduces to the following system, which we will call the Majda-Rosales-Schonbek (MRS) system.

$$(1.6) \quad \begin{aligned} u_t + \left(\frac{1}{2}u^2\right)_x &= v \\ v_t + \left(\frac{1}{2}v^2\right)_x &= -u. \end{aligned}$$

This particular choice of K gives us a system of PDEs, instead of integro-differential equations like equation (1.5) with general K . In addition, the MRS equations are non-dispersive, as we will show in section 3.6. The non-dispersive nature gives rise to some complicated dynamics, which we will demonstrate in section 3.1.

Note that the asymptotic derivation above is on the formal level. It has been proved by Schochet in [41] that weak solutions of the non-isentropic compressible Euler equations (1.1) with $O(\epsilon)$ initial data tend to the solution of the asymptotic MRS equations as $\epsilon \rightarrow 0$. Therefore, the MRS system indeed describes the asymptotic behavior of resonant interactions between high frequency, small amplitude, spatially periodic sound waves in the non-isentropic Euler equations.

1.3. Motivation for Extended Lifespan

Suppose we let $k = 0$ in (1.5), then (1.5) becomes the decoupled inviscid Burgers equations

$$\begin{aligned} u_t + \left(\frac{1}{2}u^2\right)_x &= 0 \\ v_t + \left(\frac{1}{2}v^2\right)_x &= 0. \end{aligned}$$

We know for non-zero periodic smooth initial data, solutions form shocks in time $\frac{1}{\epsilon|M|}$, where M is the minimum of the space derivative of the initial data [53]. Therefore, the initial value problem with $|M| \leq \epsilon$ has smooth solutions on $t \in [0, \frac{1}{\epsilon}]$. However, when $K \neq 0$, the interaction between u and v could delay the formation of shocks. For example, the author of [38] constructed global smooth solutions to the equations (1.5) with

$$K = -4\pi \sin 4\pi x$$

that never develop shocks.

We expect the coupling in (1.6) to delay or prevent breaking. We can see this effect by looking at the linearized equations

$$u_t = v, \quad v_t = -u.$$

For short time (t), the solutions should behave almost linearly. Consider the following solution

$$u = \sin(t)f(x), \quad v = \cos(t)f(x)$$

where $f(x)$ is some arbitrary function of x .

During the cycle $t \in [0, 2\pi)$, we can see that the non-linear terms uu_x, vv_x – responsible for the shock formation – have opposite signs during the first half half of the period ($t \in [0, \pi)$) and the second half ($t \in [\pi, 2\pi)$). The oscillation in u, v produces half compression effect and half expansion effect in each cycle. The nonlinear effect that enables shocks to form is offsetting itself during each cycle and could therefore lead to a longer lifespan of smooth solutions.

1.4. The DQS Equation

Standard asymptotic expansion of the MRS equations gives us a Degenerate Quasilinear Schrodinger (DQS) equation. The derivation is on a formal level, but it provides more insight into the behavior of $O(\epsilon)$ solutions of the MRS system on $O(\frac{1}{\epsilon^2})$ timescale. The DQS equation is given by

$$(1.7) \quad iA_t + (|A|^2 A_x)_x = 0$$

where the A corresponds to the MRS variables u, v on the leading order by the following relation

$$A = -i\sqrt{\frac{3}{2}}(u + iv).$$

For simplicity, we will rename the function A as u . The DQS equation then becomes

$$(1.8) \quad iu_t + (|u|^2 u_x)_x = 0.$$

The time variable t in (1.8) is evaluated on the $O(\frac{1}{\epsilon^2})$. In other words, the behavior of the DQS equation at $t = T$ corresponds to the behavior of the MRS equations at time $t = \frac{T}{\epsilon^2}$. Here, we only state the equation; the full derivation will be delayed until 5.1.

The equation (1.8) is an example of degenerate dispersive equations: the dispersive effect weakens as $u \rightarrow 0$. Similar degenerate dispersive effect can be found in other equations or physics phenomenon, such as shallow water waves with the Camassa-Holm equation (see [4], [21]) and magma dynamics (see [47]).

There have been many works on well-posedness of non-degenerate quasilinear dispersive equations (e.g. [5], [26]). Kenig, Ponce and Vega's work in ([5]) is fundamental in this area; it provides general local well-posedness theory for a large class of non-degenerate quasilinear Schrodinger equations. The authors of [36] proved the short-time well-posedness for a class of quasilinear Schrodinger equations with large initial data. Unfortunately, these techniques break down when the equation is degenerate, and the equation may become ill-posed.

In particular, we can observe the difficulties that arise from the degeneracy by applying a weighted energy method to the DQS equation. The method follows from Takeuchi's work in [49] (also see [33]). The goal is to avoid the loss of derivatives in the standard H^s energy estimate. As we will show in section 5.7, the growth of the weighted energy cannot be controlled by itself due to the degeneracy.

[29] has proved that the DQS equation (1.8) is ill-posed in H^s with $s > \frac{9}{2}$. The ill-posedness of degenerate dispersive equations is not an isolated phenomenon. For example, [1] proved the H^2 ill-posedness of the degenerate quasilinear KdV equation

$$u_t = 2uu_{xxx} + 6u_xu_{xx} + 2uu_x.$$

The next hope is naturally local well-posedness in analytic functions, but standard methods such as the Cauchy-Kovalevskaya method and the Nash-Moser method also appear to fail due to the degeneracy. However, we can follow the work in [20] and prove that the DQS equation is well-posed in a highly restricted function space of compactly supported solutions that decay sufficiently fast at the endpoints.

1.5. Outline

In chapter 2, we study the Burgers-Hilbert equation, which resembles the MRS system in many ways. We will discuss the similarities between the Burgers-Hilbert equation and the MRS system, and present various methods previous works have employed to prove the small solution lifespan. We

will then show the difficulties we encountered when applying these methods to the MRS system in chapter 3. In 4, we present some numerical simulations that support the $O(\frac{1}{\epsilon^2})$ lifespan hypothesis and also note the behavior of some interesting initial data. In chapter 5, we first show the derivation of the asymptotic DQS equation and study some of its basic properties. We then discuss its ill-posedness in H^s spaces, and prove a well-posedness result in a subspace following the method in [20]. In chapter 6, we present a hypothesis on compactly supported solutions which our numerical simulations suggest.

Part 1

CHAPTER 2

The Burgers-Hilbert Equation

The MRS system shares some similarities with the following quasi-linear equation, called the Burgers-Hilbert equation

$$(2.1) \quad u_t + \epsilon \left(\frac{1}{2}u^2\right)_x = H[u]$$

where $H[u]$ is the Hilbert transform of u , given on \mathbb{R} by

$$(2.2) \quad H[u](t, x) = \frac{1}{\pi} p.v. \int_{-\infty}^{\infty} \frac{u(t, y)}{x - y} dy.$$

Apply Hilbert Transform to (2.1) and let $h := H[u]$, we obtain the following system

$$(2.3) \quad u_t + \epsilon \left(\frac{1}{2}u^2\right)_x = h$$

$$(2.4) \quad h_t + \epsilon H\left[\left(\frac{1}{2}u^2\right)_x\right] = -u.$$

We can see that the system has the same linear terms as the MRS system (3.1). The dispersion relation of the Burgers-Hilbert equation, though different from that of the MRS equations, exhibits similar complicated behavior. In particular, both the Burgers-Hilbert equation and the MRS equations have 4-wave resonances, but not 3-wave resonances. A more detailed discussion on this topic will be delayed until section 3.1.

The work in [22], [23], and [40] proved the $O(\frac{1}{\epsilon^2})$ lifespan of smooth solutions of the Burgers-Hilbert equation. We quote the following theorem from [22]

THEOREM 2.0.1. *Suppose that $u_0 \in H^2(\mathbb{R})$. There are constants $k > 0$ and $\epsilon_0 > 0$, depending only on $\|u_0\|_{H^2}$, such that for every ϵ with $|\epsilon| < \epsilon_0$ there exists a solution*

$$u \in C(I^\epsilon; H^2(\mathbb{R})) \cap C^1(I^\epsilon; H^1(\mathbb{R}))$$

of (2.1) defined on the time interval $I^\epsilon = \left[-\frac{k}{\epsilon^2}, \frac{k}{\epsilon^2}\right]$.

[22] proves the above theorem using a method called Normal Form Flow (NFF), while [23] uses a modified energy method to reach the same result. Both methods are motivated by the standard Normal Form Transformation (NFT). As we will show in 2.3, direct application of NFT does not work on Burgers-Hilbert equation, therefore, the authors devised these workarounds to solve the difficulties. The same problem can be observed when applying the NFT method to the MRS system. Therefore, we will study the aforementioned methods and attempt to apply them to the MRS system.

Outline of Chapter 2: We first give an overview on the standard NFT method and explain how, when combined with energy estimates, it's used to prove the $O(\frac{1}{\varepsilon^2})$ lifespan. In section 2.3, we show that the naive NFT method on the Burgers-Hilbert equation causes loss of derivatives, and does not prove the extended lifespan we want. In sections 2.4 and 2.6, we show the two methods mentioned above: the modified energy method, and the NFF method. In section 2.5, we show that the time-resonance method (see [12]) can be used to prove the $O(\frac{1}{\varepsilon^2})$ lifespan of the Burgers-Hilbert equation as well.

2.1. Proving Local Existence with Method of Energy Estimates

The method of energy estimates is one of the most widely used methods in proving local existence of solutions. We first give a brief discussion on the standard energy estimate arguments. In the next section, we will show how the NFT method can be employed to extend this lifespan.

Since both the MRS system and the Burgers-Hilbert equation are quasi-linear hyperbolic PDEs, we will show the application of the energy estimate arguments on this particular class of equations. Consider a quasi-linear hyperbolic system

$$\begin{aligned}
 & a_0(t, x, u) \frac{\partial u}{\partial t} + \sum_{j=1}^m a_j(t, x, u) \frac{\partial u}{\partial x_j} = f(t, x, u) \\
 & u(0, x) = u_0(x) \\
 & 0 \leq t \leq T, \quad x \in \mathbb{R}^m, \quad u(t, x) \in \mathbb{R}^n.
 \end{aligned}
 \tag{2.5}$$

There are many well-established results on the local existence of quasi-linear hyperbolic systems (see [30] [50]). In general, we can expect local existence of the initial value problem (2.5) with $u_0 \in H^s$, provided that the coefficients a_j are sufficiently smooth and s is large enough.

The key idea of the argument is to obtain an estimate, called the energy estimate, that controls the time evolution of the energy, most commonly taken to be the Sobolev norm of the solution (see [27]). In the simplest case, we hope to prove

$$(2.6) \quad \frac{d}{dt} \|u\|_{H^s} \leq C(\|u\|_{H^s})^n$$

where the constant C is independent of u and $n > 1$. By Gronwall's inequality, if $u(t, \cdot)$ exists, then

$$(2.7) \quad \|u(t, \cdot)\|_{H^s} < \infty \quad \text{when } 0 < t < T$$

where $T = \frac{1}{C} \|u_0\|_{H^s}^{1-n}$.

Combining (2.7), local existence theory of (2.5), and using an open and closed argument, we can prove the initial value problem (2.5) has a solution $u \in C[0, T; H^s(\mathbb{R})]$.

Note that although H^s norm is a common choice for energy, sometimes it does not produce a good estimate like (2.6). One possible fix is to construct a different energy $E(u)$ that's more suitable for the specific equation. The modified energy method in 2.4 is one example of this approach.

2.2. Normal Form Transformation

A normal form transformation is typically used to improve the energy estimate and obtain a longer lifespan for small solutions by eliminating lower order nonlinear terms.

This method was first developed in the theory of Ordinary Differential Equations (see [2]). Jalal Shatah (see [42]) then introduced it to PDE and used it to prove long time existence of a nonlinear Klein-Gordon equation

$$(2.8) \quad \begin{aligned} (\partial_t^2 - \Delta + 1)u + f(u, \partial u, \partial^2 u) &= 0 \\ u(0) &= u_0 \quad \partial_t u(0) = u_1 \end{aligned}$$

where f is a smooth function of degree 2. Both the Burgers-Hilbert equation and the MRS system are quasi-linear hyperbolic PDEs with symmetric quadratic non-linearity. Therefore, we will work with the following more general form

$$(2.9) \quad u_t = L(u) + Q(u, u), \quad u(t, x) = u_0$$

where $L(u)$ is linear and $Q(u, u)$ is a symmetric bilinear operator.

The goal is to prove for some $\epsilon \ll 1$, if the initial data is small enough

$$\|u_0\|_{H^s} \leq \epsilon$$

then there exists solution $u \in C\left(0, \frac{\alpha}{\epsilon^2}\right)$ of the equation (2.9), where α is a constant.

To make things easier, we first re-scale the equation u by a factor of $\frac{1}{\epsilon}$ and get the following equivalent problem

$$(2.10) \quad u_t = L(u) + \epsilon Q(u, u).$$

In this form, the question becomes showing the solution exists up to time $T^* = \frac{\alpha}{\epsilon^2}$ for initial data $\|u_0\|_{H^s} \leq 1$. In other words, the initial value problem (2.9) with $\|u_0\|_{H^s} \leq \epsilon$ is equivalent to the rescaled problem (2.10) with $\|u_0\|_{H^s} \leq 1$.

Since the nonlinear term in (2.10) is quadratic (with coefficient ϵ), standard energy estimate on the equation, if closed, will give us an order $O(\epsilon)$ inequality

$$\frac{\partial}{\partial t} \|u\|_{H^s} \lesssim \epsilon f(\|u\|_{H^2})$$

for some function f . Therefore, we only get existence on time scale $O(\frac{1}{\epsilon})$ at best.

The objective of the NFT method is to use the linear term to cancel out the quadratic term and obtain a cubic non-linearity which is of order $O(\epsilon^2)$. We apply the following transformation, called the normal form transformation, on the variable u

$$(2.11) \quad v = u + \frac{\epsilon}{2} A(u, u)$$

where A is also a symmetric bilinear operator. We then get an equation on the transformed variable v

$$v_t = L(v) - \frac{\epsilon}{2} L(A(u, u)) + \epsilon A(u, L(u)) + \epsilon Q(u, u) + \epsilon^2 A(u, \epsilon Q(u, u)).$$

To remove the quadratic term in the equation, the operator A must satisfy the homological equation

$$(2.12) \quad \frac{1}{2} L(A(u, u)) - A(u, Lu) = Q(u, u).$$

This gives a cubically nonlinear equation

$$v_t = L(v) + \epsilon^2 A(u, Q(u, u)).$$

If the energy of v is equivalent to the energy of u , i.e. $\|v\|_{H^s} \sim \|u\|_{H^s}$, then we can try to obtain an energy estimate on v . The energy estimate, if successfully closed, may then lead to existence of solutions on time scale $O(\frac{1}{\epsilon^2})$.

2.3. NFT on Burgers-Hilbert

We start by applying the standard NFT method on the Burgers-Hilbert equation. Using the homological equation (2.12), we can obtain the NFT variable of the equation

$$(2.13) \quad v = u + \frac{1}{2}\epsilon|\partial_x|(h^2).$$

Here, $h = H[u]$ and $|\partial_x| = H\partial_x$. Taking the Hilbert transform of the equation and letting $g = H[v]$, we get

$$(2.14) \quad g = h - \epsilon h h_x.$$

The transformed equation is given by

$$v_t = H[v] - \epsilon^2 |\partial_x| [hH[uu_x]].$$

However, direct energy estimate on v gives

$$(2.15) \quad \frac{d}{dt} \|\partial_x^k v\|_{L^2}^2 \lesssim \epsilon^2 \|u_x\|_{L^\infty}^2 \|u\|_{H^{k+1}}^2$$

and it doesn't close due to the loss of derivative.

2.4. Modified Energy method

The Normal Form Transform (2.14) gives rise to a modified energy method [23]. As we mentioned above, the energy estimate (2.15) doesn't close. However, a direct energy estimate on u does close. The disparity is caused by the fact that H^k norms of u, v are not comparable.

From (2.13), we can calculate directly

$$\|\partial_x^k v\|_{L^2}^2 = \|\partial_x^k u\|_{L^2}^2 + 2\epsilon \langle \partial_x^k u, \partial_x^k H[HuHu_x] \rangle + \epsilon^2 \|\partial_x^k H[HuHu_x]\|_{L^2}^2.$$

We can see the third term $\epsilon^2 \|\partial_x^k H[HuHu_x]\|_{L^2}$ is the term that causes the loss of derivatives in the energy estimate. However, this term does not affect the fact that the energy estimate is cubically non-linear. In other words, if we drop the last term and only keep the first two terms, defining a modified energy

$$(2.16) \quad E_k(u) = \frac{1}{2} \|\partial_x^k u\|_{L^2}^2 + \epsilon \langle \partial_x^k u, \partial_x^k H[HuHu_x] \rangle,$$

the energy estimate $\frac{d}{dt} E_k(u)$ is still of order $O(\epsilon^2)$, and we should be able to close the energy estimate now that the problematic term is gone.

Lemma 2 in [23] shows that the energy defined as (2.16) is comparable to the standard H^k energy for $\epsilon \ll 1$. The authors then proved this modified energy indeed closes the estimate.

2.5. Time Resonance

In this section, we show that we can use a different approach – the time resonance method – to obtain the same modified energy as we discussed in 2.4. This method was developed by Germain, Masmoudi, and Shatah (see [15], [16], [17]), and an overview can be found at [12]. We will show that this method gives us the modified energy (2.16).

The Hilbert Transform (2.2) is a multiplier operator with the multiplier being $-i \operatorname{sgn} \xi$, i.e.

$$\mathcal{F}(H[u])(\xi) = -i \operatorname{sgn} \xi \mathcal{F}(u)(\xi)$$

where the Fourier transform is defined by

$$\mathcal{F}(u)(\xi) = \hat{u}(\xi) = \frac{1}{2\pi} \int_{-\infty}^{\infty} u(x) e^{-i\xi x} dx.$$

Since it's much easier to handle the symbol of Hilbert Transform than Hilbert Transform itself, we will work in the frequency domain. Taking the Fourier Transform of the Burgers-Hilbert equation (2.1), we get

$$(2.17) \quad \hat{u}_t + \epsilon \hat{u} * \widehat{u_x} = -i \operatorname{sgn} \xi \hat{u}.$$

We first find solutions to the linearized Initial Value Problem

$$u_t = H[u]$$

$$u(0, x) = u_0(x).$$

Again, taking the Fourier Transform, we get

$$\hat{u}_t = -i \operatorname{sgn}(\xi) \hat{u}$$

$$\hat{u}_t(0, \xi) = \hat{u}_0(\xi).$$

The solution is then given by

$$\hat{u}(t, \xi) = e^{-i \operatorname{sgn}(\xi)t} \hat{u}_0(\xi).$$

Define $v : \mathbb{R}^2 \rightarrow \mathbb{R}$ by

$$(2.18) \quad \hat{u}(t, \xi) = e^{-i \operatorname{sgn}(\xi)t} \hat{v}(t, \xi).$$

Then equation (2.17) becomes

$$(2.19) \quad \begin{aligned} & e^{-i \operatorname{sgn}(\xi)t} \hat{v}_t - i \operatorname{sgn}(\xi) e^{-i \operatorname{sgn}(\xi)t} \hat{v} + \epsilon (e^{-i \operatorname{sgn}(\xi)t} \hat{v}) * (i \xi e^{-i \operatorname{sgn}(\xi)t} \hat{v}) = -i \operatorname{sgn}(\xi) e^{-i \operatorname{sgn}(\xi)t} \hat{v} \\ & \hat{v}_t(t, \xi) = -\epsilon e^{i \operatorname{sgn}(\xi)t} \int_{-\infty}^{\infty} i \tau e^{-i(\operatorname{sgn}(\xi-\tau)+\operatorname{sgn}(\tau))t} \hat{v}(t, \xi - \tau) \hat{v}(t, \tau) d\tau. \end{aligned}$$

We can rewrite the solution v as:

$$\hat{v}(t, \xi) = \hat{v}_0(\xi) - \epsilon \int_0^t e^{i \operatorname{sgn}(\xi)s} \int_{-\infty}^{\infty} i \tau e^{-i(\operatorname{sgn}(\xi-\tau)+\operatorname{sgn}(\tau))s} \hat{v}(s, \xi - \tau) \hat{v}(s, \tau) d\tau ds.$$

Using integration by parts, we get

$$(2.20) \quad \begin{aligned} \hat{v}(t, \xi) &= \hat{v}_0(\xi) - \epsilon \int_0^t \int_{-\infty}^{\infty} \frac{1}{\operatorname{sgn}(\xi) - \operatorname{sgn}(\xi - \tau) - \operatorname{sgn}(\tau)} \frac{d}{ds} (e^{i(\operatorname{sgn}(\xi) - \operatorname{sgn}(\xi - \tau) - \operatorname{sgn}(\tau))s}) \tau \hat{v}(s, \xi - \tau) \hat{v}(s, \tau) d\tau ds \\ &= \hat{v}_0(\xi) - \epsilon \int_{-\infty}^{\infty} \frac{\tau}{\operatorname{sgn}(\xi) - \operatorname{sgn}(\xi - \tau) - \operatorname{sgn}(\tau)} e^{i(\operatorname{sgn}(\xi) - \operatorname{sgn}(\xi - \tau) - \operatorname{sgn}(\tau))t} \hat{v}(t, \xi - \tau) \hat{v}(t, \tau) d\tau \\ &\quad + \epsilon \int_{-\infty}^{\infty} \frac{\tau}{\operatorname{sgn}(\xi) - \operatorname{sgn}(\xi - \tau) - \operatorname{sgn}(\tau)} \hat{v}_0(\xi - \tau) \hat{v}_0(\tau) d\tau \\ &\quad + \epsilon \int_0^t \int_{-\infty}^{\infty} \frac{\tau e^{i(\operatorname{sgn}(\xi) - \operatorname{sgn}(\xi - \tau) - \operatorname{sgn}(\tau))s}}{\operatorname{sgn}(\xi) - \operatorname{sgn}(\xi - \tau) - \operatorname{sgn}(\tau)} (\hat{v}_t(s, \xi - \tau) \hat{v}(s, \tau) + \hat{v}(s, \xi - \tau) \hat{v}_t(s, \tau)) d\tau ds. \end{aligned}$$

Combining (2.19) and (2.20), we get

(2.21)

$$\begin{aligned}
\hat{v}(t, \xi) &= \hat{v}_0(\xi) - \epsilon \int_{-\infty}^{\infty} \frac{\tau}{\operatorname{sgn}(\xi) - \operatorname{sgn}(\xi - \tau) - \operatorname{sgn}(\tau)} e^{i(\operatorname{sgn}(\xi) - \operatorname{sgn}(\xi - \tau) - \operatorname{sgn}(\tau))t} \hat{v}(t, \xi - \tau) \hat{v}(t, \tau) d\tau \\
&+ \epsilon \int_{-\infty}^{\infty} \frac{\tau}{\operatorname{sgn}(\xi) - \operatorname{sgn}(\xi - \tau) - \operatorname{sgn}(\tau)} \hat{v}_0(\xi - \tau) \hat{v}_0(\tau) d\tau \\
&- \epsilon^2 \int_0^t \int_{-\infty}^{\infty} \int_{-\infty}^{\infty} \frac{i\tau\eta e^{i(\operatorname{sgn}(\xi) - \operatorname{sgn}(\tau) - \operatorname{sgn}(\xi - \tau - \eta) - \operatorname{sgn}(\eta))s}}{\operatorname{sgn}(\xi) - \operatorname{sgn}(\xi - \tau) - \operatorname{sgn}(\tau)} \hat{v}(s, \xi - \tau - \eta) \hat{v}(s, \eta) \hat{v}(s, \tau) d\eta d\tau ds \\
&- \epsilon^2 \int_0^t \int_{-\infty}^{\infty} \int_{-\infty}^{\infty} \frac{i\tau\eta e^{i(\operatorname{sgn}(\xi) - \operatorname{sgn}(\xi - \tau) - \operatorname{sgn}(\tau - \eta) - \operatorname{sgn}(\eta))s}}{\operatorname{sgn}(\xi) - \operatorname{sgn}(\xi - \tau) - \operatorname{sgn}(\tau)} \hat{v}(s, \tau - \eta) \hat{v}(s, \eta) \hat{v}(s, \xi - \tau) d\eta d\tau ds.
\end{aligned}$$

We can simplify equation (2.21) by defining the following variables

$$\begin{aligned}
\alpha &= \operatorname{sgn}(\xi) - \operatorname{sgn}(\xi - \tau) - \operatorname{sgn}(\tau) \\
\beta &= \operatorname{sgn}(\xi) - \operatorname{sgn}(\tau) - \operatorname{sgn}(\xi - \tau - \eta) - \operatorname{sgn}(\eta) \\
\gamma &= \operatorname{sgn}(\xi) - \operatorname{sgn}(\xi - \tau) - \operatorname{sgn}(\tau - \eta) - \operatorname{sgn}(\eta).
\end{aligned}$$

Then (2.21) becomes

$$\begin{aligned}
\hat{v}(t, \xi) &= \hat{v}_0(\xi) - \epsilon \int_{-\infty}^{\infty} \frac{\tau}{\alpha} e^{i\alpha t} \hat{v}(t, \xi - \tau) \hat{v}(t, \tau) d\tau + \epsilon \int_{-\infty}^{\infty} \frac{\tau}{\alpha} \hat{v}_0(\xi - \tau) \hat{v}_0(\tau) d\tau \\
&- \epsilon^2 \int_0^t \int_{-\infty}^{\infty} \int_{-\infty}^{\infty} \frac{i\tau\eta}{\alpha} e^{i\beta s} \hat{v}(s, \xi - \tau - \eta) \hat{v}(s, \eta) \hat{v}(s, \tau) d\eta d\tau ds \\
&- \epsilon^2 \int_0^t \int_{-\infty}^{\infty} \int_{-\infty}^{\infty} \frac{i\tau\eta}{\alpha} e^{i\gamma s} \hat{v}(s, \tau - \eta) \hat{v}(s, \eta) \hat{v}(s, \xi - \tau) d\eta d\tau ds.
\end{aligned}$$

Differentiating with respect to t gives

$$\begin{aligned}
(2.22) \quad \frac{d}{dt} (\hat{v} + \epsilon B) &= -\epsilon^2 (I_1 + I_2) \\
B &= \int_{-\infty}^{\infty} \frac{\tau}{\alpha} e^{i\alpha t} \hat{v}(t, \xi - \tau) \hat{v}(t, \tau) d\tau \\
I_1 &= \int_{-\infty}^{\infty} \int_{-\infty}^{\infty} \frac{i\tau\eta}{\alpha} e^{i\beta s} \hat{v}(s, \xi - \tau - \eta) \hat{v}(s, \eta) \hat{v}(s, \tau) d\eta d\tau \\
I_2 &= \int_{-\infty}^{\infty} \int_{-\infty}^{\infty} \frac{i\tau\eta}{\alpha} e^{i\gamma s} \hat{v}(s, \tau - \eta) \hat{v}(s, \eta) \hat{v}(s, \xi - \tau) d\eta d\tau.
\end{aligned}$$

Since taking k derivatives is equivalent to multiplying by $(i\xi)^k$ in the Fourier space, we multiply the previous equation by $\xi^{2k}\hat{v}^*$ and integrate with respect to ξ .

$$(2.23) \quad \int_{-\infty}^{\infty} \xi^{2k}\hat{v}^*(t, \xi)\hat{v}_t(t, \xi) d\xi + \epsilon \int_{-\infty}^{\infty} \xi^{2k}\hat{v}^*(t, \xi)B_t d\xi = -\epsilon^2 \int_{-\infty}^{\infty} \xi^{2k}\hat{v}^*(I_1 + I_2) d\xi.$$

To construct an energy, we have to move the time derivative in the second term of (2.23) to the outside. Applying the product rule and using (2.19) gives us

$$(2.24) \quad \begin{aligned} \int_{-\infty}^{\infty} \xi^{2k}\hat{v}^*(t, \xi)B_t d\xi &= \frac{d}{dt} \int_{-\infty}^{\infty} \xi^{2k}\hat{v}^*(t, \xi)B d\xi - \int_{-\infty}^{\infty} \xi^{2k}\hat{v}_t^*(t, \xi)B d\xi \\ &= \frac{d}{dt} \int_{-\infty}^{\infty} \xi^{2k}\hat{v}^*(t, \xi)B d\xi - \epsilon \int_{-\infty}^{\infty} \int_{-\infty}^{\infty} i\xi^{2k}\tau e^{-i\alpha t}\hat{v}^*(t, \xi - \tau)\hat{v}^*(t, \tau)B d\tau d\xi. \end{aligned}$$

Combining (2.23) and (2.24), we get

$$\int_{-\infty}^{\infty} \xi^{2k}\hat{v}^*(t, \xi)\hat{v}_t(t, \xi) d\xi + \epsilon \frac{d}{dt} \int_{-\infty}^{\infty} \xi^{2k}\hat{v}^*(t, \xi)B d\xi = -\epsilon^2 \left[\int_{-\infty}^{\infty} \xi^{2k}\hat{v}^*(I_1 + I_2) d\xi + G \right],$$

where $G = -\int_{-\infty}^{\infty} \int_{-\infty}^{\infty} i\xi^{2k}\tau e^{-i\alpha t}\hat{v}^*(t, \xi - \tau)\hat{v}^*(t, \tau)B d\tau$. Adding the complex conjugate and multiplying by $\frac{1}{2}$, we get

$$(2.25) \quad \frac{d}{dt} \left\{ \frac{1}{2} \int_{-\infty}^{\infty} \xi^{2k}|\hat{v}|^2 d\xi + \epsilon \Re \left[\int_{-\infty}^{\infty} \xi^{2k}\hat{v}^*(t, \xi)B d\xi \right] \right\} = -\frac{\epsilon^2}{2} \left[\int_{-\infty}^{\infty} \xi^{2k}\hat{v}^*(I_1 + I_2) d\xi + G \right].$$

We then define the energy to be

$$(2.26) \quad E_k = \frac{1}{2} \int_{-\infty}^{\infty} \xi^{2k}|\hat{v}|^2 d\xi + \epsilon \Re \left[\int_{-\infty}^{\infty} \xi^{2k}\hat{v}^*(t, \xi)B d\xi \right].$$

Obviously, this energy satisfies the requirement $\frac{d}{dt}E_k = O(\epsilon^2)$, which is necessary to prove $O(\frac{1}{\epsilon^2})$ lifespan of small smooth solutions. It remains to check this definition is the same as the modified energy (2.16).

Using (2.26), (2.22), and (2.18), we get

$$(2.27) \quad \begin{aligned} E_k &= \frac{d}{dt} \left\{ \frac{1}{2} \int_{-\infty}^{\infty} \xi^{2k}|\hat{v}|^2 d\xi + \epsilon \Re \left[\int_{-\infty}^{\infty} \int_{-\infty}^{\infty} \xi^{2k}\frac{\tau}{\alpha} e^{i\alpha t}\hat{v}(t, \xi - \tau)\hat{v}(t, \tau)\hat{v}^*(t, \xi) d\tau d\xi \right] \right\} \\ &= \frac{d}{dt} \left\{ \frac{1}{2} \int_{-\infty}^{\infty} \xi^{2k}|\hat{u}|^2 d\xi + \epsilon \Re \left[\int_{-\infty}^{\infty} \int_{-\infty}^{\infty} \xi^{2k}\frac{\tau}{\alpha} \hat{u}(t, \xi - \tau)\hat{u}(t, \tau)\hat{u}^*(t, \xi) d\tau d\xi \right] \right\}. \end{aligned}$$

Using the fact $\alpha = \text{sgn}(\xi) - \text{sgn}(\xi - \tau) - \text{sgn}(\tau) = -\alpha = \text{sgn}(\xi) \text{sgn}(\xi - \tau) \text{sgn}(\tau)$, it can be easily verified that (2.27) is equivalent to the modified energy (2.16), and (2.25) gives closed energy estimates as before.

2.6. Normal Form Flow

In [22], the authors propose to replace the NFT (2.14) by a continuous flow, which we call the Normal Form Flow (NFF).

In the naive NFT scheme (2.14), we are transforming the variable h into g . We can construct a transformation flow $G(x, t; \epsilon')$ explicitly. The function G takes the value h at $\epsilon' = 0$, and flows it to the value g at $\epsilon' = \epsilon$.

$$(2.28) \quad \begin{aligned} G_\tau &= -hh_x \\ G(x, t; 0) &= h, \quad G(x, t; \epsilon) = g. \end{aligned}$$

Since $h = G(x, t; 0)$, the Normal Form Transformation (2.28) is essentially a first order approximation of the following continuous flow, which we call the Normal Form Flow

$$(2.29) \quad \begin{aligned} G_{\epsilon'} &= -GG_x \\ G(t, x; 0) &= h(t, x). \end{aligned}$$

Here, G is a continuous flow with initial data h and we consider the flow G at $\epsilon' = \epsilon$.

Equation (2.29) can be solved explicitly using characteristics:

$$(2.30) \quad G(t, \xi; \epsilon) = h(t, x), \quad x = \xi - \epsilon G(t, x; \epsilon).$$

The map $h(t, x) \rightarrow G(t, x; \epsilon)$ is bounded and invertible. The inverse map is also bounded. Therefore, it suffices to show that $G(t, x; \epsilon)$ has cubic energy estimate.

From (2.30), we get the following equalities by the chain rule

$$(2.31) \quad h_t = \frac{G_t}{1 - \epsilon G_\xi}, \quad h_x = \frac{G_\xi}{1 - \epsilon G_\xi}, \quad h_{xx} = \frac{G_{\xi\xi}}{(1 - \epsilon G_\xi)^3}.$$

Using the Cotlar's identity, we can rewrite equation (2.4) as

$$(2.32) \quad h_t + \epsilon \{H[hh_x] - H[h_x]h - H[h]h_x\} = H[h].$$

Combine (2.4) and (2.31), we get the following equation for G

$$g_t = \text{p.v.} \frac{1}{\pi} \int_{-\infty}^{\infty} \frac{\tilde{g} + \epsilon(g - 2\tilde{g})\tilde{g}\tilde{g}_{\tilde{\xi}} - \epsilon^2(g - \tilde{g})g_{\tilde{\xi}}\tilde{g}_{\tilde{\xi}}}{\xi - \tilde{\xi} - \epsilon(g - \tilde{g})} d\tilde{\xi}$$

where $g = G(t, \xi; \epsilon)$ and $\tilde{g} = G(t, \tilde{\xi}; \epsilon)$.

The authors of [22] then proceed to show the flow has good energy estimates.

2.7. Reduced NFT

[8] provides an alternative approach, which we will call the reduced NFT method. The method was originally implemented using para-differential operators. Here, we outline the main idea of this method using a transformation type argument instead of para-differential operators. In the naive NFT method above, we used the transformation to remove the entire quadratic term in the MRS equations. However, the quadratic term can be written as the sum of a 1st-order skew self-adjoint term and a 0th-order self-adjoint term. The skew self-adjoint term is harmless in the energy estimate, therefore we consider a reduced NFT method that only cancels out the self-adjoint part of the quadratic term.

First, define $w = \partial_x^s u$. Taking s derivatives of equation (2.1), we get

$$w_t + \epsilon \partial_x^s (uw_x) = H[w].$$

We can rewrite the equation as

$$(2.33) \quad w_t + \epsilon(uw_x + (s+1)u_x w + l.o.t.) = H[w],$$

where $l.o.t. = \sum_{j=2}^{s-1} \binom{s+1}{j} \partial_x^j u \partial_x^{s+1-j} u$. The key idea of the reduced NFT method is to split the highest-order quadratic terms $uw_x + (s+1)u_x w$ into two parts, as below

$$w_t + \epsilon\left(\frac{1}{2}(u\partial_x + \partial_x u) + \left(s + \frac{1}{2}\right)u_x\right)w + \epsilon(l.o.t.) = H[w],$$

where $u\partial_x + \partial_x u$ is an operator, defined as $(u\partial_x + \partial_x u)w = uw_x + (uw)_x$. Note that the operator $u\partial_x + \partial_x u$ is a 1st-order skew-symmetric operator, which vanishes in the energy estimates. Therefore,

the only problematic term is $(s + \frac{1}{2})u_x w$, and we will choose a normal form transformation to eliminate it.

Define $w = v + \epsilon \tilde{v}$, we get

$$v_t + \epsilon \tilde{v}_t + \frac{\epsilon}{2}(u\partial_x + \partial_x u)(v + \epsilon \tilde{v}) + \epsilon(s + \frac{1}{2})u_x v + \epsilon(l.o.t.) + \epsilon^2(s + \frac{1}{2})u_x \tilde{v} = H[v] + \epsilon H[\tilde{v}].$$

We choose $\tilde{v} = (s + \frac{1}{2})H[u_x]v$, then

$$v_t + \epsilon(s + \frac{1}{2})H[u_x]v_t - \epsilon^2(s + \frac{1}{2})H[(\frac{u^2}{2})_{xx}]v + \frac{\epsilon}{2}(u\partial_x + \partial_x u)(v + \epsilon \tilde{v}) + \epsilon^2(s + \frac{1}{2})u_x \tilde{v} + \epsilon(l.o.t.) = H[v + \epsilon \tilde{v}].$$

Define the operators $M[v] = v + \epsilon(s + \frac{1}{2})H[u_x]v$ and $D_u = u\partial_x + \partial_x u$, then the equation can be written as

$$(2.34) \quad Mv_t = -\frac{\epsilon}{2}D_u Mv - \epsilon(l.o.t.) + \epsilon^2 f + H Mv,$$

where $f = (s + \frac{1}{2})H[(\frac{u^2}{2})_{xx}]v - (s + \frac{1}{2})u_x \tilde{v}$.

To obtain energy estimates on the transformation variable v , we first apply the inverse operator M^{-1} to (2.34)

$$v_t = -\frac{\epsilon}{2}D_u v - \frac{\epsilon}{2}M^{-1}[D_u, M]v - \epsilon M^{-1}(l.o.t.) + \epsilon^2 M^{-1}f + Mv + M^{-1}[H, M]v,$$

where $[D_u, M]v = D_u Mv - M D_u v$, and $[H, M]v = H[M[v]] - M[H[v]]$. L^2 energy estimates on v is then given by

$$(2.35) \quad \left(\frac{1}{2} \|v\|_{L^2}^2 \right)_t = \int \left[-\frac{\epsilon}{2} M^{-1}[D_u, M]v - \epsilon M^{-1}(l.o.t.) + \epsilon^2 M^{-1}f + M^{-1}[H, M]v \right] v \, dx.$$

Direct calculation of the commutators gives us

$$\begin{aligned} [D_u, M]v &= 2\epsilon(s + \frac{1}{2})uH[u_{xx}]v \\ [H, M]v &= \epsilon(s + \frac{1}{2})(H[H[u_x]v] - H[u_x]H[v]). \end{aligned}$$

Both $\frac{\epsilon}{2}M^{-1}[D_u, M]v$ and $\epsilon^2 M^{-1}f$ are of order ϵ^2 , and consequently produce good energy estimates.

By sobolev inequalities, we get

$$\int \left[-\frac{\epsilon}{2} M^{-1}[D_u, M]v + \epsilon^2 M^{-1}f \right] v \, dx \lesssim \|v\|_{L^2}^4,$$

where the inequality depends on s .

Private communications with Delort ([8]) suggest that we can use an additional normal form transformation to eliminate the order ϵ term $-\epsilon M^{-1}(l.o.t.) + M^{-1}[H, M]v$, thus closing the energy estimate (2.35).

The main purpose of this procedure is to devise a transformation that eliminates only the 0th-order symmetric term in (2.33). By doing so, we then introduced an additional $O(\epsilon^2)$ term $\frac{\epsilon}{2}M^{-1}[D_u, M]v$. Therefore, one crucial factor in the success of this method is that $[D_u, M]v$ does not lose derivatives. Otherwise, the energy estimate (2.35) cannot be closed. However, this is not the case in the MRS equations, as we will show in section 3.7. This is a key difference between the Burgers-Hilbert equation and the MRS equations.

CHAPTER 3

The Majda-Rosales-Schonbek System

3.1. Background

Since we are studying the lifespan of small solutions of the MRS equations, the notation will be simpler if we factor out the small parameter. Rescaling both u and v by ϵ , the MRS equations become

$$(3.1) \quad \begin{aligned} u_t + \epsilon \left(\frac{1}{2} u^2 \right)_x &= v \\ v_t + \epsilon \left(\frac{1}{2} v^2 \right)_x &= -u. \end{aligned}$$

The initial value problem (1.6) with initial data $\|u\|_{H^s} + \|v\|_{H^s} \leq \epsilon$ is equivalent to the rescaled problem (3.1) with $\|u\|_{H^s} + \|v\|_{H^s} \leq 1$. We will work with the form (3.1) throughout this paper.

Similarly, the general intro-differential equations (1.5) can be rescaled as

$$(3.2) \quad \begin{aligned} u_t + \epsilon \left(\frac{1}{2} u^2 \right)_x + \int_0^1 K(x-y)v(y,t)dy &= 0 \\ v_t + \epsilon \left(\frac{1}{2} v^2 \right)_x - \int_0^1 K(y-x)u(y,t)dy &= 0. \end{aligned}$$

We first examine the dispersion relation of the general MRS equations (3.2). Linearizing (3.2) gives us

$$(3.3) \quad \begin{aligned} u_t &= - \int_0^1 K(x-y)v(y,t)dy \\ v_t &= \int_0^1 K(y-x)u(y,t)dy. \end{aligned}$$

Let u, v be plane waves with the expressions $u = ae^{-i\omega t + ikx}$ and $v = be^{-i\omega t + ikx}$. Taking Fourier transform of (3.3), we get

$$-i\omega \begin{bmatrix} \hat{u} \\ \hat{v} \end{bmatrix} = \begin{bmatrix} 0 & -2\pi \hat{K}(k) \\ 2\pi \hat{K}^*(k) & 0 \end{bmatrix} \begin{bmatrix} \hat{u} \\ \hat{v} \end{bmatrix},$$

where \hat{K}^* is the complex conjugate of \hat{K} and K is assumed to be real. We then obtain the dispersion relation

$$(3.4) \quad \omega^2 = 4\pi^2 |\hat{K}(k)|^2.$$

We now turn to the MRS equations (3.1). Similarly, we first linearize the MRS equations (3.1)

$$(3.5) \quad \begin{bmatrix} u \\ v \end{bmatrix}_t = \begin{bmatrix} 0 & 1 \\ -1 & 0 \end{bmatrix} \begin{bmatrix} u \\ v \end{bmatrix}.$$

The dispersion relation is then given by

$$(3.6) \quad \omega^2 = 1.$$

We can also obtain the dispersion relation by using (3.4) and $K(x) = \delta(x)$ and $\hat{K}(k) = \frac{1}{2\pi}$.

Since the frequency is independent of the wave number, the MRS system is a non-dispersive equation. The dispersion relation also implies that the problem generates 4-wave resonances, and not 3-wave resonances.

For general dispersive waves whose linearized solutions take the form

$$u(x, t) = \sum_k A(k) e^{i(kx - \omega(k)t)},$$

the problem has 3-wave resonances if it admits three pairs $\{k_i, \omega(k_i)\}$, with $k_i \neq 0$ for $i = 1, 2, 3$ satisfying the relationship

$$k_1 \pm k_2 \pm k_3 = 0, \quad \omega(k_1) \pm \omega(k_2) \pm \omega(k_3) = 0.$$

For the MRS system, the above equations do not have any solutions since the dispersion relation (3.6) gives us $\omega = \pm 1$.

However, if we consider four pairs $\{k_i, \omega(k_i)\}$, with $k_i \neq 0$ for $i = 1, 2, 3, 4$, we get the following 4-wave resonance relationship

$$(3.7) \quad k_1 \pm k_2 \pm k_3 \pm k_4 = 0, \quad \omega(k_1) \pm \omega(k_2) \pm \omega(k_3) \pm \omega(k_4) = 0.$$

The equation (3.8) admits a very large set of solutions. For any wave numbers that satisfy $k_1 + k_2 - k_3 - k_4 = 0$, we can choose $\omega(k_1) = \omega(k_2) = \omega(k_3) = \omega(k_4) = 1$ and they satisfy the relation

$$(3.8) \quad k_1 + k_2 - k_3 - k_4 = 0, \quad \omega(k_1) + \omega(k_2) - \omega(k_3) - \omega(k_4) = 0.$$

Therefore, the MRS system has a large number of 4-wave resonant interactions and these interactions cause some complicated behavior.

Similar 4-wave resonances can be observed in the Burgers-Hilbert equation. The dispersion relation of the Burgers-Hilbert equation (2.1) is given by

$$(3.9) \quad \omega = \text{sgn}(k).$$

For any choice of four positive wave numbers

$$k_1 + k_2 - k_3 - k_4 = 0, \quad k_1, k_2, k_3, k_4 \in (0, \infty)$$

the frequencies are given by $\omega_1 = \omega_2 = \omega_3 = \omega_4 = 1$ and satisfy the same 3-wave resonance relation (3.8). Therefore, the dispersion relation of the Burgers-Hilbert equation gives rise to a very large number of 4-wave resonant interactions, just like the MRS system.

One interesting fact is that when written into a system of two equations, the Burgers-Hilbert equation (2.3) (2.4) have the same linear terms as the MRS system (3.1), but the dispersion relations (3.6) (3.9) are different. The reason is that the variables u, v in the MRS system are independent, while the variables u, h in the Burgers-Hilbert system are not (h is defined as $h = H[u]$). In particular, the dispersion relation of the Burgers-Hilbert equation is "half" of that of the MRS system. This observation corresponds to splitting the linear equation (3.5)

$$(\partial_t - H)(\partial_t + H)u = 0.$$

A plane wave that satisfies (3.5) must have

$$\omega = \text{sgn}(k) \quad \text{or} \quad \omega = -\text{sgn}(k).$$

3.2. Smooth Solution Lifespan

Standard energy estimate on the MRS equation (3.1) gives existence of smooth solutions up to time $O(\frac{1}{\epsilon})$. Define energy as $\int |\partial_x^k u|^2 + |\partial_x^k v|^2 dx$, then it's easy to see that the linear terms cancel out and the energy estimate is exactly the same as that of the Burger's equation

$$\frac{d}{dt} \int |\partial_x^k u|^2 + |\partial_x^k v|^2 dx \lesssim \epsilon (\|u_x\|_{L^\infty} + \|v_x\|_{L^\infty}) \int |\partial_x^k u|^2 + |\partial_x^k v|^2 dx.$$

It follows by a standard argument that the solution exists up to time $O(\frac{1}{\epsilon})$.

Wagonmaker then improved this result and extended the lifespan of smooth solutions to $O(\frac{\ln(\epsilon)}{\epsilon})$ in [52].

Standard energy estimates give us $O(\frac{1}{\epsilon})$ lifespan because the nonlinear term is quadratic. However, we may be able to use the linear term to control the quadratic term and ultimately get cubic non-linearity.

3.3. Naive NFT

To obtain the naive NFT, we first write the MRS equations in the vector form

$$\mathbf{u}_t = L(\mathbf{u}) + \epsilon Q(\mathbf{u}, \mathbf{u})$$

$$\mathbf{u} = \begin{bmatrix} u \\ v \end{bmatrix}, \quad L(\mathbf{u}) = \begin{bmatrix} 0 & 1 \\ -1 & 0 \end{bmatrix} \mathbf{u}, \quad Q(\mathbf{u}, \mathbf{u}) = \begin{bmatrix} (-\frac{u^2}{2})_x \\ -(\frac{v^2}{2})_x \end{bmatrix}.$$

Solving the homological equation (2.12) with the above vector valued operators, we get

$$(3.10) \quad \begin{aligned} U &= u + \frac{1}{3}\epsilon \partial_x (u^2 - uv + \frac{1}{2}v^2) \\ V &= v - \frac{1}{3}\epsilon \partial_x (\frac{1}{2}u^2 - uv + v^2). \end{aligned}$$

Direct calculation gives the following equations on U, V

$$\begin{aligned} U_t &= V + \frac{\epsilon^2}{3} \partial_x (-2u^2 u_x + uvu_x + uvv_x - v^2 v_x) \\ V_t &= -U + \frac{\epsilon^2}{3} \partial_x (u^2 u_x - uvu_x - uvv_x + 2v^2 v_x). \end{aligned}$$

Direct energy estimates results in the same loss of derivatives as occurs for the Burgers-Hilbert equation

$$\frac{d}{dt} \int |\partial_x^k U|^2 + |\partial_x^k V|^2 dx \lesssim \epsilon^2 (\|u\|_{H^{k+1}} + \|v\|_{H^{k+1}})^2 (\|u\|_{L^\infty} + \|v\|_{L^\infty}),$$

where the inequality depends on k .

3.4. Modified Energy

Since direct energy estimate on the NFT variables U, V loses derivatives, we attempt to replicate the modified energy method here. Straight forward calculation gives us the standard energy

$$\begin{aligned} \|\partial_x^k U\|_{L^2}^2 + \|\partial_x^k V\|_{L^2}^2 &= \|\partial_x^k u\|_{L^2}^2 + \|\partial_x^k v\|_{L^2}^2 + \frac{2}{3}\epsilon < \partial_x^k u, \partial_x^{k+1}(u^2 - uv + \frac{1}{2}v^2) > - \frac{2}{3}\epsilon < \partial_x^k v, \partial_x^{k+1}(\frac{1}{2}u^2 - uv + v^2) > \\ &+ \frac{1}{9}\epsilon^2 \|\partial_x^{k+1}(u^2 - uv + \frac{1}{2}v^2)\|_{L^2}^2 + \frac{1}{9}\epsilon^2 \|\partial_x^{k+1}(\frac{1}{2}u^2 - uv + v^2)\|_{L^2}^2. \end{aligned}$$

As explained in 2.4, the $O(\epsilon^2)$ term does not affect the cubically non-linear energy estimate. Dropping the $O(\epsilon^2)$ term gives us the modified energy

$$(3.11) \quad E_k := \|\partial_x^k u\|_{L^2}^2 + \|\partial_x^k v\|_{L^2}^2 + \frac{2}{3}\epsilon < \partial_x^k u, \partial_x^{k+1}(u^2 - uv + \frac{1}{2}v^2) > - \frac{2}{3}\epsilon < \partial_x^k v, \partial_x^{k+1}(\frac{1}{2}u^2 - uv + v^2) > .$$

Taking the time derivative of the energy E_k , we get

$$(3.12) \quad \begin{aligned} \frac{dE_k}{dt} &= \frac{2\epsilon^2}{3} \int \left[\partial_x^k u \partial_x^{k+1} (-2u^2 u_x + uvu_x + uvv_x - v^2 v_x) - \partial_x^k v \partial_x^{k+1} (-u^2 u_x + uvu_x + uvv_x - 2v^2 v_x) \right. \\ &\quad \left. - \partial_x^k (uu_x) \partial_x^{k+1} (u^2 - uv + \frac{1}{2}v^2) + \partial_x^k (vv_x) \partial_x^{k+1} (\frac{1}{2}u^2 - uv + v^2) \right] dx. \end{aligned}$$

Straight forward calculation gives us

$$\frac{dE_k}{dt} = \frac{(k-1)\epsilon^2}{3} \int (u^2 - v^2)_x (\partial_x^{k+1} u \partial_x^k v - \partial_x^k u \partial_x^{k+1} v) + (l.o.t.) dx,$$

where $l.o.t.$ contains only derivatives of order less than or equal to k and gives good energy estimates.

Unlike the Burgers-Hilbert equation, the modified energy estimate suffers from loss of derivatives as well, i.e. we need order- $(k+1)$ derivatives of u, v to control $\frac{dE_k}{dt}$.

3.5. Time Resonance

We show that the modified energy (3.11) can be derived from the time resonance method as well.

To simplify the algebra, we write the system (3.1) in complex form for $F = u + iv$

$$F_t + \epsilon \frac{1}{8}(1-i) \left[F^2 + 2i|F|^2 + \overline{F}^2 \right]_x = -iF.$$

To eliminate the linear term, we define $F(t, x) = e^{-it}G(t, x)$, then

$$(3.13) \quad G_t + \epsilon \frac{1}{8}(1-i) \left[e^{-it}G^2 + 2i|G|^2 + e^{3it}\overline{G}^2 \right]_x = 0.$$

Integrating (3.13), we get

$$G = G_0 - \epsilon \frac{1}{8}(1-i) \partial_x \int_0^t e^{-is}G^2 + 2ie^{is}|G|^2 + e^{3is}\overline{G}^2 ds,$$

where $G_0(x) = G(0, x)$. Integration by parts gives

$$(3.14) \quad G = G_0 + J - \epsilon \frac{1}{8}(1-i) \partial_x \left[ie^{-it}G^2 + 2e^{it}|G|^2 - \frac{i}{3}e^{3is}\overline{G}^2 \right] + \epsilon \frac{1}{8}(1-i) \partial_x \left[iG_0^2 + 2|G_0|^2 - \frac{i}{3}\overline{G_0}^2 \right]$$

$$J = \epsilon \frac{1}{8}(1-i) \partial_x \int_0^t ie^{-is}(G^2)_t + 2e^{is}(|G|^2)_t - \frac{i}{3}e^{3is}(\overline{G}^2)_t ds.$$

Using (3.13), we can calculate

$$J = \frac{i}{16}\epsilon^2 \partial_x \int_0^t [ie^{-is}G + e^{is}\overline{G}] \partial_x [e^{-is}G^2 + 2ie^{is}|G|^2 + e^{3is}\overline{G}^2] ds$$

$$- \frac{1}{16}\epsilon^2 \partial_x \int_0^t [e^{is}G - \frac{i}{3}e^{3is}\overline{G}] \partial_x [e^{is}\overline{G}^2 - 2ie^{-is}|G|^2 + e^{-3is}G^2] ds.$$

After some simplification, we can get

$$(3.15) \quad J = \frac{i}{4}\epsilon^2 \partial_x \int_0^t \left[ie^{-2is}G^2\overline{G}_x + \frac{4i}{3}e^{2is}|G|^2\overline{G}_x + \frac{2}{3}|G^2|G_x + \frac{i}{4}\overline{G}^2G_x + \frac{2}{3}\overline{G}^2\overline{G}_x \right] ds.$$

Combining (3.14) and (3.15), then differentiating with respect to t , we get

$$(3.16) \quad \frac{d}{dt}(G + \epsilon B) = \frac{i}{4}\epsilon^2 \partial_x \left[ie^{-2it}G^2\overline{G}_x + \frac{4i}{3}e^{2it}|G|^2\overline{G}_x + \frac{2}{3}|G^2|G_x + \frac{i}{4}\overline{G}^2G_x + \frac{2}{3}\overline{G}^2\overline{G}_x \right]$$

$$B = \frac{1}{8}(1-i) \partial_x \left[ie^{-it}G^2 + 2e^{it}|G|^2 - \frac{i}{3}e^{3it}\overline{G}^2 \right].$$

Applying ∂_x^k to (3.16), we get

$$(3.17) \quad \frac{d}{dt}(\partial_x^k G - \epsilon \partial_x^k B) = \frac{i}{4} \epsilon^2 \partial_x^{k+1} \left[i e^{-2it} G^2 \overline{G}_x + \frac{4i}{3} e^{2it} |G|^2 \overline{G}_x + \frac{2}{3} |G^2| G_x + \frac{i}{4} \overline{G}^2 G_x + \frac{2}{3} \overline{G}^2 \overline{G}_x \right].$$

We then multiply (3.17) by $\partial_x^k \overline{G}$ and integrate over x

$$(3.18) \quad \int_{-\infty}^{\infty} \frac{d}{dt}(\partial_x^k G - \epsilon \partial_x^k B) \partial_x^k \overline{G} dx = \epsilon^2 I_1$$

$$I_1 = \frac{i}{4} \partial_x \int_0^t \left[i e^{-2is} G^2 \overline{G}_x + \frac{4i}{3} e^{2is} |G|^2 \overline{G}_x + \frac{2}{3} |G^2| G_x + \frac{i}{4} \overline{G}^2 G_x + \frac{2}{3} \overline{G}^2 \overline{G}_x \right] ds.$$

From product rule, we get

$$(3.19) \quad \epsilon \frac{d}{dt} \partial_x^k B \partial_x^k \overline{G} = \epsilon \frac{d}{dt} \left(\partial_x^k B \partial_x^k \overline{G} \right) - \epsilon \partial_x^k B \partial_x^k \overline{G}_t$$

$$= \epsilon \frac{d}{dt} \left(\partial_x^k B \partial_x^k \overline{G} \right) + \epsilon^2 \frac{1}{8} (1+i) \partial_x^k B \partial_x^{k+1} \left[e^{it} \overline{G}^2 - 2i |G|^2 + e^{-3it} G^2 \right].$$

Combine (3.18), and (3.19), then add the complex conjugate, we get

$$\frac{d}{dt} \left[\left\| \partial_x^k G \right\|_{L^2} - 2\epsilon \int_{-\infty}^{\infty} \Re \left(\partial_x^k B \partial_x^k \overline{G} \right) \right] dt = \epsilon^2 (I_1 + I_2) + c.c.$$

$$I_2 = \int_{-\infty}^{\infty} \frac{1}{8} (1-i) \partial_x^k B \partial_x^{k+1} \left[e^{it} \overline{G}^2 - 2i |G|^2 + e^{-3it} G^2 \right] dx.$$

We then define the energy to be

$$E_k = \left\| \partial_x^k G \right\|_{L^2} - 2\epsilon \int_{-\infty}^{\infty} \Re \left(\partial_x^k B \partial_x^k \overline{G} \right).$$

It is straight forward to check the definition is equivalent to the modified energy (3.11), and therefore suffers from the same loss of derivatives as in (3.12).

3.6. Normal Form Flow

Following the same procedure in section 2.6, we replace naive NFT (3.10) with continuous flows $U(t, x; \tau)$ and $V(t, x; \tau)$

$$(3.20) \quad U_\tau - \frac{1}{3} \epsilon \partial_x (U^2 - UV + \frac{1}{2} V^2) = 0$$

$$V_\tau + \frac{1}{3} \epsilon \partial_x (\frac{1}{2} U^2 - UV + V^2) = 0$$

$$U(t, x; 0) = u(t, x), V(t, x; 0) = v(t, x).$$

Notice that the naive NFT equations (3.10) is a first-order forward Euler approximation to the continuous flows (3.20).

The system can be put into the matrix form

$$\begin{bmatrix} U \\ V \end{bmatrix}_\tau + \frac{1}{3}\epsilon \begin{bmatrix} -2U + V & U - V \\ U - V & -U + 2V \end{bmatrix} \begin{bmatrix} U_x \\ V_x \end{bmatrix} = 0.$$

This is a symmetric hyperbolic system and the matrix has eigenvalues

$$\begin{aligned} \lambda_1 &= \frac{1}{2}(-3U + 3V + \sqrt{5U^2 - 6UV + 5V^2}) \\ \lambda_2 &= \frac{1}{2}(-3U + 3V - \sqrt{5U^2 - 6UV + 5V^2}) \end{aligned}$$

with eigenvectors

$$\mathbf{r}_1 = \begin{bmatrix} U - V \\ \frac{1}{2} \left(U + V + \sqrt{5U^2 - 6UV + 5V^2} \right) \end{bmatrix}, \quad \mathbf{r}_2 = \begin{bmatrix} U - V \\ \frac{1}{2} \left(U + V - \sqrt{5U^2 - 6UV + 5V^2} \right) \end{bmatrix}.$$

However, unlike the Burgers-Hilbert equation, where one can get an explicit expression of the normal form flow, it appears that an explicit expression for the normal variables cannot be easily obtained.

3.7. Reduced NFT

In this section, we present the loss of derivatives in the commutator when we apply the reduced NFT method to the MRS equations, marking a crucial difference from the Burgers-Hilbert equation (2.1). Following the same procedure in section 2.7, we first define $a = \partial_x^s u, b = \partial_x^s v$. Taking s derivatives on (3.1) gives us

$$\begin{aligned} (3.21) \quad a_t + \epsilon \left(\frac{1}{2} (u \partial_x + \partial_x u) + \left(s + \frac{1}{2} \right) u_x \right) a + \epsilon (l.o.t.) &= b \\ b_t + \epsilon \left(\frac{1}{2} (v \partial_x + \partial_x v) + \left(s + \frac{1}{2} \right) v_x \right) b + \epsilon (l.o.t.) &= -a, \end{aligned}$$

where the $\partial_x u$ is interpreted as an operator defined by $[\partial_x u] a = (ua)_x$.

We then look for a transformation that eliminates the harmful terms $s + \frac{1}{2} u_x a$ and $s + \frac{1}{2} v_x b$. Recall that when applying the reduced NFT method to the Burgers-Hilbert equation (section 2.7), it produces another harmful term which is the commutator of the transformation and the linear term on

the right hand side, which we then eliminated with a second normal form transformation. However, when working with the MRS system, it turns out we can combine these two transformations and use only one transformation instead.

We first write the equation in the matrix form. Define the vector $\mathbf{r} = \begin{bmatrix} a \\ b \end{bmatrix}$, and operators $D_u = u\partial_x + \partial_x u, D_v = v\partial_x + \partial_x v$, then equation (3.21) can be written as

$$(3.22) \quad \mathbf{p}_t = \epsilon L\mathbf{p} + \epsilon K\mathbf{p} + \epsilon(l.o.t.) - J\mathbf{p} = 0,$$

where the operators L, K, J are given by $L = \begin{bmatrix} \frac{1}{2}D_u & 0 \\ 0 & \frac{1}{2}D_v \end{bmatrix}$, $K = \begin{bmatrix} (s + \frac{1}{2})u_x & 0 \\ 0 & (s + \frac{1}{2})v_x \end{bmatrix}$ and

$$J = \begin{bmatrix} 0 & 1 \\ -1 & 0 \end{bmatrix}.$$

Define the transformation $\mathbf{p} = M\mathbf{r}$, then we have

$$(3.23) \quad (M\mathbf{r})_t = \epsilon LM\mathbf{r} + \epsilon KM\mathbf{r} + \epsilon(l.o.t.) - JM\mathbf{r} = 0.$$

Assume M is a multiplier operator, i.e. M can be represented by some 2×2 matrix, then we have

$$(3.24) \quad M\mathbf{r}_t + M_t\mathbf{r} + \epsilon ML\mathbf{r} + \epsilon[L, M]\mathbf{r} + \epsilon KM\mathbf{r} - MJ\mathbf{r} - [J, M]\mathbf{r} + \epsilon(l.o.t.) = 0.$$

We choose an operator M such that $(M_t + \epsilon KM - [J, M])\mathbf{r} = O(\epsilon^2)$. Direct calculations give us the solution

$$M = \begin{bmatrix} 1 + \epsilon \left(-\frac{2}{3}(1 + \frac{1}{2})u_x + \frac{1}{3}(1 + \frac{1}{2})v_x \right) & \epsilon \left(\frac{1}{3}(1 + \frac{1}{2})u_x - \frac{1}{3}(1 + \frac{1}{2})v_x \right) \\ \epsilon \left(\frac{1}{3}(1 + \frac{1}{2})u_x - \frac{1}{3}(1 + \frac{1}{2})v_x \right) & 1 + \epsilon \left(-\frac{1}{3}(1 + \frac{1}{2})u_x + \frac{2}{3}(1 + \frac{1}{2})v_x \right) \end{bmatrix}.$$

Then we have

$$(3.25) \quad \begin{aligned} M_t + \epsilon KM - [J, M] = & \epsilon^2 \left(s - \frac{1}{2} \right) \begin{bmatrix} \frac{2}{3}(uu_x)_x - \frac{1}{3}(vv_x)_x & -\frac{1}{3}(uu_x)_x + \frac{1}{3}(vv_x)_x \\ -\frac{1}{3}(uu_x)_x + \frac{1}{3}(vv_x)_x & \frac{1}{3}(uu_x)_x - \frac{2}{3}(vv_x)_x \end{bmatrix} \\ & + \epsilon^2 \left(s - \frac{1}{2} \right)^2 \begin{bmatrix} \left(-\frac{2}{3}u_x^2 + \frac{1}{3}u_x v_x \right) & \frac{1}{3}u_x^2 - \frac{1}{3}u_x v_x \\ \frac{1}{3}u_x v_x - \frac{1}{3}v_x^2 & -\frac{1}{3}u_x v_x + \frac{2}{3}v_x^2 \end{bmatrix}. \end{aligned}$$

Writing $F = M_t + \epsilon KM - [J, M]$, then the equation (3.24) becomes

$$(3.26) \quad M\mathbf{r}_t + \epsilon M L \mathbf{r} + \epsilon [L, M] \mathbf{r} - M J \mathbf{r} + \epsilon(l.o.t.) + F \mathbf{r} = 0.$$

Applying the inverse operator M^{-1} to equation (3.26), we get

$$\mathbf{r}_t + \epsilon L \mathbf{r} + \epsilon M^{-1} [L, M] \mathbf{r} - J \mathbf{r} + \epsilon(l.o.t.) + \epsilon^2 M^{-1} F v = 0.$$

From (3.26), we see that $M^{-1} F v$ is of order $O(\epsilon^2)$ does not contain any derivatives of \mathbf{r} . Therefore, it produces good energy estimates. Similar to the Burgers-Hilbert equation, we expect that the term $\epsilon(l.o.t.)$ can be taken care of by another normal form transformation since it contains only lower order derivatives. We now look at $\epsilon M^{-1} [L, M] \mathbf{r}$. Using the properties

$$\begin{aligned} D_u[fg] &= D_u[f]g + D_u[g]f - u_x fg \\ D_v[fg] &= D_v[f]g + D_v[g]f - v_x fg, \end{aligned}$$

we can obtain

$$(3.27) \quad \begin{aligned} \epsilon [L, M] &= \epsilon^2 \frac{1}{3} \left(s - \frac{1}{2} \right) \begin{bmatrix} (u_x - v_x) D_{u-v} [b_0] \\ -(u_x - v_x) D_{u-v} [a_0] \end{bmatrix} \\ &+ \epsilon^2 \begin{bmatrix} D_u [2u_x - v_x] a_0 - u_x (2u_x - v_x) a_0 + D_u [u_x - v_x] b_0 - u_v (u_x - v_x) b_0 \\ D_v [u_x - v_x] a_0 - u_x (u_x - v_x) a_0 + D_v [u_x - 2v_x] b_0 - v_x (u_x - 2v_x) b_0 \end{bmatrix}, \end{aligned}$$

where $\mathbf{r} = \begin{bmatrix} a_0 \\ b_0 \end{bmatrix}$

We can see that the first term in (3.27) loses derivatives, while the second term is good. As a result, the energy estimate cannot be closed. The fact that the commutator $[L, M]$ loses derivatives suggests an important difference between the Burgers-Hilbert equation (2.1) and the MRS system (3.1). Although they both have the Burgers non-linearity and a skew-symmetric linear term, but we lose the commutativity of the transformation operator M and the skew-symmetric operator L (i.e. the commutator $[L, M]$ loses derivatives) when going from an 1×1 equation to a 2×2 system.

CHAPTER 4

Numerical Results for the MRS System

4.1. Numerical Scheme

We consider the initial value problem for MRS

$$\begin{aligned}u_t + \epsilon\left(\frac{1}{2}u^2\right)_x &= v \\v_t + \epsilon\left(\frac{1}{2}v^2\right)_x &= -u \\u(x, 0) &= u_0(x) \\v(x, 0) &= v_0(x).\end{aligned}$$

We use a Weighted Essentially Non-Oscillatory (WENO) method (see [45], [46]) on a grid of size $N = 2^k$ to calculate the spatial derivatives. Our algorithm implements a 5th-order WENO flux described in [45] and uses the method of lines. An earlier work [44] by the same author provides more background information on the WENO scheme. The time derivatives are calculated using the MATLAB Runge-Kutta solver "ODE45". The MATLAB code was provided by Prof. John Hunter ([25]).

4.2. Shock

We first study the case where u_0 contains a single shock and v_0 is uniformly 0.

$$u_0 = \begin{cases} \epsilon & x \leq \pi \\ -\epsilon & x \geq \pi \end{cases}$$
$$v_0 = 0,$$

where we choose $\epsilon = 0.03$

The numerical result suggests a periodic exchange between shock and rarefaction. The visualizations below shows this exchange within one time period. The initial profile at $t = 0$ is shown in ??.

As t increases, the shock in u forces a rarefaction wave to form in v , which will in turn causes the shock to shrink. The shock in u will eventually turn into a rarefaction due to the expansion effect forced by the rarefaction in v . Once the rarefaction wave forms in u , it produces a shocking effect on v . The rarefaction in v will then turn into a shock and forces a shock to form in u . As a result, the solutions u and v will alternate between shocks and rarefactions in a periodic manner. This alternating behavior is visualized in figure 4.1 and 4.2, which are two snapshots of the solution at $t = \frac{\pi}{4}$ and $t = \frac{5\pi}{4}$. See [here](#) (URL at (1)) for a movie of the solutions.

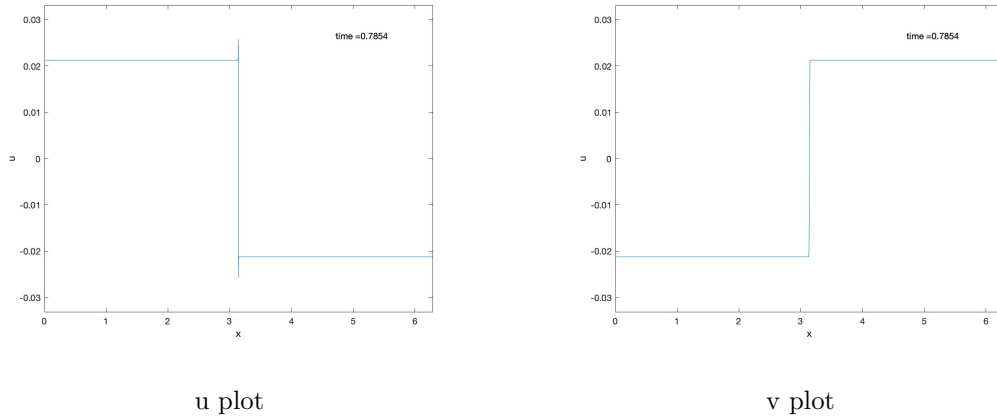


FIGURE 4.1. $t = \frac{\pi}{4}$

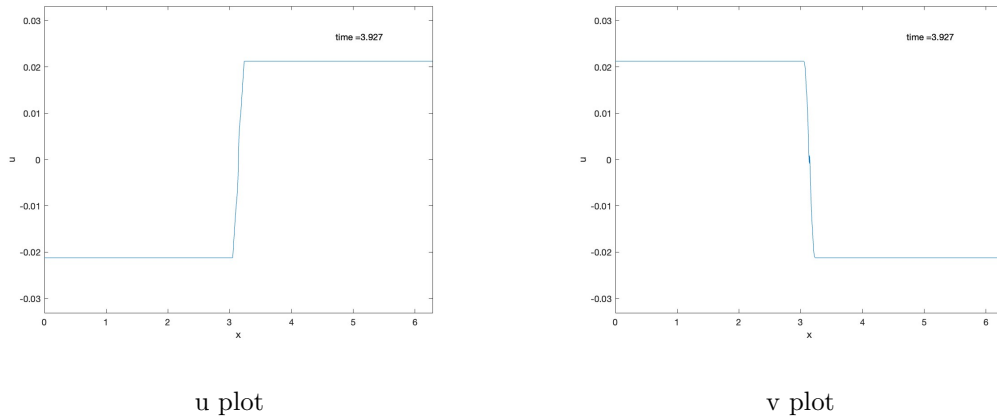
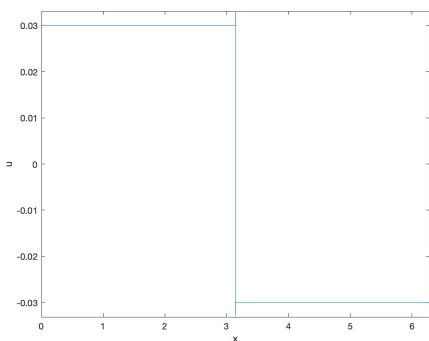


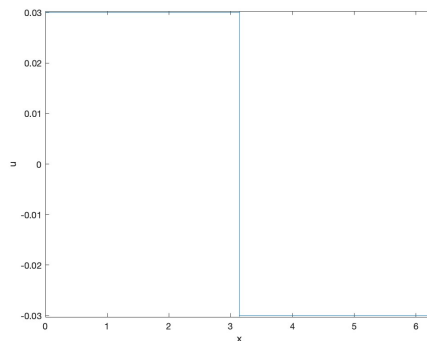
FIGURE 4.2. $t = \frac{5\pi}{4}$

An interesting phenomenon is the presence of spikes both at the top and bottom of the shock and the middle of the shock. We believe the top and bottom spikes are numerical because they can be significantly reduced by adding a dissipation.

We tried an alternate WENO method suggested by [39]. The alternate method adds a 4th order correction term that acts as viscosity. Therefore, the method is 5th order accurate, but includes more dissipation than the standard WENO scheme. The code is provided in B Figure 4.3 shows a comparison between the standard WENO scheme and the alternate WENO scheme at $t = \frac{\pi}{100}$. We see that the solution obtained using the standard WENO scheme develops spikes at the top and bottom of the shock almost immediately, whereas the alternate WENO solution remains flat outside the shock and the absolute value does not exceed $\epsilon = 0.03$.



u plot - standard WENO scheme



u plot - alternate WENO scheme

FIGURE 4.3. $t = \frac{\pi}{100}$

However, the spikes at the middle of the shock does not seem to disappear with the addition of dissipation. We believe this is a real property of the solutions. Figure 4.4 shows a zoomed-in plot of the spike at the middle of the v solution at $t = 3.4086$. Same middle spikes can be observed in u solutions as well. We are using a grid of 2^{15} evenly spaced points on $[0, 2\pi)$. A crude estimate shows that the spike in figure 4.4 spans across approximately 260 spatial points. Therefore, we believe this is a real property of the solutions, and not caused by the numerical scheme. We are currently running more experiments to study this phenomenon and will update if we make any progress.

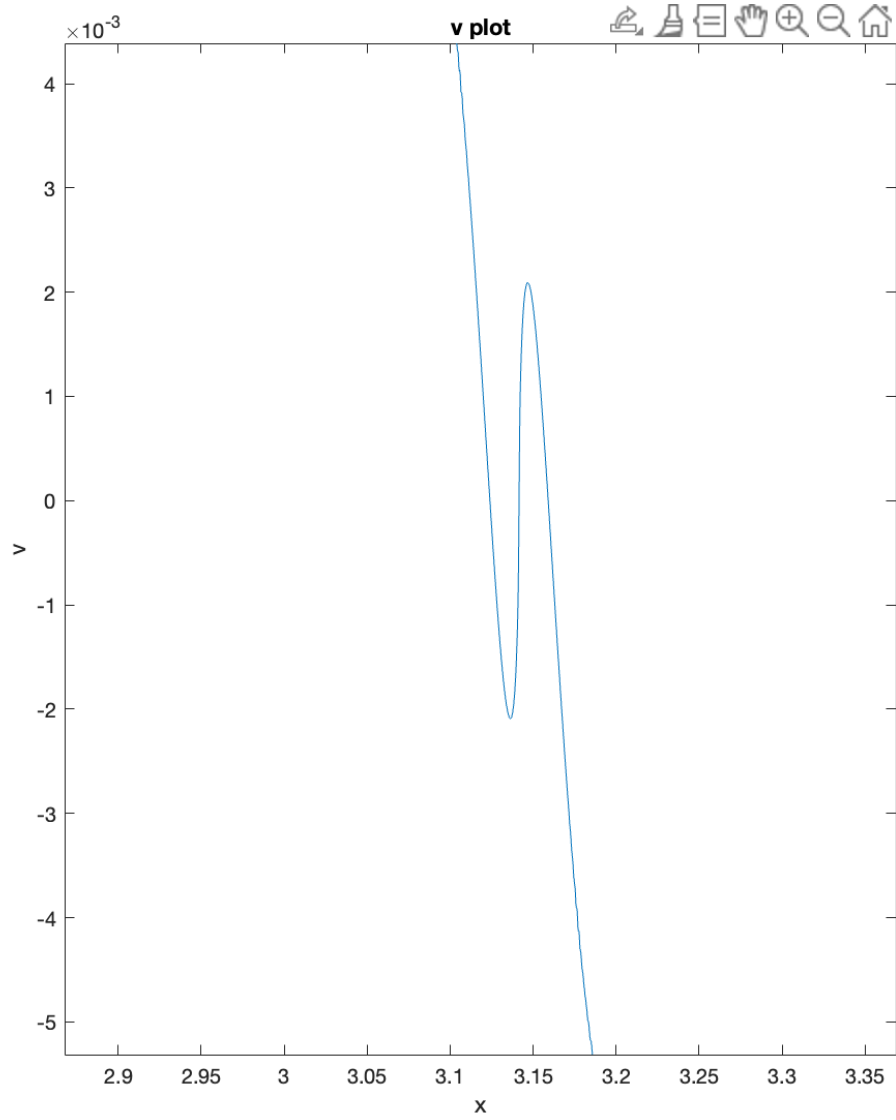


FIGURE 4.4

4.3. Shock with Zero Boundary Value

We have made some interesting observations with the following piece-wise initial data. The initial data u_0 contains a shock at $x = \pi$, but has value 0 at the end points,

$$u_0 = \begin{cases} 0 & x \in [0, \frac{\pi}{2}] \cup (\frac{3}{2}\pi, 2\pi] \\ x - \frac{\pi}{2} & x \in (\frac{\pi}{2}, \pi] \\ \frac{3}{2}\pi - x & x \in (\pi, \frac{3\pi}{2}] \end{cases}$$

$$v_0 = 0.$$

Figure 4.5 plots the solutions u, v at $t = 32\pi$, and see [here](#) (URL at (2)) for a movie of the numerical simulation. The solutions develop oscillations at the shock $x = \pi$. The oscillations gradually spread toward the corners, but never passing the corners. The numerical result seems to suggest that the oscillations die down as they approach the corners, but the reason behind this behavior is unclear.

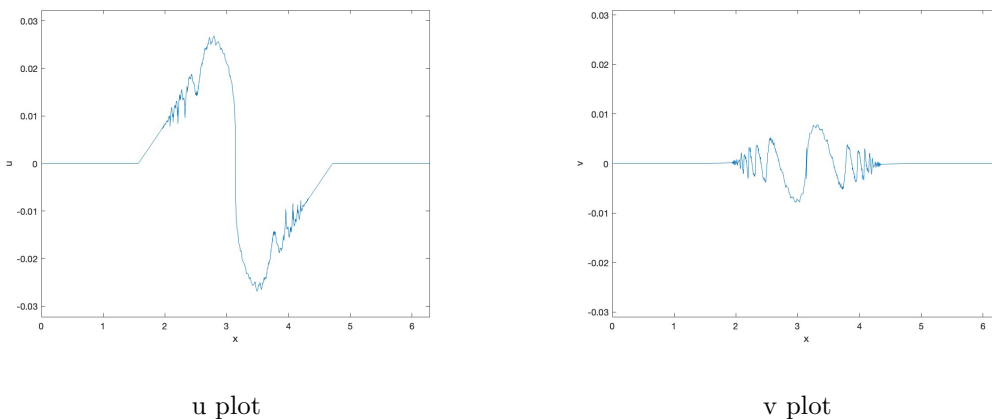


FIGURE 4.5. $t = 32\pi$

4.4. Lifespan

Here, we provide some numerical evidence to the $O(\epsilon^2)$ lifespan hypothesis. Consider the initial profile

$$(4.1) \quad \begin{aligned} u_0 &= \epsilon \cos(x)e^{\sin x} + \frac{\epsilon}{10} \sin(10x) \\ v_0 &= \epsilon(e^{\sin(x-\frac{\pi}{4})} - e^{\frac{1}{\sqrt{2}}}). \end{aligned}$$

u_0, v_0 both pass through 0 at $x = \frac{\pi}{2}$, which is where the singularity will form. We add the fast oscillation $\frac{\epsilon}{10} \sin(10x)$ to speed up the singularity formation. Without the fast oscillation, the singularity takes much longer to form, making our numerical result less accurate.

The L_2 norm of the solution starts to decay when the singularity forms. Therefore, we use the time derivative of the L_2 norm to detect the formation of the singularity. For example, 4.6 shows the entropy derivative with $\epsilon = 0.03$. The entropy derivative becomes negative at approximately $t = 108.322$, suggesting the formation of a singularity.

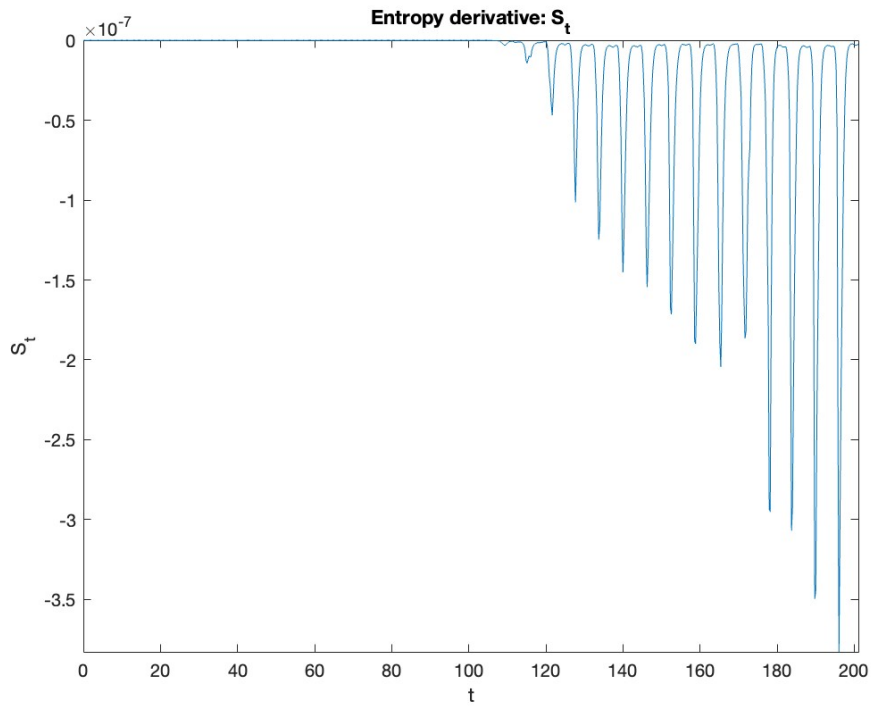


FIGURE 4.6

Figure 4.7 is a log-log plot of the singularity formation time T versus ϵ . The red curve shows the actual singularity formation time T versus ϵ , while the blue curve is the approximation obtained by polynomial fitting. The best exponential approximation of the singularity formation time T as a function of ϵ is $T = 0.298\epsilon^{-1.708}$. This result is fairly close to our $O(\frac{1}{\epsilon^2})$ lifespan hypothesis.

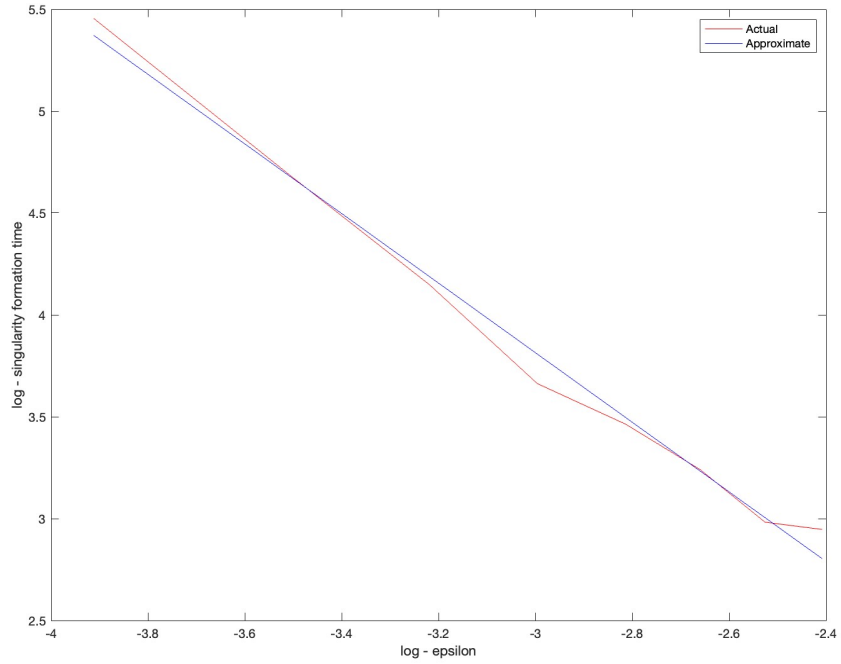


FIGURE 4.7

Similar outcomes can be observed with other initial data. For example, if we replace the perturbation in the initial data (4.1) by $\frac{\epsilon}{10} \cos(10x)$, i.e.

$$u_0 = \epsilon \cos(x)e^{\sin x} + \frac{\epsilon}{10} \cos(10x)$$

$$v_0 = \epsilon(e^{\sin(x-\frac{\pi}{4})} - e^{\frac{1}{\sqrt{2}}}),$$

the log-log plot of the actual and approximate singularity formation time versus ϵ is shown in figure 4.8. The exponential approximation of the singularity formation time T as a function of ϵ is $T = 0.118\epsilon^{-1.913}$, which again seems to follow the $O(\frac{1}{\epsilon^2})$ lifespan hypothesis.

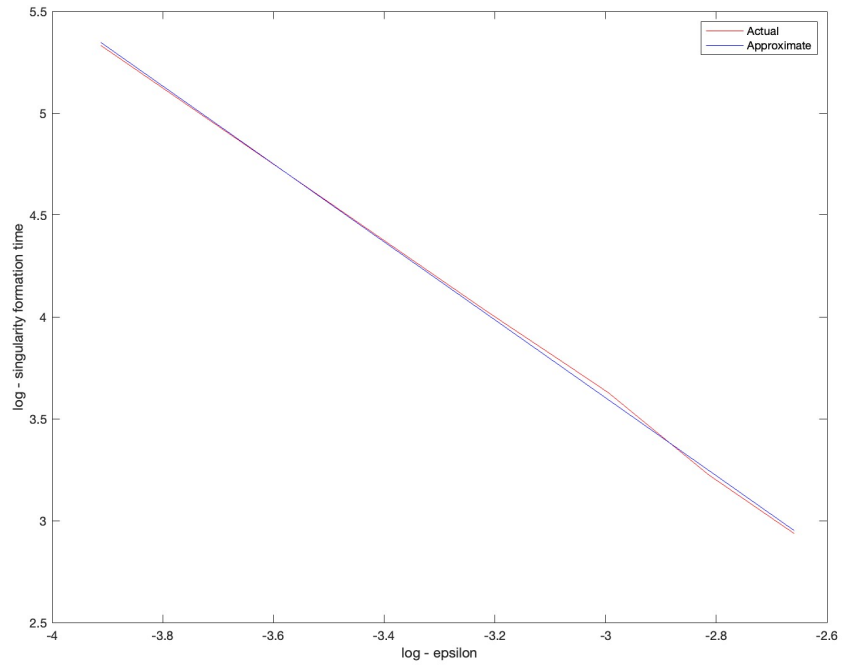


FIGURE 4.8

We have tested with a variety of different initial data, and all of the results appear to have $O(\frac{1}{\epsilon^2})$ lifespan. We have not found any initial data that violates this hypothesis.

Part 2

The Degenerate Quasi-linear Schrodinger Equation

Outline: Section 5.1 shows the derivation of the DQS equation through an asymptotic expansion of the MRS system. We then show the equation's Hamiltonian structure and the conservation laws that arise from the equation in section 5.2. In section 5.5, we apply the modulation theory to obtain a system of modulation equations. Before discussing the ill-posedness in H^s , we first demonstrate the difficulties introduced by the degeneracy in this problem. Section 5.6 shows the loss of derivatives in the standard energy method. In 5.7, we show a weighted energy method which overcomes the loss of derivatives, but fails due to the degeneracy. In section 5.8, we present a result in [29] by Jeong and Oh that shows the DQS equation is ill-posedness in H^s spaces. In section 5.9, we follow the method used in [20] to prove the equation is well-posed in a more restrictive function space.

5.1. Derivation

We first discuss the derivation of the following degenerate quasi-linear Schrödinger equation (1.8). This equation is obtained through an asymptotic expansion of the MRS system (3.1). Suppose u and v depends explicitly on $\tau = \epsilon^2 t$ (i.e. $u = u(t, x, \tau), v = v(t, x, \tau)$). Then, expand $u(t, x, \tau) = u_1(x, t, \tau) + \epsilon u_2(x, t, \tau) + \dots$ and $v = v(x, t, \tau) = v_1(x, t, \tau) + \epsilon v_2(x, t, \tau) + \dots$ and match terms with the same order, we get a system of equations.

At the leading order (order $O(\epsilon)$), we get the equations

$$\begin{aligned} u &= u(x, t, \tau) = \epsilon u_1(x, t, \tau) + \epsilon^2 u_2(x, t, \tau) + \dots \\ v &= v(x, t, \tau) = \epsilon v_1(x, t, \tau) + \epsilon^2 v_2(x, t, \tau) + \dots \end{aligned}$$

We can solve u_1 and v_1 explicitly:

$$\begin{aligned} u_1 &= iA(x, \tau)e^{-it} - \overline{iA(x, \tau)}e^{it} \\ v_1 &= A(x, \tau)e^{-it} + \overline{A(x, \tau)}e^{it}, \end{aligned}$$

where A is an arbitrary function.

At order $O(\epsilon^2)$, we get the equations

$$u_{2t} + u_1 u_{1x} = v_2$$

$$v_{2t} + v_1 v_{1x} = -u_2.$$

The solution to the order ϵ^2 equation is given by

$$u_2 = \frac{1+2i}{3} A A_x e^{-2it} + \frac{1-2i}{3} \overline{A A_x} e^{2it} - |A|_x^2$$

$$v_2 = \frac{1-2i}{3} A A_x e^{-2it} + \frac{1+2i}{3} \overline{A A_x} e^{2it} + |A|_x^2,$$

where we use the notation $|A|_x^2 = \partial_x(|A|^2)$. At order ϵ^3 , we get the equations

$$u_{1\tau} + u_{3t} + (u_1 u_2)_x = v_3$$

$$v_{1\tau} + v_{3t} + (v_1 v_2)_x = -u_3.$$

Plugging in u_1, u_2, v_1, v_2 , we get

$$u_{3t} - v_3 = -i A_\tau e^{-it} + i \overline{A_\tau} e^{it} -$$

$$\left(\frac{-2+i}{3} A^2 A_x e^{-3it} + \frac{2+i}{3} A \overline{A A_x} e^{it} - i A |A|_x^2 e^{-it} + \frac{2-i}{3} A \overline{A A_x} e^{-it} + \frac{-2-i}{3} \overline{A^2 A_x} e^{3it} + i \overline{A} |A|_x^2 e^{it} \right)_x$$

$$v_{3t} + u_3 = -A_\tau e^{-it} - \overline{A_\tau} e^{it} -$$

$$\left(\frac{1-2i}{3} A^2 A_x e^{-3it} + \frac{1+2i}{3} A \overline{A A_x} e^{it} + A |A|_x^2 e^{-it} + \frac{1-2i}{3} A \overline{A A_x} e^{-it} + \frac{1+2i}{3} \overline{A^2 A_x} e^{3it} + \overline{A} |A|_x^2 e^{it} \right)_x.$$

We can see that u_1, v_1 consist only of modes ± 1 , and u_2, v_2 consist only of modes ± 2 . However, at order ϵ^3 , we get resonant terms with modes ± 1 . Let

$$u_3 = u_3^{(0)} + u_3^{(1)} + c.c., \quad v_3 = v_3^{(0)} + v_3^{(1)} + c.c.$$

$$u_3^{(0)} = U(x, \tau) e^{-it}, \quad u_3^{(1)} = F(x, \tau) e^{-3it}$$

$$v_3^{(0)} = V(x, \tau) e^{-it}, \quad v_3^{(1)} = G(x, \tau) e^{-3it},$$

where $c.c.$ stands for complex conjugate.

Then $u_3^{(0)}, v_3^{(0)}$ are the resonant components of u_3, v_3 . Collect terms with mode -1 , we get

$$\begin{aligned} u_{3t} - v_3 &= -e^{-it} \left(iA_\tau - (iA|A|_x^2 - \frac{2-i}{3}|A|^2 A_x)_x \right) \\ v_{3t} + u_3 &= -e^{-it} \left(A_\tau + (A|A|_x^2 + \frac{1-2i}{3}|A|^2 A_x)_x \right). \end{aligned}$$

Multiply the second equation by i , plus the first equation, we get the solvability condition

$$iA_\tau + \frac{2}{3}(|A|^2 A_x)_x = 0.$$

Letting

$$(5.1) \quad u = \sqrt{\frac{3}{2}} A$$

and renaming τ as t gives us (1.8)

Since the DQS equation is derived from the MRS equation and the MRS equation is derived from gas dynamics, we expect that one can derive the DQS equation from gas laws directly. This approach is detailed in [48] and [24].

5.2. Basic Properties

5.2.1. Hamiltonian Structure. The DQS equation is Hamiltonian with the Hamiltonian structure

$$(5.2) \quad \begin{aligned} u_t + \partial_x \left[\frac{\delta \mathcal{H}}{\delta u^*} \right] &= 0 \\ \mathcal{H}(u, u^*) &= \frac{1}{4} \int i|u|^2 (uu_x^* - u^* u_x) dx \end{aligned}$$

with the non-canonical Hamiltonian operator ∂_x .

5.2.2. Variational Approach. The DES equation (1.8) can also be formulated as the variational equation $\frac{\delta S}{\delta \phi^*}[\phi, \phi^*] = 0$, where $u = \phi_x$ and

$$S[\phi, \phi^*] = \int \frac{1}{2} (\phi_t \phi_x^* + \phi_t^* \phi_x) + \frac{i}{4} \phi_x \phi_x^* (\phi_x \phi_{xx}^* + \phi_x^* \phi_{xx}) dx dt.$$

5.2.3. Conservation Laws. The DQS equation has the following associated conservation laws:

- (1) The DQS equation (1.8) itself is in conservation form. Therefore, the first conservation law is the DQS equation (1.8) itself.
- (2) The conservation of momentum $\rho(u, u^*) = \int uu^* dx$, associated with its spatial translation invariance:

$$(5.3) \quad \partial_t [|u|^2] + \partial_x [i|u|^2(uu_x^* - u^*u_x)]_x = 0.$$

- (3) The conservation of energy \mathcal{H} , associated with its temporal translation invariance:

$$(5.4) \quad \partial_t [i|u|^2(uu_x^* - u^*u_x)] + \partial_x \{6|u|^4|u_x|^2 + |u|^2 [(|u|^2)_x]^2 - \frac{1}{3}(|u|^6)_{xx}\} = 0.$$

- (4) The conservation of action, associated with its phase invariance:

$$(5.5) \quad \partial_t [i(\phi^*u - \phi u^*)] + \partial_x [|u|^2(\phi^*u_x + \phi u_x^*) + m^*\phi + m\phi^* - |u|^4] = 0.$$

where $m = m(t)$ is given by

$$i\phi_t + |\phi_x|^2\phi_{xx} = m(t).$$

5.3. Special Exact Solutions of the DQS Equation

We present the construction of a few exact solutions to the DQS equation. Evans and Hunter [10] have constructed other exact solutions as well.

5.3.1. Cube Root Solution. The cube root function

$$u(t, x) = Cx^{1/3}$$

where $C \in \mathbb{R}$ is a constant, is a solution to the DQS equation (1.8). However, we can not obtain a weak solution by extending by zero. The following function is not a weak solution to the DQS equation (1.8).

$$u(t, x) = \begin{cases} Cx^{1/3} & x > 0 \\ 0 & x \leq 0 \end{cases}$$

5.3.2. Linear Solution. The DQS equation has the linear solution

$$u(t, x) = xe^{2it}.$$

It's easy to check we can obtain a weak solution by extending by zero, i.e. the function

$$u(t, x) = \begin{cases} xe^{2it} & x > 0 \\ 0 & x \leq 0 \end{cases}$$

is a weak solution to the DQS equation.

5.3.3. Traveling Wave Solutions. We study the traveling wave solutions in the form of

$$u(x, t) = AU(kx - \omega t, s)$$

where $\omega = |A|^2 k^2$ and $A \in \mathbb{C}, s \in \mathbb{R}$ are both constants. Here, s is derived as a constant of integration. This class of solutions is discussed in [10].

Writing $\theta = kx - \omega t$, we then get an ODE for $U(\theta; s)$

$$(i + s)U = |U|^2 U_\theta.$$

We make a change of variable, defining ξ by $\frac{d\xi}{d\theta} = \frac{1}{|U|^2}$, we get the equation

$$U_\xi - iU = is.$$

The solution to this ODE is given by

$$(5.6) \quad U = ce^{i\xi} - s,$$

where c is given by $c^2 + s^2 = 1$. It follows that $\theta = \xi - 2cs \sin \xi$ with $s \in [0, 1]$. Figure 5.1 shows the plots of the traveling wave solutions with $s_1 = 0.8$, $s_2 = \frac{1}{\sqrt{2}}$, $s_3 = 0.3$, and $s_4 = 0.1$.

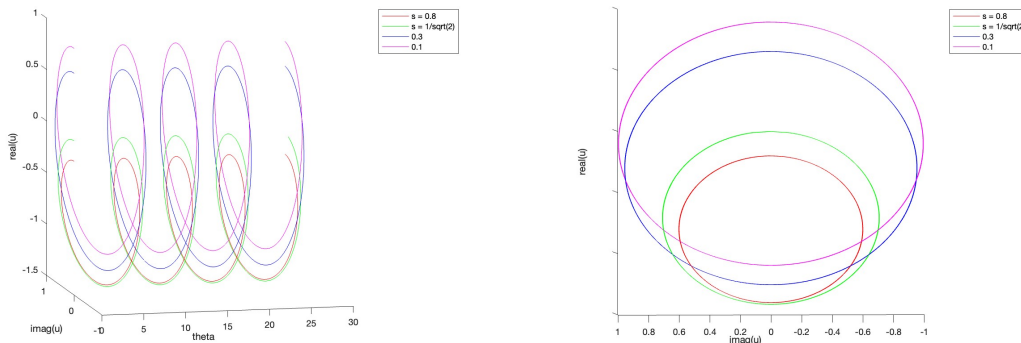


FIGURE 5.1. Traveling Wave Solutions

Observe that the solution does not have any singularity ($u = 0$) if $s \neq \frac{1}{\sqrt{2}}$. When $s = \frac{1}{\sqrt{2}}$, the solution has singularities at $\theta = 0$. The second plot shows a side view of the solutions. We can see the maximum real value of the solutions approaches 1 as $s \rightarrow 0$.

5.3.4. Generalized Traveling Wave. We look at an equation for generalized traveling wave solutions $u(x, t) = v(\theta)e^{i\alpha t}$ with $\theta = x - t$. Using (1.8), we get

$$iv' - (|v|^2v')' + \alpha v = 0.$$

Multiplying the equation by $|v|^2$, we get

$$i|v|^2v' - |v|^2(|v|^2v')' + \alpha|v|^2v = 0.$$

Choose new coordinate ξ such that $\frac{d}{d\xi} = |v|^2 \frac{d}{d\theta}$, then

$$(5.7) \quad iv' - v'' + \alpha|v|^2v = 0.$$

Notice that (5.7) gives the traveling wave solution $u(x - t) = v(\theta)$, where $\theta = x - t$ to the NLS equation

$$iu_t + u_{xx} - \alpha|u|^2u = 0.$$

Therefore, each generalized traveling wave solution of the DQS equation corresponds to a traveling wave solution of the NLS equation.

Here, we show how to obtain one class of traveling wave solutions for the NLS equation. Define $v(\theta) = \phi(\theta)e^{\frac{i}{2}\theta}$ where ϕ is real, then

$$\phi'' + \frac{1}{4}\phi - \alpha\phi^3 = 0.$$

Multiply the equation by ϕ' and integrate, we get the energy equation

$$\frac{1}{2}(\phi')^2 + \int (\frac{1}{4} - \alpha\phi^2)\phi d\phi = E_0.$$

Let $V(\phi) = \int (\frac{1}{4} - \alpha\phi^2)\phi d\phi = \frac{1}{8}\phi^2 - \frac{\alpha}{4}\phi^4$, then the solution is given by

$$\theta - \theta_0 = \int \frac{d\phi}{\sqrt{2(E_0 - V(\phi))}}.$$

The roots of $E_0 - V(\phi)$ are all real when $0 \leq \alpha E_0 \leq \frac{1}{64}$. Denote them by $\phi_1, \phi_2, \phi_3, \phi_4$, where $\phi_1 > \phi_2 > \phi_3 > \phi_4$.

- When $0 < \alpha E_0 < \frac{1}{64}$:

Using Jacobi Elliptic functions and the Möbius transformation, we get

$$\phi = \phi_1 + \frac{(\phi_2 - \phi_4)\phi_1 - (\phi_1 - \phi_4)\phi_2 \operatorname{sn}^2[\sqrt{\frac{\alpha(\phi_1 - \phi_3)(\phi_2 - \phi_4)}{8}}(\theta - \theta_0), \frac{(\phi_1 - \phi_4)(\phi_2 - \phi_3)}{(\phi_1 - \phi_3)(\phi_2 - \phi_4)}]}{(\phi_2 - \phi_4) - (\phi_1 - \phi_4) \operatorname{sn}^2[\sqrt{\frac{\alpha(\phi_1 - \phi_3)(\phi_2 - \phi_4)}{8}}(\theta - \theta_0), \frac{(\phi_1 - \phi_4)(\phi_2 - \phi_3)}{(\phi_1 - \phi_3)(\phi_2 - \phi_4)}]}.$$

Then the solution to the DQS equation is $u = \phi(x - t)e^{i(\frac{x-t}{2} + \alpha t)}$.

- When $\alpha E_0 = \frac{1}{64}$:

We get $\phi' = \sqrt{\frac{\alpha}{2}}\phi^2 - \sqrt{\frac{1}{32\alpha}}$ when $\phi^2 \geq \frac{1}{4\alpha}$.

Define $\phi = \sqrt{\frac{1}{4\alpha}}\tilde{\phi}$, we get $\tilde{\phi}' = \sqrt{\frac{1}{8}}(\tilde{\phi}^2 - 1)$.

Then $\tilde{\phi} = -\tanh(\frac{\theta}{\sqrt{8}})$, when $|\tilde{\phi}| < 1$. Translating back to ϕ , we get $\phi = -\sqrt{\frac{1}{4\alpha}}\tanh(\frac{\theta}{\sqrt{8}})$.

Then the solution to the DQS equation is $u = -\sqrt{\frac{1}{4\alpha}}\tanh(\frac{x-t}{\sqrt{8}})e^{i(\frac{x-t}{2} + \alpha t)}$.

5.4. Solutions with Cube Root Singularity

In this section, we will study solutions with cube root singularities. We start with a more general class of solutions

$$u(x, t) = AU(\theta; s),$$

where $k = \theta_x$ and $\omega = \theta_t$ are not necessarily constants. In the case that they are constants, then it reduces to the traveling wave solution (5.6). A cube root singularity means $U(\theta^*; s) = 0$ for some θ^* , and $U \sim (\theta - \theta^*)^{\frac{1}{3}}$ as $\theta \rightarrow \theta^*$.

Suppose u has a cube root singularity, we can expand u by

$$(5.8) \quad u = \sum_{j=1}^{\infty} A_j \theta^{\frac{j}{3}},$$

where A_j are functions of x and t . Applying the expansion (5.8) in the DQS equation (1.8) and equating the coefficients, we obtain the following two leading order equations.

On order $O(\theta^{-\frac{2}{3}})$, we get

$$(5.9) \quad -\frac{i}{3}wA_1 + \frac{k^2}{3}(|A_1|^2A_2 + \frac{1}{3}A_1^2\overline{A_2}) = 0.$$

On order $O(\theta^{-\frac{1}{3}})$, we get

$$(5.10) \quad -\frac{2i}{3}\omega A_2 + \frac{2k^2}{3}\left(\frac{4}{3}|A_1|^2A_3 + \frac{1}{3}A_1^2\overline{A_3} + |A_2|^2A_1 + \frac{2}{3}A_2^2\overline{A_1}\right) = 0.$$

From (5.9), we get

$$(5.11) \quad \frac{w}{k^2} = -i(\overline{A_1}A_2 + \frac{1}{3}A_1\overline{A_2}),$$

then (5.10) can be simplified to

$$\frac{4}{3}|A_1|^2A_3 + \frac{1}{3}A_1^2\overline{A_3} + \frac{2}{3}|A_2|^2A_1 - \frac{1}{3}A_2^2\overline{A_1} = 0.$$

Note that the traveling wave solution (5.6) has a singularity at $\xi = 0$ if $s = \frac{1}{\sqrt{2}}$. We can use (5.11) to calculate the speed of this singularity. Suppose $s = \frac{1}{\sqrt{2}}$, then as $\xi \rightarrow 0$, we have

$$\theta = \frac{1}{6}\xi^3 + O(\xi^5).$$

Then,

$$(5.12) \quad U = \frac{1}{\sqrt{2}}(\cos \xi + i \sin \xi - 1) = \frac{1}{\sqrt{2}}\left(6^{\frac{1}{3}}i\theta^{\frac{1}{3}} - \frac{6^{\frac{2}{3}}}{2}\theta^{\frac{2}{3}} - i\theta\right) + O(\theta^{4/3}).$$

Therefore, we have $A_1 = \frac{6^{1/3}i}{\sqrt{2}}$ and $A_2 = -\frac{6^{2/3}}{2\sqrt{2}}$, and equation (5.11) gives us the speed of the traveling wave

$$\frac{\omega}{k} = k.$$

5.5. Modulation System

We use the method of multiple scales to derive the modulation system. We assume the solution u depends on slow variables x, t and a fast phase variable θ .

$$\begin{aligned} u &= u(\theta, X, T; \epsilon) \\ \theta &= \frac{\phi(X, T)}{\epsilon}, \quad X = \epsilon x, \quad T = \epsilon t. \end{aligned}$$

Since θ is the phase variable, we require u to be 2π -periodic in θ . We then expand

$$u = u_0(\theta, X, T) + \epsilon u_1(\theta, X, T) + O(\epsilon^2)$$

and match coefficients of the same order. On the leading order, we get the equation

$$-i\omega u_{0\theta} + k^2(|u_0|^2 u_{0\theta})_\theta = 0,$$

where $\omega = -\phi_T$ and $k = \phi_X$. The solution is given by

$$(5.13) \quad u_0(\theta, X, T) = A(X, T)U(\theta; s), \quad \omega = |A|^2 k^2,$$

where ω, k, A, s are functions of (X, T) , and U is the traveling wave solution (5.6).

The order $O(\epsilon)$ equation is given by

$$(5.14) \quad -i\omega u_{1\theta} + iu_{0T} + k^2[|u_0|^2 u_{1\theta} + (u_0^* u_1 + u_0 u_1^*) u_{0\theta}^*]_\theta + k(|u_0|^2 u_{0\theta})_X + (k|u_0|^2 u_{0X})_\theta = 0.$$

We can rewrite equation (5.14) into the following form

$$\begin{aligned} \omega L u_1 + f(u_0) &= 0 \\ L u_1 &= k^2[|u_0|^2 u_{1\theta} + (u_0^* u_1 + u_0 u_1^*) u_{0\theta}^*]_\theta \\ f(u_0) &= iu_{0T} + k(|u_0|^2 u_{0\theta})_X + (k|u_0|^2 u_{0X})_\theta. \end{aligned}$$

The solvability conditions in order to obtain 2π -periodic solutions for u_1 are

$$(5.15) \quad \frac{1}{2\pi} \oint f(u_0) d\theta = 0$$

$$(5.16) \quad \frac{1}{2\pi i} \oint [u_0^* f(u_0) - u_0 f^*(u_0)] d\theta = 0.$$

where \oint denotes the integral over a 2π -period.

Define $\langle U \rangle := \frac{1}{2\pi} \oint U d\theta$ and $\rho = |u_0|^2$. Apply the solution (5.13) for u_0 to the first solvability condition (5.15) gives

$$i[A\langle U \rangle]_T + [k\rho A\langle |U|^2 U_\theta \rangle]_X = 0.$$

From the solution (5.6) for U , we can easily calculate

$$\langle U \rangle = -s(1 + c^2),$$

where c is given by $c^2 + s^2 = 1$. Then, we get the equation

$$[s(1 + c^2)A]_t + (\rho k c^2 s A)_x = 0.$$

Similarly, after some simplification, the second solvability condition (5.16) gives

$$[\rho(1 + 2c^2 s^2)]_t + [2\rho^2 k c^2 (1 + s^2)]_x = 0.$$

Combining the equation $k_t + \omega_x = 0$ and the above two equations, we get the equations

$$(5.17) \quad k_t + (\rho k^2)_x = 0$$

$$(5.18) \quad [s(1 + c^2)A]_t + (\rho k c^2 s A)_x = 0$$

$$(5.19) \quad [\rho(1 + 2c^2 s^2)]_t + [2\rho^2 k c^2 (1 + s^2)]_x = 0.$$

The equations correspond to the average of the conservation laws in 5.2.3. Equation (5.18) corresponds to the conservation of mean, which is the DQS equation (1.8) itself. Equation (5.19) corresponds to the conservation of momentum (5.3). If we take $u = AU$ in the equations (1.8), (5.3), and average them out over a 2π -period, we get (5.18), (5.19). Writing it into a system for

(ρ, k, s) requires further simplifications. Let $A = \sqrt{\rho}e^{i\eta}$, we get two real equations from (5.18).

$$(5.20) \quad [\sqrt{\rho}s(1+c^2)]_t + [\rho^{\frac{3}{2}}kc^2s] = 0$$

$$(5.21) \quad s(1+c^2)\eta_t + \rho kc^2s\eta_x = 0.$$

Equation (5.21) can be decoupled from the remaining equations since we can solve for (ρ, k, s) first and determine η afterwards.

Collecting (5.17), (5.19), and (5.20), we get the modulation equations on the variables ρ, k, s

$$\begin{aligned} k_t + (\rho k^2)_x &= 0 \\ [\rho(1+2c^2s^2)]_t + [2\rho^2kc^2(1+s^2)]_x &= 0 \\ [\sqrt{\rho}s(1+c^2)]_t + [\rho^{\frac{3}{2}}kc^2s] &= 0. \end{aligned}$$

Equivalently, it can be written as the following non-conservative form

$$(5.22) \quad \begin{bmatrix} 1 & 0 & 0 \\ 0 & 1+2s^2-2s^4 & 4s\rho(1-2s^2) \\ 0 & s(2-s^2) & 2\rho(2-3s^2) \end{bmatrix} \begin{bmatrix} k \\ \rho \\ s \end{bmatrix}_t + \begin{bmatrix} 2\rho k & k^2 & 0 \\ 2\rho^2c^2(1+s^2) & 4\rho kc^2(1+s^2) & 2\rho 2k(1-s^4) \\ 2\rho^2s(1-s^2) & 3\rho ks(1-s^2) & 2\rho^2k(1-3s^2) \end{bmatrix} \begin{bmatrix} k \\ \rho \\ s \end{bmatrix}_x = 0.$$

The eigenvalues of (5.22) is given by

$$\lambda = \rho k \mu(s),$$

where $\mu(s)$ satisfies

$$(5.23) \quad (4-6s^2+4s^6)\mu^3 - (26-50s^2+20s^4+12s^6)\mu^2 + (36-80s^2+40s^4+12s^6)\mu - (12-36s^2+20s^4+4s^6) = 0.$$

All three roots of (5.23) are real, and Figure 5.2 plots the roots as functions of s .

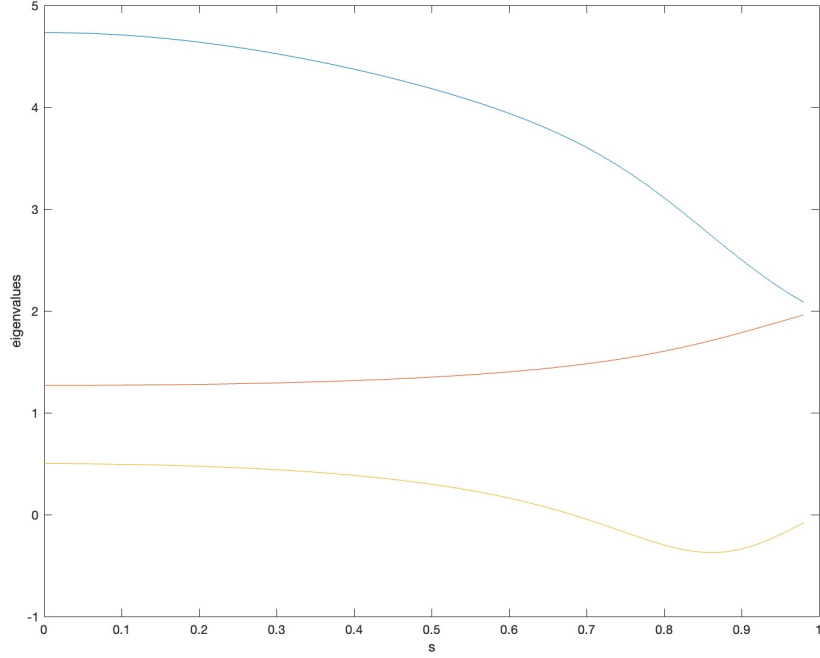


FIGURE 5.2

In section 6.5, we study a special case of the modulation system with $s = 0$ uniformly.

5.6. Energy Estimates

We first compute the standard energy estimate in H^s with $s \geq 3$,

$$\partial_t \|\partial_x^s u\|_{L^2}^2 = I_1 + I_2 \quad \text{where}$$

$$I_1 = -i \int \partial_x^{s+1} \bar{u} [\partial_x^s (|u|^2) u_x + s(|u|^2)_x \partial_x^s u] - \partial_x^{s+1} u [\partial_x^s (|u|^2) \bar{u}_x + s(|u|^2)_x \partial_x^s \bar{u}] dx$$

$$I_2 = i \sum_{j=2}^{s-1} \binom{s}{j} \int \partial_x^s \bar{u} [\partial_x^{j+1} |u|^2 \partial_x^{s-j+1} u + \partial_x^j |u|^2 \partial_x^{s-j+2} u] - \partial_x^s u [\partial_x^{j+1} |u|^2 \partial_x^{s-j+1} \bar{u} + \partial_x^j |u|^2 \partial_x^{s-j+2} \bar{u}] dx.$$

By Holder's inequality and Sobolev inequality, we can bound the second integral I_2 by $I_2 \lesssim \|U\|_{H^s}^4$.

However, the first integral I_1 can only be controlled by $\|U\|_{H^{s+1}}$. For example, if $s = 3$, then we have

$$I_1 = 2\Im \left(\int \overline{u_{xxxx}} [(|u|^2)_{xxx} u_x + 3(|u|^2)_x u_{xxx}] dx \right),$$

where $\Im(\cdot)$ means the imaginary part. It's clear I_1 cannot be controlled by the H^s norm. Hence, the energy estimate does not close due to the loss of derivatives in I_1 .

5.7. Weighted Energy Estimates

One way to resolve the loss of derivatives in the standard energy estimate is to replace the H^s energy with a weighted energy. Writing $\rho = |u|^2$ and differentiating (1.8) s times, we get

$$(\partial_x^s u)_t = i\partial_x^{s+1}(\rho u_x).$$

We simplify the notation by writing $v = \partial_x^s u$

$$\begin{aligned} v_t &= i \left[\rho v_{xx} + (s + \frac{3}{2})\rho_x v_x + \frac{1}{2}(\bar{u}u_x - u\bar{u}_x)v_x + uu_x\bar{v}_x \right. \\ &\quad \left. + \frac{s(s+1)}{2}\rho_{xx}v + (s+1)(u_x\bar{u}_x + u_{xx}\bar{u})v + (s+1)(u_x^2 + uu_{xx})\bar{v} \right] + f \\ f &= \sum_{j=3}^{s-1} \binom{s+1}{j} \partial_x^j \rho \partial_x^{s+2-j} u + \sum_{j=2}^{s-1} \binom{s+1}{j} \partial_x^j u \partial_x^{s+1-j} \bar{u} u_x + (s+1) \sum_{j=1}^{s-1} \binom{s}{j} \partial_x^j u \partial_x^{s-j} \bar{u} u_{xx}. \end{aligned}$$

The goal is to use a weighted energy $E_s = \|e^{-\phi(u)} v\|_{L^2}$ to replace the standard energy $\|v\|_{L^2}$ as shown in 5.6 and hopefully get good energy estimates. We chose to write the weight $e^{-\phi(u)}$ in this particular form so that it's easier to find the appropriate weight to use, as we will show below.

Define w by $v = e^\phi w$, then the energy can be written as $E_s = \|w\|_{L^2}$. Direct calculation yields

$$\begin{aligned} w_t &= i \left[\partial_x(\rho w_x) + (2\rho\phi_x + (s + \frac{1}{2})\rho_x)w_x + \frac{1}{2}(\bar{u}u_x - u\bar{u}_x)w_x + uu_x\bar{w}_x \right] \\ &\quad + i \left[\frac{s(s+1)}{2}\rho_{xx} + (s+1)(u_x\bar{u}_x + u_{xx}\bar{u}) + (\rho\phi_x^2 + \rho\phi_{xx} + (s + \frac{3}{2})\rho_x\phi_x + \frac{1}{2}(\bar{u}u_x - u\bar{u}_x)\phi_x) \right] w \\ &\quad + i \left[(s+1)(u_x^2 + uu_{xx}) + uu_x\bar{\phi}_x \right] \bar{w} + fe^{-\phi}. \end{aligned}$$

For simplicity, we rewrite this as

$$w_t = N_1 + N_2 + N_3 + f e^{-\phi}$$

$$N_1 = i \left[\partial_x(\rho w_x) + (2\rho\phi_x + (s + \frac{1}{2})\rho_x)w_x + \frac{1}{2}(\bar{u}u_x - u\bar{u}_x)w_x + uu_x\bar{w}_x \right]$$

$$N_2 = i \left[\frac{s(s+1)}{2}\rho_{xx} + (s+1)(u_x\bar{u}_x + u_{xx}\bar{u}) + (\rho\phi_x^2 + \rho\phi_{xx} + (s + \frac{3}{2})\rho_x\phi_x + \frac{1}{2}(\bar{u}u_x - u\bar{u}_x)\phi_x) \right] w$$

$$N_3 = i \left[(s+1)(u_x^2 + uu_{xx}) + uu_x\bar{\phi}_x \right] \bar{w}.$$

To get the time derivative of the energy, we multiply w_t by \bar{w} , add the complex conjugate and integrate over time. Let's look at the terms one by one and determine which one could break the energy estimate. N_2 and N_3 are obviously good terms since they do not involve space derivatives of w and the coefficients are lower order derivatives of u . The term $f e^{-\phi}$ consists of only lower order derivatives of u , therefore it does not cause any loss of derivatives. In N_1 , both $i\partial_x(\rho\partial_x)$ and $\frac{i}{2}(\bar{u}u_x - u\bar{u}_x)\partial_x$ are skew-symmetric and will vanish in the energy estimate. The term $i uu_x\bar{w}_x$, when multiplied with \bar{w} , can be written as $\frac{i}{2}uu_x\partial_x(\bar{w}^2)$ and we can move the derivative onto the lower order coefficient uu_x using integration by parts. Therefore, the only term that causes loss of derivatives is $i(2\rho\phi_x + (s + \frac{1}{2})\rho_x)w_x$ and we pick the weight by making it zero, i.e. we choose ϕ so that $2\rho\phi_x + (s + \frac{1}{2})\rho_x = 0$. The solution is then given by

$$\phi = -\left(\frac{s}{2} + \frac{1}{4}\right) \ln \rho, \quad w = e^{-\phi} v = |u|^{s+\frac{1}{2}} v.$$

We then compute the energy estimate

$$\partial_t \|w\|_{L^2}^2 = \int N_1 \bar{w} + \bar{N}_1 w \, dx + \int N_2 \bar{w} + \bar{N}_2 w \, dx + \int N_3 \bar{w} + \bar{N}_3 w \, dx + \int (f\bar{w} + \bar{f}w) |u|^{s+\frac{1}{2}} \, dx.$$

Using Sobolev inequality $\|u_x\|_{L^\infty} \lesssim \|U\|_{H^1}$ and integration by parts, we can bound the first integral by

$$(5.24) \quad \begin{aligned} \int N_1 \bar{w} + \bar{N}_1 w \, dx &= -i \int \frac{1}{2}(\bar{u}u_x - u\bar{u}_x)_x |w|^2 \, dx - \frac{i}{2} \int (uu_x)_x \bar{w}^2 \, dx + \frac{i}{2} \int (\bar{u}\bar{u}_x)_x w^2 \, dx \\ &\lesssim \|U\|_{H^3}^2 \|w\|_{L^2}^2. \end{aligned}$$

Direct application of the Sobolev inequality can bound the remaining three integrals

$$(5.25) \quad \int N_2 \bar{w} + \overline{N_2 w} \, dx + \int N_3 \bar{w} + \overline{N_3 w} \, dx + \int (f \bar{w} + \overline{f w}) |u|^{s+\frac{1}{2}} \, dx \lesssim \|U\|_{H^3}^2 \|w\|_{L^2}^2.$$

Combining (5.24) and (5.25), and choosing $s \geq 3$, we get

$$\partial_t \|w\|_{L^2}^2 \lesssim \|U\|_{H^3}^2 \|w\|_{L^2}^2 \lesssim \|v\|_{L^2}^2 \|w\|_{L^2}^2,$$

where the second inequality follows from Sobolev inequality.

The weighted energy method does resolve the loss of derivatives as we expected. However, $\|v\|_{L^2}$ cannot be controlled by the weighted energy $\|W\|_{L^2}$ due to the degeneracy of the equation. If the initial data is non-degenerate, then $\|v\|_{L^2}$ is comparable to $\|W\|_{L^2}$, closing the energy estimate, and the local well-posedness then follows from a standard Gronwall argument. But when the initial data is degenerate, the comparability between $\|v\|_{L^2}$ and $\|W\|_{L^2}$ breaks down and we cannot obtain a good energy estimate.

5.8. Ill-posedness in H^s

Jeong and Oh ([29], [28]) showed that the DQS equation is ill-posedness in H^s for $s > \frac{9}{2}$. In particular, they prove the following theorem

THEOREM 5.8.1. *For any $s > \frac{9}{2}$, there exists an initial data $u_0 \in H^2 \cap C^\infty(\mathbb{R})$ for which there is no corresponding solution to (1.8) in $L^\infty([0, \delta]; H^s(\mathbb{R}))$ with any $\delta > 0$.*

The authors considered a perturbation around the solution $f(t, x) = x e^{2it}$. They then performed a modified energy estimate on this perturbation and showed that this modified energy does not decay to 0. They finally showed this modified energy can be used to find a lower bound that blows up arbitrarily fast for the L_2 energy. The goal of the modified energy is to obtain a self-adjoint operator that consists of higher-order terms so that it cancels out in the energy estimate. [49] also gives an example of this method.

The key idea of the proof is that the support of the perturbation will shrink, and it will blow up around $x = 0$. We can construct perturbations that blow arbitrarily fast.

5.9. Well-posedness Result

[20] proves a well-posedness result in a more restricted space for a similar Quasi-linear Schrodinger equation

$$(5.26) \quad iu_t + \bar{u}(uu_x)_x = \mu|u^2|u,$$

where $\mu \in \{-1, 0, 1\}$.

Although equation (5.9) is similar to our DQS equation (1.8) in many ways, the Hamiltonian structure is very different. The hamiltonian of equation (5.9) is given by

$$\begin{aligned} u_t + i \left[\frac{\delta \mathcal{H}}{\delta u^*} \right] &= 0 \\ \mathcal{H}(u, u^*) &= \frac{1}{2} \int -(u^*)^2 (uu_x)_x + \mu |u|^4 dx. \end{aligned}$$

Note that the Hamiltonian form of the DQS equation (5.2) has the non-canonical operator ∂_x , whereas equation (5.9) can be written in the Hamiltonian form with the canonical operator i .

Since non-linear term in equation is very similar to the non-linear term in the DQS equation, we expect to obtain well-posedness in the same function space. In this chapter, we show that the same method used in [20] can be applied to our DQS equation to prove well-posedness on the set of initial data U_0 that is smooth, non-zero on an interval $I := (-x_0, x_0)$, supported on $\bar{I} = [-x_0, x_0]$, and has sufficient decay at the endpoints to ensure

$$(5.27) \quad \frac{1}{|u_0|} \notin L^1((-\infty, 0)) \cup L^1((0, \infty)).$$

5.9.1. Main result.

THEOREM 5.9.1. *Let $x_0 > 0$ and $I = (-x_0, x_0)$. Then there exists a set $S \subset L^2$ of functions that are non-zero and smooth on I , supported on \bar{I} and satisfy (5.27) so that for any $u_0 \in S$ there exists a time $T > 0$ and a unique $u \in C([0, T]; L^2)$ that satisfies (1.8) in the sense of distributions. Further, for all $t \in [0, T]$ the solution map $u_0 \rightarrow u(t)$ is Lipschitz continuous with respect to the L^2 -topology.*

Outline of Proof: The proof mainly consists of three parts. We first apply a change of variables to get a system of new equations. We then prove we can obtain solutions of this system with

good energy estimates. The final piece of the proof is to show that the solutions we constructed have sufficient regularity so that we can invert the change of variables and obtain a solution to the original equation (1.8).

The change of variables is the same as that used in [20] and is discussed in section 5.9.2. The equations are different from those in [20], but we can obtain the same well-posedness result. In 5.9.7, we show that we can adapt the proof in [20] to our equation and the calculations all work out. This last part of the proof depends only on the change of variables applied and the regularity of the new variables, and not on the equations of the new variables. Since we are using the same change of variables as in [20] and the new variables satisfy the same regularity conditions, this part of the proof will be exactly the same as Section 6 of [20] and we omit it here.

5.9.2. Change of Variables. We introduce the independent variable

$$(5.28) \quad y(t, x) = \int_0^x \frac{1}{|u(t, \zeta)|} d\zeta + c(t).$$

Using the change of variable we define

$$\begin{aligned} U(t, y(t, x)) &= u(t, x) \\ W(t, y(t, x)) &= w(t, x) = \frac{\overline{u(t, x)}u_x(t, x)}{|u(t, x)|}. \end{aligned}$$

The variable W is related to U by the identity

$$W = \frac{\overline{U}U_y}{|U|^2}.$$

We denote the real and imaginary part of W as

$$\alpha = \operatorname{Re}(W) \quad \text{and} \quad \beta = \operatorname{Im}(W).$$

Use α and β to fix our gauge by taking $c(t)$ to solve the equation

$$\begin{cases} c_t(t) = \beta(t, c(t)) + 3 \int_0^{c(t)} \alpha(t, \zeta) \beta(t, \zeta) \zeta \\ c(0) = 0 \end{cases},$$

and defining function $b(t, y)$ by

$$b(t, y) = 3 \int_0^y \alpha(t, \zeta) \beta(t, \zeta) d\zeta.$$

The equation (1.8) can be written as

$$(5.29) \quad i(U_t + b(t, y)U_y) + U_{yy} + (\alpha(t, y) - i\beta(t, y))U_y = 0.$$

As we mentioned, we also need to control W , which satisfies

$$(5.30) \quad i(W_t + bW_y) = -3i\alpha\beta W - \overline{W}W_y - 3WW_y - W_{yy}.$$

5.9.3. Function Spaces. [20] defines the following function spaces:

In the case of linear endpoint decay, Example 2.1 in [20] suggests that we should not expect W to decay as $|y| \rightarrow \infty$. This motivates the definition of the space Z^s with norm

$$\|f\|_{Z^s} := \|f\|_{L^\infty} + \|f_y\|_{H^{s-\frac{1}{2}}}.$$

Given a function $m : \mathbb{R} \rightarrow \mathbb{C}$ we define the Fourier multiplier

$$m(D_y)f(x) := \frac{1}{\sqrt{2\pi}} \int m(\xi) \hat{f}(\xi) e^{ix\xi} d\xi.$$

Given $\tau > 0$ and a Banach space X of tempered distributions on \mathbb{R} with norm $\|\cdot\|_X$, we define the subspace AX_τ of X to consist of $f \in X$ with finite norm

$$\|f\|_{AX_\tau} := \|(e^{\tau D_y} f, e^{-\tau D_y} f)\|_X,$$

where we make the convention that if $g = (g_1, g_2, \dots, g_n)$ then

$$\|g\|_X = \sum_{j=1}^n \|g_j\|_X.$$

5.9.4. Preliminary Inequalities. The proof requires the following results from [20]. We state the inequalities here and the proof can be found in [20]:

- Symmetric product bounds. If $s \geq 0$, then

$$(5.31) \quad \|fg_y\|_{AH_\tau^s} \lesssim \|f\|_{AL_\tau^\infty} \|g_y\|_{AH_\tau^s} + \|f_y\|_{AH_\tau^s} \|g\|_{AL_\tau^\infty}$$

$$(5.32) \quad \|fg\|_{AZ_\tau^s} \lesssim \|f\|_{AL_\tau^\infty} \|g\|_{AZ_\tau^s} + \|f\|_{AZ_\tau^s} \|g\|_{AL_\tau^\infty}$$

- Asymmetric product bounds. If $0 < s \leq \frac{1}{2}$, then

$$(5.33) \quad \|fg_y\|_{AH_\tau^{s-\frac{1}{2}}} \lesssim \|f\|_{AZ_\tau^0} \|g_y\|_{AH_\tau^{s-\frac{1}{2}}}$$

5.9.5. Existence for U, W . In order to prove existence of solutions to the DQS equation (1.8), we need to first prove existence of a solution to the equation (5.29). Here, we will treat the equations (5.29) and (5.30) as a system, where the initial data is not necessarily related.

THEOREM 5.9.2. *Let $0 < s \leq \frac{1}{2}$ and $0 < \tau_0 \leq 1$. Then given any*

$$U_0 \in AH_{\tau_0}^s, \quad W_0 \in AZ_{\tau_0}^s,$$

there exists some $T > 0$, a non-increasing, continuously differentiable function $\tau : [0, T] \rightarrow (0, \infty)$ so that $\tau(0) = \tau_0$, and a solution $U \in C_w([0, T]; AH_\tau^s), W \in C_w([0, T]; AZ_\tau^s)$ of the system (5.29) (5.30) with initial data $U(0) = U_0, W(0) = W_0$. Further, we have the estimates

$$(5.34) \quad \|U\|_{L_T^\infty AH_\tau^s} \lesssim \|U_0\|_{AH_{\tau_0}^s}$$

$$(5.35) \quad \|W\|_{L_T^\infty AZ_\tau^s} \lesssim \|W_0\|_{AZ_{\tau_0}^s}.$$

5.9.6. Regularized System. We take $\phi \in C_c^\infty$ to be an even function, identically 1 on $[-1, 1]$ and supported in $(-2, 2)$. We define the Littlewood-Paley projection $P_0 = \phi(D_y)$ and for $j \geq 1$ we define $P_j = \phi(2^{-j}D_y) - \phi(2^{1-j}D_y)$. We then consider the following regularized system

$$(5.36a) \quad \begin{cases} iU_t = P_{\leq j} [-iBU_{\leq j, y} + U_{\leq j, yy} + W_{\leq j}U_{\leq j, y}] \end{cases}$$

$$(5.36b) \quad \begin{cases} iW_t = P_{\leq j} [-iBW_{\leq j, y} + W_{\leq j, yy} + \overline{W_{\leq j}}W_{\leq j, y} - 3W_{\leq j}W_{\leq j, y} - 3i\alpha_{\leq j}\beta_{\leq j}W_{\leq j}] \end{cases}.$$

LEMMA 5.9.2.1. *Given $0 < s \leq \frac{1}{2}$, $0 \leq \tau_0 \leq 1$ and $(U_0, W_0) \in AH_{\tau_0}^s \times AZ_{\tau_0}^s$, there exists a time $T_0 > 0$ and a solution $(U, W) \in C^1([0, T_0]; AH_{\tau_0}^s \times AZ_{\tau_0}^s)$ of (5.36) with initial data $(U, W)(0) = (U_0, W_0)$.*

PROOF. We first bound the velocity B by

$$\|B\|_{L^\infty} \lesssim 2^j \|\alpha_{\leq j}\|_{L^\infty} \|\beta_{\leq j}\|_{L^\infty} \lesssim 2^j \|W\|_{L^\infty}^2.$$

We then apply Bernstein's inequality and Sobolev inequality to bound

$$\begin{aligned}
\|RHS((5.36a))\|_{AH_{\tau_0}^s} &\lesssim e^{\tau_0 2^j} 2^{sj} \|(RHS(5.36a))\|_{L^2} \\
&\lesssim e^{\tau_0 2^j} 2^{sj} [\|B\|_{L^\infty} \|U_{\leq j, y}\|_{L^2} + \|U_{\leq j, yy}\|_{L^2} + \|W_{\leq j}\|_{L^\infty} \|U_{\leq j, y}\|_{L^2}] \\
&\lesssim \|U\|_{L^2} e^{\tau_0 2^j} 2^{sj} [2^{2j} \|W\|_{L^\infty}^2 + 2^{2j} + 2^j \|W\|_{L^\infty}] \\
&\lesssim_{\tau_0, j} (1 + \|(U, W)\|_{AH_{\tau_0}^s \times AZ_{\tau_0}^s})^2 \|(U, W)\|_{AH_{\tau_0}^s \times AZ_{\tau_0}^s} \\
\|RHS((5.36b))\|_{AL_{\tau_0}^\infty} &\lesssim e^{\tau_0 2^j} \|-iBW_{\leq j, y} + W_{\leq j, yy} + \overline{W_{\leq j}}W_{\leq j, y} - 3W_{\leq j}W_{\leq j, y} - 3i\alpha_{\leq j}\beta_{\leq j}W_{\leq j}\|_{L^\infty} \\
&\lesssim e^{\tau_0 2^j} [2^{2j} \|W\|_\infty^3 + 2^{2j} \|W\|_\infty + 2^j \|W\|_\infty^2 + \|W\|_\infty^3] \\
&\lesssim_{\tau_0, j} (1 + \|(U, W)\|_{AH_{\tau_0}^s \times AZ_{\tau_0}^s})^2 \|(U, W)\|_{AH_{\tau_0}^s \times AZ_{\tau_0}^s} \\
\|\partial_y RHS((5.36b))\|_{H^{s-\frac{1}{2}}} &\lesssim e^{\tau_0 2^j} [2^{2j} \|W\|_{L^\infty}^2 \|W_y\|_{L^2} + 2^{2j} \|W_y\|_{L^2} + 2^j \|W\|_{L^\infty} \|W_y\|_{L^2} + \|W\|_{L^\infty}^2 \|W_y\|_{L^2}] \\
&\lesssim_{\tau_0, j} (1 + \|(U, W)\|_{AH_{\tau_0}^s \times AZ_{\tau_0}^s})^2 \|(U, W)\|_{AH_{\tau_0}^s \times AZ_{\tau_0}^s}.
\end{aligned}$$

Using the above bounds, we see that $RHS((5.36a))$ and $RHS((5.36b))$ are Lipschitz continuous as maps from $AH_{\tau_0}^s \times AZ_{\tau_0}^s$ to itself. The existence of the solution $(U, W) \in C^1([0, T_0]; AH_{\tau_0}^s \times AZ_{\tau_0}^s)$ then follows from the Picard-Lindelöf Theorem. \square

5.9.7. Proof of Theorem 5.9.2.

PROOF. We make the bootstrap assumption that for some $0 < T \leq T_*$ we have

$$(5.37) \quad \sup_{t \in [0, T]} \|U\|_{AH_\tau^s} + \sqrt{M\tau_0} \|U\|_{L_T^2 AH_\tau^{\frac{1}{2}}} + \sup_{t \in [0, T]} \|W\|_{AZ_\tau^s} + \sqrt{M\tau_0} \|W_y\|_{L_T^2 AL_\tau^2} \leq \frac{\sqrt{M}}{K}.$$

Remember that $B(t, y; j) = -3sech(2^{-j}y) \int_0^y \alpha_{\leq j}(t, \zeta) \beta_{\leq j}(t, \zeta) d\zeta$. We need to first obtain a bound for B_y . Since the definition of B is the same as that in [20], we will quote the result directly without providing the calculations and readers can refer to [20] for proof of the following inequality

$$(5.38) \quad \|B_y\|_{AZ_\tau^0} \lesssim \|W\|_{AL_\tau^\infty} \|W\|_{AZ_\tau^0} \lesssim \frac{M}{K^2}.$$

Using lemma 4.1 in [20], we obtain the following bound for U

$$(5.39) \quad \sup_{t \in [0, T]} \|U\|_{AH_\tau^s} + \sqrt{M\tau_0} \|U\|_{L_T^2 AH_\tau^{s+\frac{1}{2}}} \lesssim \|U_0\|_{AH_{\tau_0}^s} + \frac{1}{\sqrt{M\tau_0}} \|W_{\leq j} U_{\leq j, y}\|_{L_T^2 AH_\tau^{s-\frac{1}{2}}}.$$

(5.40)

Using (5.33) and the bootstrap assumption (5.37), we can then get

$$(5.41) \quad \begin{aligned} \frac{1}{\sqrt{M\tau_0}} \|W_{\leq j} U_{\leq j, y}\|_{L_T^2 AH_\tau^{s-\frac{1}{2}}} &\lesssim \frac{1}{\sqrt{M\tau_0}} \left\| \|W\|_{AZ_\tau^0} \|U_y\|_{AH_\tau^{s-\frac{1}{2}}} \right\|_{L_T^2} \\ &\lesssim \frac{1}{\sqrt{M\tau_0}} \|W\|_{L_T^\infty AZ_\tau^0} \|U\|_{L_T^2 AH_\tau^{s+\frac{1}{2}}} \\ &\lesssim \frac{1}{\sqrt{M\tau_0}} \|W\|_{L_T^\infty AZ_\tau^s} \|U\|_{L_T^2 AH_\tau^{s+\frac{1}{2}}} \\ &\lesssim \frac{1}{K\sqrt{\tau_0}} \|U\|_{L_T^2 AH_\tau^{s+\frac{1}{2}}}. \end{aligned}$$

Combining (5.39) and (5.41) and choosing K to be sufficiently large, we get

$$\sup_{t \in [0, T]} \|U\|_{AH_\tau^s} + \sqrt{M\tau_0} \|U\|_{L_T^2 AH_\tau^{s+\frac{1}{2}}} \lesssim_K \|U_0\|_{AH_{\tau_0}^s}$$

uniformly in $M \geq 1$. Finally, provided M is sufficiently large, we have

$$\sup_{t \in [0, T]} \|U\|_{AH_\tau^s} + \sqrt{M\tau_0} \|U\|_{L_T^2 AH_\tau^{s+\frac{1}{2}}} \leq \frac{\sqrt{M}}{20K},$$

which closes the first part of the bootstrap.

Next, we consider bounds for W_y . Differentiate (5.36b) by y , we get

$$\begin{aligned} iW_{ty} + iP_{\leq j} B W_{\leq j, yy} &= P_{\leq j} W_{\leq j, yyy} \\ &+ P_{\leq j} [\overline{W}_{\leq j} W_{\leq j, y} - 3W_{\leq j} W_{\leq j, y}]_y \\ &+ iP_{\leq j} [-B_y W_{\leq j, y} - 3\alpha_{\leq j, y} \beta_{\leq j} W_{\leq j} - 3\alpha_{\leq j} \beta_{\leq j, y} W_{\leq j} - 3\alpha_{\leq j} \beta_{\leq j} W_{\leq j, y}]. \end{aligned}$$

Applying the estimate (5.31), we may bound

$$\begin{aligned}
\|(\overline{W}_{\leq j} W_{\leq j, y} - 3W_{\leq j} W_{\leq j, y})_y\|_{L_T^2 AH_\tau^{s-1}} &\lesssim \|\overline{W}_{\leq j} W_{\leq j, y} - 3W_{\leq j} W_{\leq j, y}\|_{L_T^2 AH_\tau^s} \\
&\lesssim \left\| \|W\|_{AL_\tau^\infty} \|W_y\|_{AH_\tau^s} \right\|_{L_T^2} \\
&\lesssim \|W\|_{L_T^\infty AL_\tau^\infty} \|W_y\|_{L_T^2 AH_\tau^s} \\
&\lesssim \frac{\sqrt{M}}{K} \|W_y\|_{L_T^2 AH_\tau^s}.
\end{aligned}$$

Using the fact that $T \lesssim \frac{1}{M}$, with (5.32), (5.33), and the bootstrap assumption (5.37), we can bound

$$\begin{aligned}
&\|\alpha_{\leq j, y} \beta_{\leq j} W_{\leq j} + \alpha_{\leq j} \beta_{\leq j, y} W_{\leq j} + \alpha_{\leq j} \beta_{\leq j} W_{\leq j, y}\|_{L_T^1 AH_\tau^{s-\frac{1}{2}}} \\
&\lesssim \left\| \|\alpha\beta\|_{AZ_\tau^0} \|W_y\|_{AH_\tau^{s-\frac{1}{2}}} \right\|_{L_T^1} \\
&\lesssim \left\| \|W\|_{AL_\tau^\infty} \|W\|_{AZ_\tau^0} \|W_y\|_{AH_\tau^{s-\frac{1}{2}}} \right\|_{L_T^1} \\
&\lesssim \frac{1}{K^2} \|W_y\|_{L_T^\infty AH_\tau^{s-\frac{1}{2}}},
\end{aligned}$$

and using $T \lesssim \frac{1}{M}$ again, with the estimates (5.38) and (5.33), we also have

$$\|B_y W_{\leq j, y}\|_{L_T^1 AH_\tau^{s-\frac{1}{2}}} \lesssim T \|B_y\|_{L_T^\infty AZ_\tau^0} \|W_y\|_{L_T^\infty AH_\tau^{s-\frac{1}{2}}} \lesssim \frac{1}{K^2} \|W_y\|_{L_T^\infty}.$$

Applying proposition 4.1 we then obtain

$$\sup_{t \in [0, T]} \|W_y\|_{AH_\tau^{s-\frac{1}{2}}} + \sqrt{M\tau_0} \|W_y\|_{L_T^2 AH_\tau^s} \lesssim \|W_{0y}\|_{AH_{\tau_0}^{s-\frac{1}{2}}} + \frac{1}{k^2} \|W_y\|_{L_T^\infty AH_\tau^{s-\frac{1}{2}}} + \frac{1}{\sqrt{\tau_0} K} \|W_y\|_{L_T^2 AH_\tau^s}.$$

Provided that $K \gg 1$ is sufficiently large, we get

$$(5.42) \quad \sup_{t \in [0, T]} \|W_y\|_{AH_\tau^{s-\frac{1}{2}}} + \sqrt{M\tau_0} \|W_y\|_{L_T^2 AH_\tau^s} \lesssim \|W_{0y}\|_{AH_{\tau_0}^{s-\frac{1}{2}}}$$

uniformly in $M \geq 1$. Provided M is sufficiently large, we can ensure that

$$(5.43) \quad \sup_{t \in [0, T]} \|W_y\|_{AH_\tau^{s-\frac{1}{2}}} + \sqrt{M\tau_0} \|W_y\|_{L_T^2 AL_\tau^2} \lesssim \frac{\sqrt{M}}{40K},$$

which closes the second part of the bootstrap.

For the final part of the bootstrap, we need to bound the following quantity

$$\sup_{t \in [0, T]} \|W\|_{AL_\tau^\infty} \leq \sup_{t \in [0, T]} \|P_{>0}W\|_{AL_\tau^\infty} + \sup_{t \in [0, T]} \|P_0W\|_{AL_\tau^\infty}.$$

The first term can be bounded by Bernstein's inequality and (5.42)

$$\begin{aligned} \sup_{t \in [0, T]} \|P_{>0}W\|_{AL_\tau^\infty} &\lesssim \sup_{t \in [0, T]} \sum_{j=1}^{\infty} \|P_jW\|_{AL_\tau^\infty} \\ &\lesssim \sup_{t \in [0, T]} \|W_y\|_{AH_\tau^{s-\frac{1}{2}}} \lesssim \|W_{0y}\|_{AH_{\tau_0}^{s-\frac{1}{2}}}. \end{aligned}$$

Using Bernstein's inequality, the estimate (5.42), and the fact $T \lesssim \frac{1}{M}$, we can bound

$$\begin{aligned} \|P_0W_{\leq j, yy}\|_{L_T^1 AL_\tau^\infty} &\lesssim T \|W_y\|_{L_T^\infty AH_\tau^{s-\frac{1}{2}}} \lesssim \frac{1}{M} \|W_{0y}\|_{AH_{\tau_0}^{s-\frac{1}{2}}} \\ \|P_0(\overline{W_{\leq j}W_{\leq j, y}} - 3W_{\leq j}W_{\leq j, y})\|_{L_T^1 AL_\tau^\infty} &\lesssim \frac{1}{M} \|W\|_{AL_\tau^\infty}^2 \lesssim \frac{1}{K\sqrt{M}} \|W\|_{L_T^\infty AL_\tau^\infty} \\ \|P_0(\alpha_{\leq j}\beta_{\leq j}W_{\leq j})\|_{L_T^1 AL_\tau^\infty} &\lesssim T \|W\|_{L_T^\infty AL_\tau^\infty}^3 \lesssim \frac{1}{K^2} \|W\|_{L_T^\infty AL_\tau^\infty}. \end{aligned}$$

Applying all these bounds, and proposition 4.4 in [20], we obtain

$$\begin{aligned} \sup_{t \in [0, T]} \|W\|_{AL_\tau^\infty} &\lesssim C(K) \|W_{0y}\|_{AH_{\tau_0}^{s-\frac{1}{2}}} + \sup_{t \in [0, T]} \|P_0W\|_{AL_\tau^\infty} \\ &\lesssim C(K) \|W_{0y}\|_{AH_{\tau_0}^{s-\frac{1}{2}}} + \|W_0\|_{AL_{\tau_0}^\infty} + \|P_0(W_{\leq j, yy} + \overline{W_{\leq j}W_{\leq j, y}} - 3W_{\leq j}W_{\leq j, y} - 3i\alpha_{\leq j}\beta_{\leq j}W_{\leq j})\|_{L_T^1 AL_\tau^\infty} \\ &\lesssim C(K) \|W_{0y}\|_{AH_{\tau_0}^{s-\frac{1}{2}}} + \|W_0\|_{AL_{\tau_0}^\infty} + \left(\frac{1}{K\sqrt{M}} + \frac{1}{K^2}\right) \|W\|_{L_T^\infty AL_\tau^\infty} \end{aligned}$$

uniformly in j , where $C(K)$ is a constant depending on K, s, τ_0 . Provided K is sufficiently large (depending on s, τ_0) we obtain

$$\sup_{t \in [0, T]} \|W\|_{AL_\tau^\infty} \lesssim \frac{\sqrt{M}}{40K},$$

which closes the bootstrap.

We've shown that if the solutions of (5.36a) and (5.36b) satisfies (5.37), then it must satisfy (5.37) with the RHS((5.37)) replaced by $\frac{\sqrt{M}}{10K}$. Applying Lemma 5.9.2.1, our solution may then be extended to time $T = T^*$ and satisfies (5.37).

We can then obtain solutions of (5.36a) and (5.36b) that satisfy the estimates (5.34) and (5.35) uniformly in j . Passing to a subsequence $j \rightarrow \infty$, we may extract a weak limit $U \in C_w([0, T]; AH_\tau^2)$ and $W \in C_w([0, T]; AH_\tau^2)$ satisfying the equations (5.29) (5.30) and estimates (5.34) (5.35). \square

Numerical Results for the DQS Equation

6.1. Motivation for Front Propagating Solutions of the DQS Equation

We ask if the DQS equation can have compactly supported solutions. One motivation comes from the fact that the porous medium equation

$$u_t = (uu_x)_x$$

has solutions with a spreading front. For the porous medium equation, if we start with a pulse at zero (i.e. initial condition is a δ -function), then dimensional analysis shows us the solution is

$$u(x, t) = t^{\frac{1}{3}} F\left(\frac{x}{t^{1/3}}\right),$$

where F can be shown to have compact support. Therefore, we get a propagating solution with compact support.

The existence of compacton solutions is a feature of many degenerate dispersive equations. In [14], the authors showed that there are compacton solutions to the degenerate nonlinear Schrodinger equation

$$-i\partial_t u + \bar{u}\partial_x(u\partial_x u) + |u|^{p-2}u = 0$$

with $p > 2$. Another example of degenerate dispersive equations with compacton solutions is the following degenerate quasilinear Korteweg-de Vries (KdV) equation studied in [13],

$$u_t + (u(uu_x)_x + \mu u^3)_x = 0.$$

Here, we ask if we can also find a compactly supported solution for the DQS equation. Since we rely on numerical simulations, we cannot use a δ -function. Instead, we require the initial data to be compactly supported with a pulse at the center. In particular, we look at the following initial

data:

$$(6.1) \quad u_0(x) = \begin{cases} C[(\frac{\pi}{2})^2 - (\pi - x)^2]^2 & |x - \pi| \leq \frac{\pi}{2} \\ 0 & \text{otherwise.} \end{cases}$$

A plot of the solution at $t = 0.15$ is shown in figure 6.1, and a movie of the solution is provided [here](#) (URL at (5)).

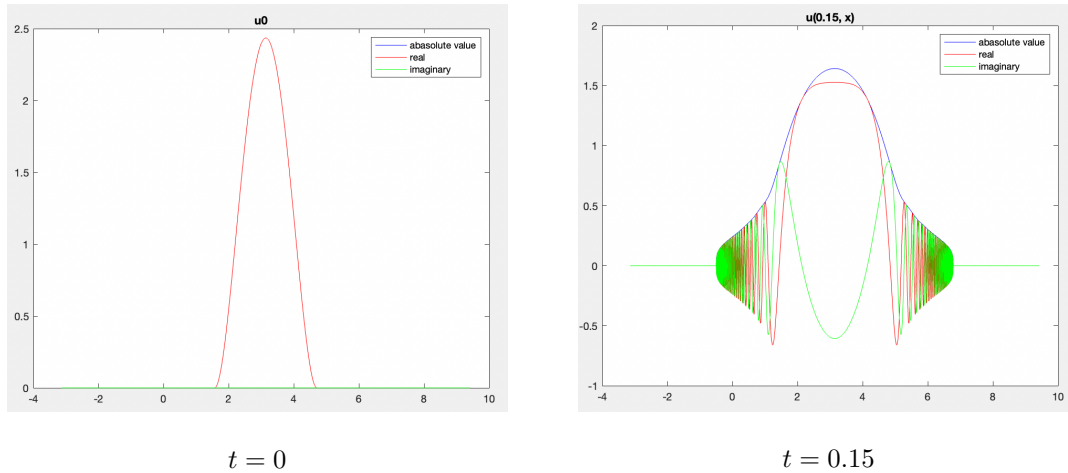


FIGURE 6.1

6.2. Previous Numerical experiment

This front solution was considered in [48] by Evan Smothers. He used a spectral scheme with artificial viscosity to compute the solution. However, the spectral scheme requires an implicit ODE solver, making it very costly under high resolutions since the system is not sparse. Therefore, we use a finite-difference scheme instead, which allows us to work with a sparse system. The time consumption and memory requirement are lower compared to the spectral method.

6.3. Numerical Method

We use a finite-difference scheme to solve the equation numerically. Take $\rho = |u|^2$, then we obtain a system of two equations:

$$(6.2) \quad \rho_t = i(\rho(u_x \bar{u} - \bar{u}_x u))_x$$

$$(6.3) \quad u_t = i(\rho u_x)_x.$$

We solve the two equations in alternation. In each iteration, we use (6.2) to update ρ first; then use (6.3) to update u .

In equation (6.2), note that $i(u_x\bar{u} - \bar{u}_x u)$ is real. Therefore equation (6.2) is similar to an advection equation. An explicit method is stable for this problem as long as we keep the CFL number small. Here, we use the Lax-Friedrichs method. One major advantage of the Lax-Friedrichs method over other methods is that it preserves positivity of ρ . For equation (6.3), we use the Backward Euler method since $i\rho$ is purely imaginary and hence a Backward Euler method is unconditionally stable. Therefore, our algorithm is 1-st order accurate in both space and time.

For the finite difference method, we use a grid size of $N = 2^k$. And to keep the CFL number small, we set $M = 2N$, where M is the number of time steps.

Let x_n^k be the k -th point on the grid at the n -th time step, and let $x_n^{k+\frac{1}{2}} = \frac{1}{2}(x_n^k + x_n^{k+1})$.

Let $u_n^k = u(x_n^k)$ and $\rho_n^{k+\frac{1}{2}} = \rho(x_n^{k+\frac{1}{2}})$. Here, u and ρ are evaluated on a staggered grid. u is evaluated on points x_n^k and ρ is evaluated on points $x_n^{k+\frac{1}{2}}$ only.

For clarity, let's also define $J = i(u_x\bar{u} - \bar{u}_x u)$. Then (6.2) becomes $\rho_t = (\rho J)_x$. To calculate the x -derivative, J must be evaluated on the same grid points as ρ . Therefore, we approximate $u_n^{k+\frac{1}{2}}$ by $u_n^{k+\frac{1}{2}} = \frac{1}{2}(u_n^k + u_n^{k+1})$. Let $J_n^{k+\frac{1}{2}} = J(u_n^{k+\frac{1}{2}})$, the numerical scheme has the form

$$(6.4) \quad \rho_{n+1}^{k+\frac{1}{2}} = \frac{1}{2}(\rho_n^{k+\frac{3}{2}} + \rho_n^{k-\frac{1}{2}}) + \frac{\Delta t}{2\Delta x}(\rho_n^{k+\frac{3}{2}} J_n^{k+\frac{3}{2}} - \rho_n^{k-\frac{1}{2}} J_n^{k-\frac{1}{2}})$$

$$(6.5) \quad \frac{u_{n+1}^k - u_n^k}{\Delta t} = \frac{i}{\Delta x^2}[\rho_{n+1}^{k+\frac{1}{2}}(u_{n+1}^{k+1} - u_{n+1}^k) - \rho_{n+1}^{k-\frac{1}{2}}(u_{n+1}^k - u_{n+1}^{k-1})].$$

The numerical scheme we used is 1-st order accurate in space and time. The code is provided in appendix A. We have attempted methods with better accuracy, such as the Crank-Nicolson method and the 2nd-order Backward Differentiation Formula (BDF2) for the Schrodinger equation, both of which are 2-nd order accurate in time. However, according to our simulations, these methods create oscillations, and our effort to find a stable but more accurate methods has been unsuccessful so far. Below, we show the comparison between the fully implicit scheme, the Crank-Nicolson scheme, and the BDF2 scheme.

The details of the numerical viscosity of the fully implicit scheme will be explained in section 6.4. For now, we will just say the fully implicit scheme has a viscous effect that inhibits the formation of oscillations. The BDF2 scheme has built-in viscosity as well, but it is weaker compared to that

of the implicit scheme. The comparison between the solutions of the fully implicit scheme and the BDF2 scheme at $t = \frac{\pi}{2}$ is shown in figure 6.3. Both schemes are run with the grid size of 2^{14} , and the initial data is set to be that of the traveling wave solution (5.6) with $s = c = \frac{1}{\sqrt{2}}$. See [here](#) (URL at (4)) for a movie of the traveling wave solution using the fully implicit scheme.

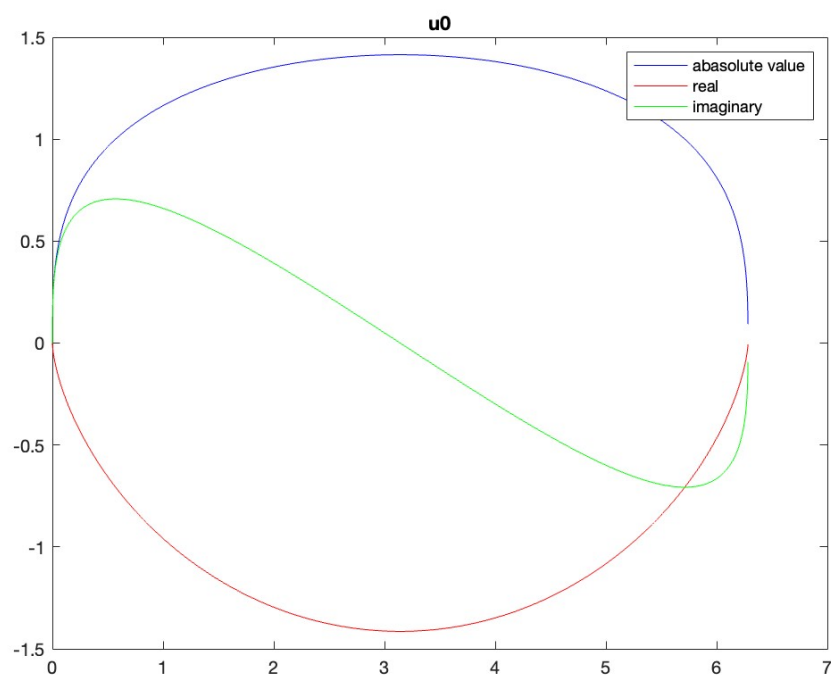
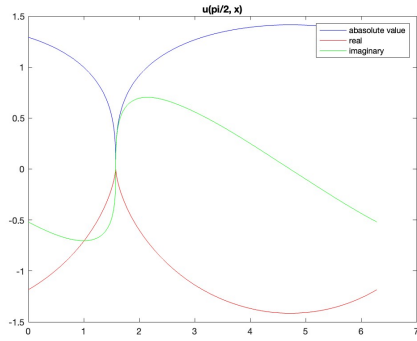
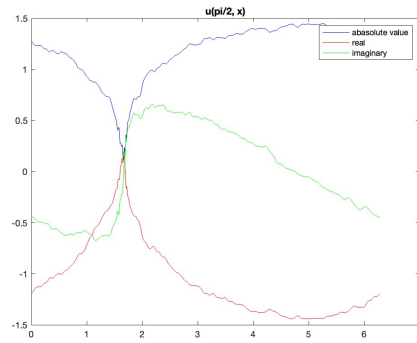


FIGURE 6.2. Initial Data

We can see the implicit scheme solution behaves exactly like the traveling wave solution with the correct speed, while the BDF2 scheme generates oscillations due to its weaker viscous effect.



Fully Implicit Scheme at $t = \pi/2$



BDF2 Scheme at $t = \pi/2$

FIGURE 6.3

Figure 6.4 shows the solution obtained with the Crank-Nicolson scheme at $t = \pi/8$. Since the Crank-Nicolson scheme has no built-in viscosity, it develops stronger oscillations much quicker.

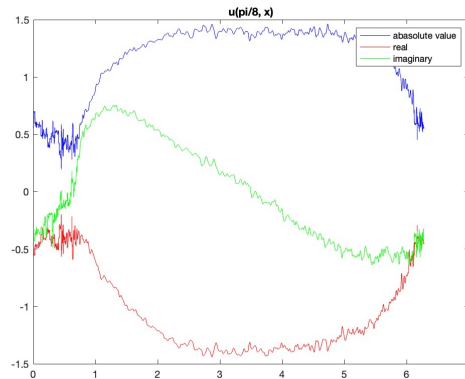


FIGURE 6.4. Crank-Nicolson Scheme at $t = \pi/8$

6.4. Front Expansion

We ran the algorithm at various resolutions (from 2^{11} spatial points to 2^{17} points) with the initial condition mentioned above. One interesting phenomenon is that the higher the resolution, the further the front propagates in unit time. Figure 6.5 shows the final location of the front at $t = 0.15$ versus resolution. The relation between the final front location and $\log(\text{resolution})$ becomes almost linear with resolution higher than 2^{14} .

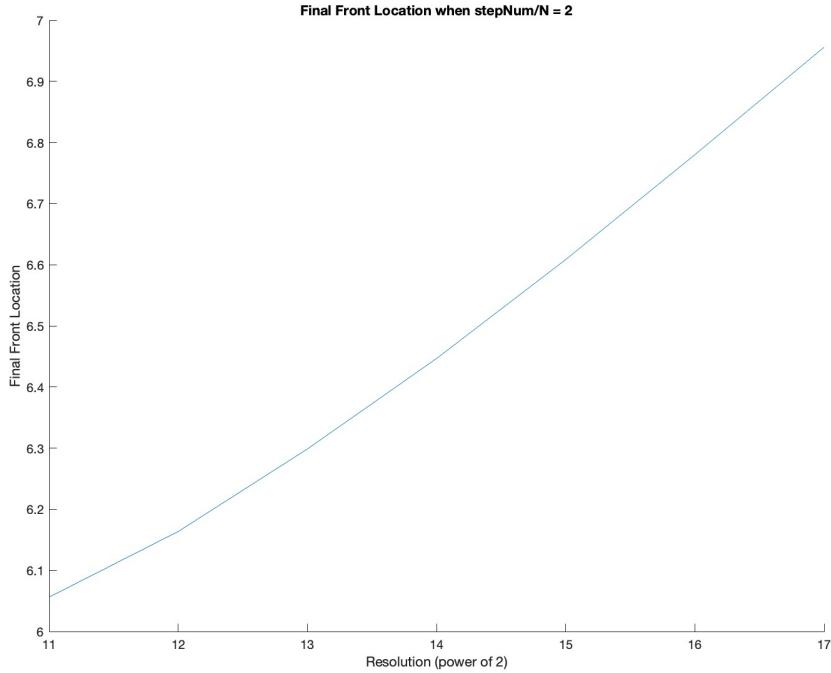


FIGURE 6.5. No artificial viscosity

Our hypothesis is that the sharp front shown in figure 6.1 is a result of the numerical viscosity in our algorithm. The exact solution may not have a propagating front. We speculate that when the front first forms in our numerical simulation, the exact solution immediately forms oscillations that spreads to $\pm\infty$.

To get a modified equation for the numerical viscosity of the scheme, we Taylor expand the left hand side of equation (6.5) in t and obtain

$$(6.6) \quad u_t(x_n^k) + \frac{\Delta t}{2} u_{tt}(x^*) = \frac{i}{\Delta x^2} [\rho_{n+1}^{k+\frac{1}{2}}(u_{n+1}^{k+1} - u_{n+1}^k) - \rho_{n+1}^{k-\frac{1}{2}}(u_{n+1}^k - u_{n+1}^{k-1})].$$

Using equation (1.8), we know that the leading order term in u_{tt} is $-\rho u_{xxxx}$. u_{tt} can be written as $u_{tt} = -\rho u_{xxxx} - f(u_x, u_{xx}, u_{xxx})$.

Therefore, equation (6.6) becomes

$$(6.7) \quad u_t(x_n^k) = \frac{i}{\Delta x^2} [\rho_{n+1}^{k+\frac{1}{2}}(u_{n+1}^{k+1} - u_{n+1}^k) - \rho_{n+1}^{k-\frac{1}{2}}(u_{n+1}^k - u_{n+1}^{k-1})] + \frac{\Delta t}{2} (\rho(x^*) u_{xxxx}(x^*) + f(u_x, u_{xx}, u_{xxx})(x^*)).$$

Here, the ρu_{xxxx} term is the viscosity produced by our numerical scheme. And since it has strength proportional to Δt , it is compatible with our observation that the front propagates further under higher resolution (which leads to small Δt).

Of course, Taylor expanding on the right hand side will also produce an error, but since the entire right hand side gets multiplied by i , it is not a viscous term.

To test the hypothesis, we add artificial viscosity to equation (6.3) and get

$$(6.8) \quad u_t = i(\rho u_x)_x + \epsilon u_{xx}.$$

The fixed dissipation ϵu_{xx} on the right hand side of the equation should dominate the numerical viscosity as $\Delta t \rightarrow 0$. Hence, we should be able to get a converging front propagation speed. Figure 6.6 shows the front location of the viscous equation (6.8) with different values of ϵ ranging from 0.001 to 0.003. The plot shows that as ϵ increases, not only does the front travel less, but the plot of the front location versus resolution also seems to converge. This confirms our hypothesis that when the artificial viscosity is sufficiently large, it will dominate the numerical viscosity which depends on Δt , and there will no longer be a visible difference between the front locations under different resolutions. Due to the high time consumption of the high resolution runs, I have not completed the run at resolutions higher than 2^{15} . But the runs from 2^{11} points to 2^{15} points do suggest a converging propagation speed for viscous fronts.

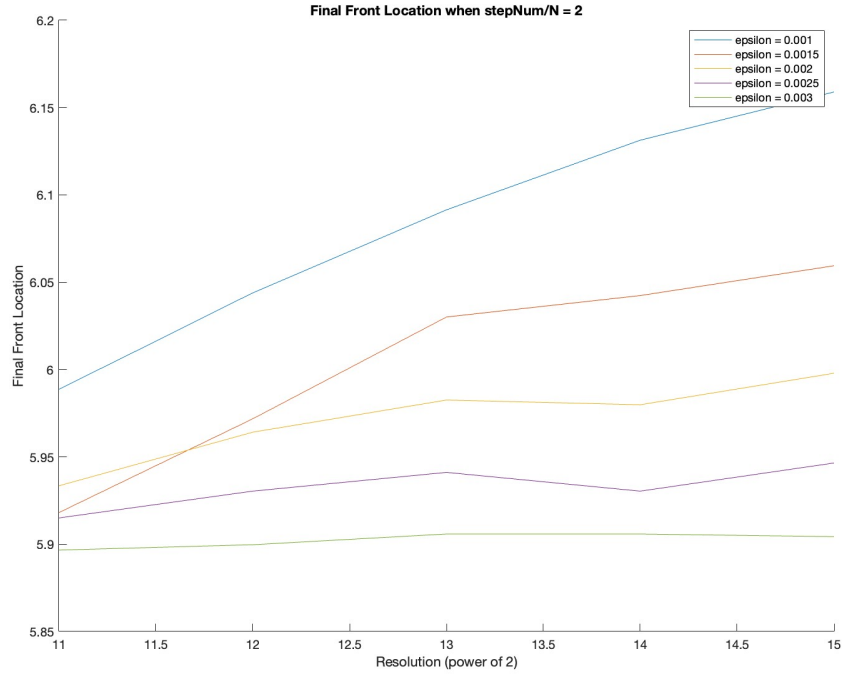


FIGURE 6.6. Artificial viscosity

6.4.1. Group Velocity Near the Front. We further study the connection between group velocity and the front location. We write $u = re^{i\phi}$, where r is the amplitude, and ϕ is the phase. The dispersion relation of the DQS equation is given by

$$\omega = \rho k^2,$$

where $k = \phi_x$ is the wave number and $\omega = -\phi_t$ is the frequency. We can then calculate the group velocity

$$\frac{\partial \omega}{\partial k} = 2\rho k.$$

We wish to study whether or not the front is propagating at the speed predicted by the dispersion relation. Therefore, we compute the group velocity and the front propagation speed, and check how well they match.

Calculating the propagation speed of the front is very straight forward. We simply find the last non-zero point from the right, and that is the location of the front. Subtracting the locations of the front in two consecutive time steps, and dividing by dt gives us the front traveling speed.

We can calculate the wave number by the following formula

$$k = \frac{1}{2i\rho}(\overline{u}u_x - u\overline{u}_x).$$

Then, the group velocity is given by

$$w = -i(\overline{u}u_x - u\overline{u}_x).$$

Below we show the comparison of the front propagation speed and the group velocity at two different resolutions: 2^{15} spatial points and 2^{17} points. We first choose the grid size of 2^{15} points. Plot 1 in figure 6.7 shows the front propagation speed as a function of time. At $t = 0.15$, the front propagation speed is approximately 16.36, while the group velocity at the front is 15.895.

Figure 6.8 shows the comparison with the grid size of 2^{17} points. At $t = 0.15$, the front propagation speed is 19.31, and the group velocity at the front is 19.02.

The data shows that the group velocity does match up with the actual propagation speed of the front. In addition, as we increase the resolution, we see larger wave number and group velocity at the front, which is compatible with our hypothesis that when the front first forms in the numerical simulation, the exact solution immediately forms oscillations that spreads to $\pm\infty$.

The front of the solution is dominated by waves with high wave numbers traveling at their corresponding group velocity. Since our algorithm samples u at finitely many points, higher wave-numbered waves are omitted in the sampling. As we increase the resolution, we preserve more higher wave-numbered waves during the sampling and that causes the front to travel faster.

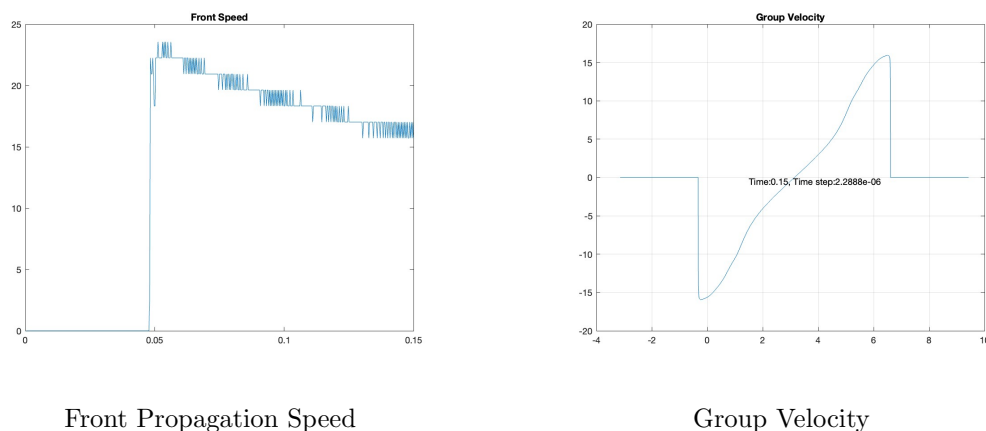
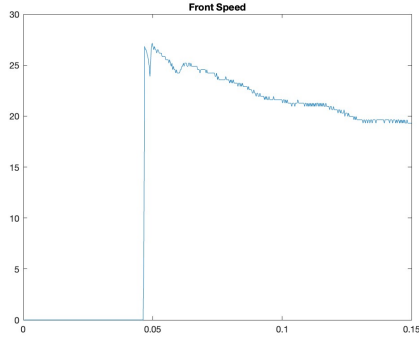
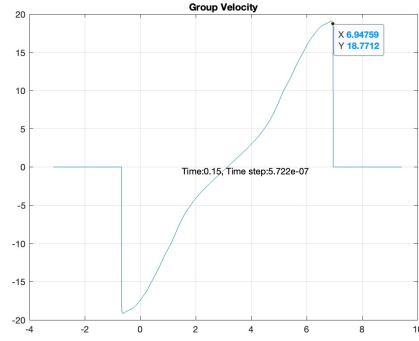


FIGURE 6.7



Front Propagation Speed



Group Velocity

FIGURE 6.8

6.5. Dispersive Shocks

As we can see in figure 6.1, the wave develops rapid oscillation with decreasing amplitude before the front. And the oscillation happens on a fast time scale, while the change in amplitude happens on a slow time scale. This suggests that the wave can be described by dispersive shocks.

Let r denote the amplitude, φ denote the phase, $k = \varphi_x$ denote the wave number and $\omega = -\varphi_t$ denote the frequency. Let ϵ be the scale of the period of the oscillations, then the phase can be written as $\frac{\varphi}{\epsilon}$. This suggests we can look at solutions in the form

$$u = \epsilon^{\frac{1}{2}} A(x, t) e^{i \frac{\varphi(x, t)}{\epsilon}}.$$

We then expand the equation by setting $u = u_1 + \epsilon u_2 + \epsilon^2 u_3 + \dots$

At order $\epsilon^{-\frac{1}{2}}$, we get the equation

$$\omega = |u_1|^2 k^2.$$

Combined with the fact $\omega_x = -k_t$, we get the first conservation law

$$(6.9) \quad k_t = -(|u_1|^2 k^2)_x.$$

At order $\epsilon^{\frac{1}{2}}$, we get the equation

$$u_{1t} = i\omega u_2 - (k|u_1|^2 u_1)_x - ik^2(2|u_1|^2 u_2 + u_1^2 \overline{u_2}).$$

Multiply both sides by $\overline{u_1}$ and add the complex conjugate, we get

(6.10)

$$|u_1|_t^2 = i\omega(u_2\overline{u_1} - \overline{u_2}u_1) - ik^2(2|u_1|^2u_2 + u_1^2\overline{u_2} - 2|u_1|^2\overline{u_2} - \overline{u_1}^2u_2) - (k|u_1|^2u_1)_x\overline{u_1} - (k|u_1|^2\overline{u_1})_xu_1.$$

Notice that the left hand side of (6.10) is real. Therefore, we must have $\Re RHS(6.10) = 0$. Since the first two terms of the right hand side of (6.10) are purely imaginary and the sum of the remaining two terms are real, we have

$$(6.11) \quad |u_1|_t^2 = -(k|u_1|^2u_1)_x\overline{u_1} - (k|u_1|^2\overline{u_1})_xu_1 = -2(k|u_1|^4)_x.$$

Let $\rho = |u_1|^2$, we can write the system of conservation laws (6.9) and (6.11) as

$$\begin{aligned} k_t + (\rho k^2)_x &= 0 \\ \rho_t + 2(k\rho^2)_x &= 0. \end{aligned}$$

The system can also be written as the following non-conservative form

$$(6.12) \quad \begin{bmatrix} k \\ \rho \end{bmatrix}_t = - \begin{bmatrix} 2k\rho & k^2 \\ 2\rho^2 & 4k\rho \end{bmatrix} \begin{bmatrix} k \\ \rho \end{bmatrix}_x.$$

Observe that the system is a special case of the 3x3 modulation system (5.22). Let $s = 0$, then (5.22) reduces to the dispersive shock system .

The system has eigenvalues $(3 \pm \sqrt{3})k\rho$, which are both real. Hence it is a hyperbolic system.

Since dispersive shocks correspond to rarefaction waves in the modulation variables (ρ, k) (see [9]), we look for the self-centered rarefaction wave $\rho(t, x) = \rho(\frac{x}{t}), k(t, x) = k(\frac{x}{t})$.

Let $\xi = \frac{x}{t}$, then we have

$$(6.13) \quad \xi \begin{bmatrix} k \\ \rho \end{bmatrix}_\xi - \begin{bmatrix} 2k\rho & k^2 \\ 2\rho^2 & 4k\rho \end{bmatrix} \begin{bmatrix} k \\ \rho \end{bmatrix}_\xi = 0.$$

Therefore, ξ is an eigenvalue and $\begin{bmatrix} k \\ \rho \end{bmatrix}_\xi$ is the corresponding eigenvector. The matrix has two

eigenvectors: $v_1 = \begin{bmatrix} k \\ (1 + \sqrt{3})\rho \end{bmatrix}$ and $v_2 = \begin{bmatrix} k \\ (1 - \sqrt{3})\rho \end{bmatrix}$. We pick $\begin{bmatrix} k \\ \rho \end{bmatrix}_\xi = \begin{bmatrix} k \\ (1 - \sqrt{3})\rho \end{bmatrix}$ since this

is the one that corresponds to a rarefaction with $\rho \rightarrow 0$ and $k \rightarrow \infty$. We want ρ to be decreasing as approaching the front. Solving the system, we get

$$(6.14) \quad \begin{aligned} k &= c_1 e^\xi \\ \rho &= c_2 e^{(1-\sqrt{3})\xi}. \end{aligned}$$

Then, $\rho \sim k^{1-\sqrt{3}}$ as $\xi \rightarrow \infty$. This describes the dispersive shock section behind the front.

Numerical experiments show that the dispersive shock theory is a good description of the solution. We take a segment before the front as shown in figure 6.9. Here, we are using a spatial grid of 2^{16} points. Polynomial fitting of the wave number and the amplitude on that segment gives the following relation:

$$(6.15) \quad \rho \sim k^{-0.7314}.$$

Figure (6.10) plots the exact values of ρ and the approximation as functions of k . We can see the approximation (6.15) is very close to the theoretical prediction (6.14).

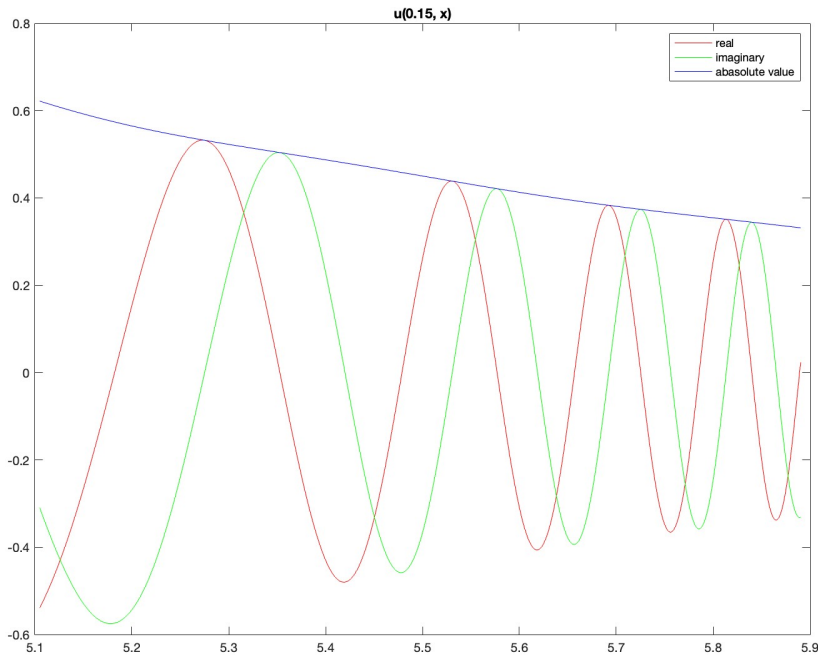


FIGURE 6.9

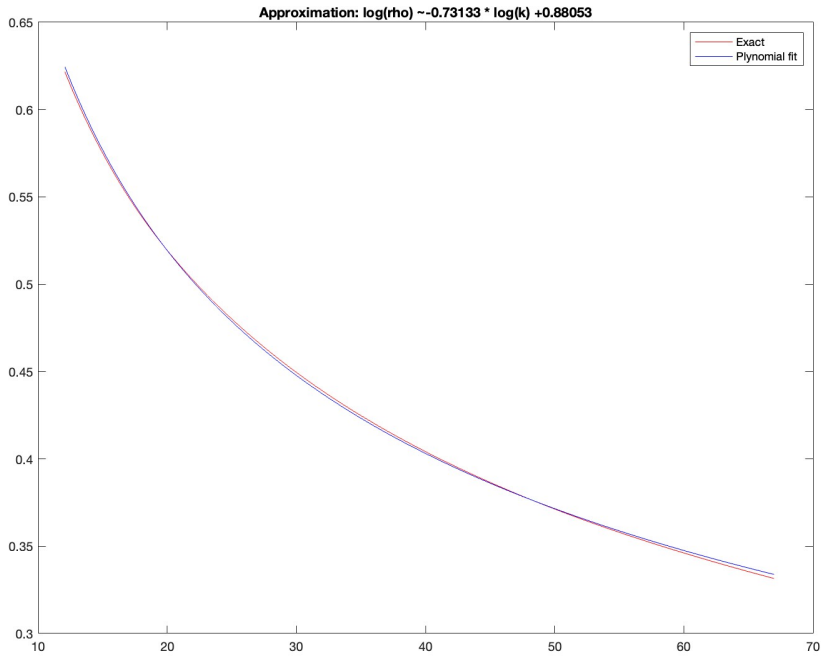


FIGURE 6.10

6.6. Comparison with the MRS numerical solution

We compare the numerical solutions of the DQS equation and the MRS system to study how well the DQS equation describes the behavior of the MRS system on $O(\epsilon^2)$ time scale. We choose an initial data for the MRS system

$$u_0 = \epsilon a(x)$$

$$v_0 = \epsilon b(x),$$

the corresponding initial value for the DQS equation is then given by

$$A_0 = \frac{1}{\sqrt{6}}a(x) + \frac{i}{\sqrt{6}}b(x).$$

In the example shown in Figure 6.11, we use the initial data

$$a(x) = \cos(x)e^{\sin x} + \frac{1}{10} \sin(10x)$$

$$b(x) = e^{\sin(x-\frac{\pi}{4})} - e^{\frac{1}{\sqrt{2}}}$$

$$\epsilon = 0.03.$$

See [here](#) (URL at (3)) for a full movie of the solution. The first plot in figure 6.11 shows that the DQS equation develops a singularity approximately at $t = 0.096$. We expect the singularity to form in the MRS system at $T = \frac{T}{\epsilon^2} = 95.11$. The singularity formation time of the MRS system, as shown in the second plot, is approximately 97.02. Similarly, we can predict the singularity formation time of the MRS system with different values of ϵ . Table 6.1 shows the comparison of the predicted singularity formation time and the actual formation time with ϵ chosen to be between 0.02 and 0.09. The DQS equation appears to provide a good prediction when $\epsilon \leq 0.05$. The error becomes more substantial with larger ϵ values.

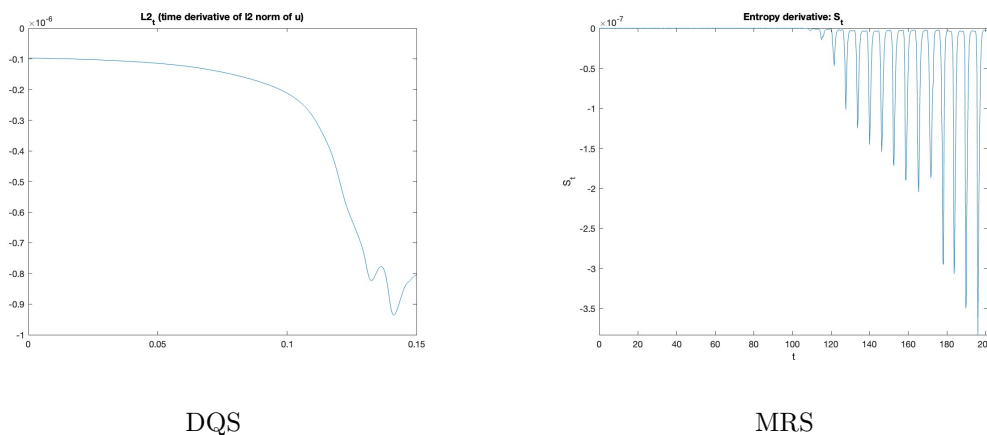


FIGURE 6.11. Entropy Derivative

We now examine how well the front solution (6.1) of the DQS equation describes the MRS system. Using the relation (??) we get the corresponding initial data for the MRS system

$$u_0(x) = \begin{cases} \epsilon[(\frac{\pi}{2})^2 - (\pi - x)^2]^2 & |x - \pi| \leq \frac{\pi}{2} \\ 0 & \text{otherwise} \end{cases},$$

$$v_0(x) = 0.$$

TABLE 6.1. Singularity Formation

ϵ	Predicted Singularity Formation Time	Actual Singularity Formation Time
0.02	240	234.049
0.03	106.667	108.322
0.04	60	63.335
0.05	38.4	38.956
0.06	26.667	31.919
0.07	19.592	25.526
0.08	15	19.733
0.09	11.852	19.046

Note that here we neglected the scaling (5.1), but it does not affect the result.

We use the standard WENO scheme to solve the initial value problem for different ϵ and compare the resulting solutions to the front solution of the DQS equation in section 6.4.

Since we chose the final time $t = 0.15$ to evaluate the location of the front for the DQS solutions, the final time T for the MRS numerical scheme should be chosen to be

$$T = \frac{0.15}{\epsilon^2}.$$

For simplicity, we will prescribe values to T instead, and choose ϵ to satisfy

$$\epsilon = \sqrt{\frac{0.15}{T}}.$$

Figure 6.12 plots the front location of $u + iv$ under different values of ϵ . Here, we choose T to be $200\pi, 400\pi, 800\pi, 1200\pi, 1600\pi$, and the corresponding ϵ values are 0.015451, 0.01093, 0.007725, 0.006308, 0.005463.

We can see that the front indeed propagates further as ϵ decreases, which is compatible with our hypothesis that the front solution of the DQS equation propagates with infinite speed once it develops a shock. It suggests that the front solution of the DQS equation offers a good qualitative description of the behavior of the MRS system on the timescale $O(\frac{1}{\epsilon^2})$ as $\epsilon \rightarrow 0$.

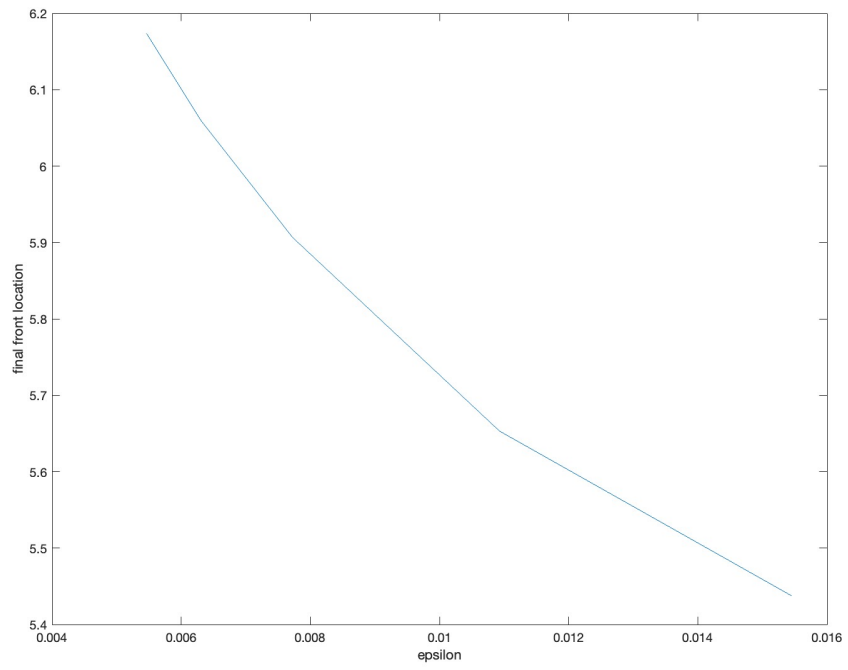


FIGURE 6.12

CHAPTER 7

Conclusion

The general MRS equations (1.5) describes the asymptotic behavior of resonant interactions between high frequency, small amplitude, spatially periodic sound waves in the non-isentropic Euler equations. In this paper, we studied the MRS system (3.1), obtained by choosing $K(x) = 1 - \sum_{n=-\infty}^{\infty} \delta(x - n)$ in (1.5). This particular choice was proposed by Majda, Rosales, and Schonbek.

Previous work has proven the $O(\frac{\log \epsilon}{\epsilon})$ lifespan of the MRS system. However, the oscillating nature of the solutions of the linear solutions suggests we may be able to obtain an $O(\frac{1}{\epsilon^2})$ lifespan. In an attempt to prove this result, we first explored the different approaches used to prove $O(\frac{1}{\epsilon^2})$ lifespan of small solutions of other quadratically quasilinear PDEs, in particular, the Burgers-Hilbert equation. We attempted to apply these methods to the MRS system, but none of them seems to be transferable. The modified energy method failed due to loss of derivatives, and the Normal Form Flow method does not give us an explicit expression of the flow variables. However, the reduced NFT method reveals a key difference between the Burgers-Hilbert equation and the MRS system, which does provide more insights on the difficulties when going from scalar Burgers-Hilbert equation to the 2×2 MRS system. In the Burgers-Hilbert equation, both the transformation and the problematic symmetric quadratic term are scalar operators, and the commutator provides good energy estimates. However, in the MRS system, the transformation and the symmetric quadratic term are 2×2 instead. The commutator of the two operators loses derivatives.

An asymptotic expansion of the MRS system gives us the DQS equation (1.8), which describes the behavior of small solutions of the MRS system on a formal level. Previous work by In-Jee Jeong and Sung-Jin Oh proved that the DQS equation is ill-posed in Sobolev spaces H^s with sufficiently large s . We followed the method proposed by Benjamin Harrop-Griffiths and Jeremy L. Marzuola to prove its well-posedness in a restrictive subspace of compactly supported solutions with sufficient endpoint decay.

The numerical simulations in Chapter 6 suggests that the DQS equation provides a good prediction of the MRS system. The predicted singularity formation time of small solutions using the DQS solution is close to the actual singularity formation time. In addition, we used the numerical method to study the possibility of compactly supported solutions. Based on our numerical results, we hypothesize that compactly supported solutions cannot remain compact once a singularity forms. Instead, it develops oscillations that immediately spread to $\pm\infty$. The numerical results of the MRS system with corresponding initial data in section 6.6 also seem to support this hypothesis. Furthermore, in section 6.5 we showed that the dispersive shock theory offers a good description of the section of the solution behind the front. The relation between the wave number and the amplitude is very close to that predicted by the dispersive shock theory.

APPENDIX A

DQS Numerical Scheme Code

Code for DQS numerical simulations:

```
function res = LF_implicit(uniform_visc, nmode, N, finalT)
    % uniform_visc: sets the strength of the uniform viscosity added to the
    % u equation, set to 0 if artificial viscosity is not needed
    % nmode: chooses initial data in file "ic.m"
    % N: spatial resolution (number of spatial grid points). Ex: N = 2^15
    % finalT: the algorithm terminates at t = finalT. Ex: finalT = 0.15

    % Solve for u_t = i(|u|^2 u_x)_x
    % Let rho = |u|^2

    % Set up spacial resolution
    a = 0;
    b = 2*pi;
    dx = (b-a)/N;
    x = dx .* (0:(N-1)) + a;

    % Set up time resolution
    stepNum = 2*N + 1;
    dt = finalT / (stepNum-1);

    % Set initial conditions
    epsilon = 0.5; % only used to set the amplitude of a few initial data
    u = ic(x, nmode, N, epsilon);
    rho = ic(x + (dx/2), nmode, N, epsilon);
    rho = abs(rho).^2;
```

```

% Set the save frequency, i.e. how many frame we will save
frameNum = 2^9+1;
frameRate = (stepNum-1) / (frameNum-1);

% Set the periodic flag
isPeriodic = "periodic";

% Build the sparsity pattern vectors
% They will be passed into function eq2 to indicate the nonzeros
% entries in the implicit method
if isPeriodic == "periodic"
    sparsityPattern_row = floor((0:(3*N)-1) / 3) + 1;
    sparsityPattern_column = (sparsityPattern_row - 1) + rem(0:(3*N)-1, 3);
    sparsityPattern_column(1) = N;
    sparsityPattern_column(3*N) = 1;
else
    sparsityPattern_row = [1, floor((3:(3*N-3)-1) / 3) + 1, N];
    sparsityPattern_column = sparsityPattern_row + [0, rem(3:(3*N-3)-1, 3)-1, 0];
end

u_allsteps = zeros(frameNum, N); % stores u at each time step
rho_allsteps = zeros(frameNum, N); % stores rho at each time step
cfl_allsteps = zeros(1, frameNum); % stores the max CFL number at each time step
u_allsteps(1, :) = u;
rho_allsteps(1, :) = rho;
cfl_allsteps(1) = cfl(u, N, dt, dx);

tic
for counter = 2:stepNum
    % Use u to update rho explicitly
    rho = eq1_LaxFriedrichs_staggered_periodic(rho, u, dt, dx, N, isPeriodic);

```

```

% Update u implicitly
u = eq2_implicit_staggered(rho, u, dt, dx, N, uniform_visc, sparsityPattern_row,
    sparsityPattern_column, isPeriodic);

if rem(counter-1, frameRate) == 0
    rho_allsteps((counter-1)/frameRate+1, :) = rho;
    u_allsteps((counter-1)/frameRate+1, :) = u;
    cfl_allsteps((counter-1)/frameRate+1) = cfl(u, N, dt, dx);
end

end

elapsedT = toc

% Save the result
fileName = "LaxFriedrichs_implicit_stagger.mat";
save(fileName, 'mnode', 'finalT', 'stepNum', 'frameRate', 'frameNum', 'a', 'b', 'N',
    'u_allsteps', 'rho_allsteps', 'cfl_allsteps', 'elapsedT', '-v7.3');
end

% The Lax_Friedrichs method is an explicit method that takes
%  $\rho_n^j = 1/2 * (\rho_n^{j+1} + \rho_n^{j-1})$ 
% It updates rho on the half grid
% It uses the values of f at 4 points: f(j-1), f(j), f(j+1), f(j+2)
function res = eq1_LaxFriedrichs_staggered_periodic(rho, u, dt, dx, N, isPeriodic)
    up1 = circshift(u, -1);
    if isPeriodic ~= "periodic"
        up1(N) = u(N);
    end

    J = -1/dx .* imag(up1-u) .* conj(up1+u);

```

```

rho_p1 = circshift(rho, -1);
rho_m1 = circshift(rho, 1);
Jp1 = circshift(J, -1);
Jm1 = circshift(J, 1);
if isPeriodic ~= "periodic"
    rho_p1(N) = rho(N);
    rho_m1(1) = rho(1);
    Jp1(N) = J(N);
    Jm1(1) = J(1);
end

rho_new = 1/2 * (rho_m1+rho_p1) + dt/2/dx * (rho_p1.*Jp1 - rho_m1.*Jm1);
res = rho_new;
end

% The implicit method preserves the structure and evaluates rho on the half
% grid
function res = eq2_implicit_staggered(rho, u, dt, dx, N, uniform_visc,
    sparsityPattern_row, sparsityPattern_column, isPeriodic)
    rho_m1 = circshift(rho, 1);
    if isPeriodic ~= "periodic"
        rho_m1(1) = rho(1);
    end

    c = 1i * dt / (dx^2);
    v = zeros(1, 3*N);
    for j = 1:N
        v(3*(j-1)+1) = -c * rho_m1(j) - uniform_visc * c;
        v(3*(j-1)+2) = 1 + c * (rho_m1(j) + rho(j)) + 2 * uniform_visc * c;
        v(3*(j-1)+3) = -c * rho(j) - uniform_visc * c;
    end

    g = u;

```

```
A = sparse(sparsityPattern_row, sparsityPattern_column, v, N, N);  
  
res = (A\('g.')).';  
end
```

APPENDIX B

Alternate WENO Scheme Code

Code for Alternate WENO scheme:

```
function u_t = alternate_WENO_burgers_5th(u,k,lx,dx, periodic)

    eps = 1e-6;

    gamma1 = 0.1;
    gamma2 = 0.6;
    gamma3 = 0.3;

    a = max(abs(fl_prime(u)));

    ujp1 = circshift(u,[0,-1]);    % u(j+1)
    ujp2 = circshift(ujp1,[0,-1]); % u(j+2)
    ujp3 = circshift(ujp2,[0,-1]); % u(j+3)
    ujm1 = circshift(u,[0,1]);     % u(j-1)
    ujm2 = circshift(ujm1,[0,1]);  % u(j-2)

    % Nonperiodic solution: we have to set the endpoints explicitly
    if periodic == "no"
        ujp1(size(u, 2)) = ujp1(size(u, 2)-1);
        ujp2(size(u, 2)) = ujp1(size(u, 2)-2);
        ujp2(size(u, 2)-1) = ujp1(size(u, 2)-2);
        ujp3(size(u, 2)) = ujp1(size(u, 2)-3);
        ujp3(size(u, 2)-1) = ujp1(size(u, 2)-3);
        ujp3(size(u, 2)-2) = ujp1(size(u, 2)-3);
        ujm1(1) = ujm1(2);
    end
end
```



```

    ujm2(1) = ujm2(3);
    ujm2(2) = ujm2(3);
end

u_app_m1 = ujm2/3 - 7*ujm1/6 + 11*u/6;
u_app_m2 = -ujm1/6 + 5*u/6 + ujp1/3;
u_app_m3 = u/3 + 5*ujp1/6 - ujp2/6;

u_app_p1 = ujp3/3 - 7*ujp2/6 + 11*ujp1/6;
u_app_p2 = -ujp2/6 + 5*ujp1/6 + u/3;
u_app_p3 = ujp1/3 + 5*u/6 - ujm1/6;

bm1 = (13/12)*(ujm2 - 2*ujm1 + u).^2 ...
      + (0.25)*(ujm2 - 4*ujm1 + 3*u).^2;
bm2 = (13/12)*(ujm1 - 2*u + ujp1).^2 ...
      + (0.25)*(ujm1 - ujp1).^2;
bm3 = (13/12)*(u - 2*ujp1 + ujp2).^2 ...
      + (0.25)*(3*u - 4*ujp1 + ujp2).^2;

bp1 = (13/12)*(ujp3 - 2*ujp2 + ujp1).^2 ...
      + (0.25)*(ujp3 - 4*ujp2 + 3*ujp1).^2;
bp2 = (13/12)*(ujp2 - 2*ujp1 + u).^2 ...
      + (0.25)*(ujp2 - u).^2;
bp3 = (13/12)*(ujp1 - 2*u + ujm1).^2 ...
      + (0.25)*(3*ujp1 - 4*u + ujm1).^2;

twp1 = gamma1./(eps+bp1).^2;
twp2 = gamma2./(eps+bp2).^2;
twp3 = gamma3./(eps+bp3).^2;
stwp = twp1+twp2+twp3;
wp1 = twp1./stwp;
wp2 = twp2./stwp;

```

```

wp3 = twp3./stwp;

twm1 = gamma1./(eps+bm1).^2;
twm2 = gamma2./(eps+bm2).^2;
twm3 = gamma3./(eps+bm3).^2;
stwm = twm1+twm2+twm3;
wm1 = twm1./stwm;
wm2 = twm2./stwm;
wm3 = twm3./stwm;

ulp_right = wp1.*u_app_p1 + wp2.*u_app_p2 + wp3.*u_app_p3;
ulm_right = wm1.*u_app_m1 + wm2.*u_app_m2 + wm3.*u_app_m3;
f_right_low = 1/2 * ((fl(ulp_right)+fl(ulm_right)) - a/2*(ulp_right-ulm_right));

fp_right_high_2 = -5/24.*fp(ujm2,a) + 4/3.*fp(ujm1,a) - 7/4.*fp(u,a) + 1/3.*fp(ujp1,a)
    + 7/24.*fp(ujp2,a);
fm_right_high_2 = 7/24.*fm(ujm1,a) + 1/3.*fm(u,a) - 7/4.*fm(ujp1,a) + 4/3.*fm(ujp2,a)
    - 5/24.*fm(ujp3,a);
f_right_high_2 = 1/24 .* (fp_right_high_2 + fm_right_high_2);

fp_right_high_4 = fp(ujm2,a) - 4.*fp(ujm1,a) + 6.*fp(u,a) - 4.*fp(ujp1,a) + fp(ujp2,a);
fm_right_high_4 = fm(ujm1,a) - 4.*fm(u,a) + 6.*fm(ujp1,a) - 4.*fm(ujp2,a) + fm(ujp3,a);
f_right_high_4 = 7/5760 .* (fp_right_high_4 + fm_right_high_4);

f_right = f_right_low + f_right_high_2 + f_right_high_4;
f_left = circshift(f_right,[0,1]);
u_t = -(f_right - f_left)/dx;
end

```

APPENDIX C

Movie Links

- (1) https://github.com/allen0chen/thesis/blob/main/mrs_stationaryShock.mp4
- (2) https://github.com/allen0chen/thesis/blob/main/mrs_continuousShock.mp4
- (3) https://github.com/allen0chen/thesis/blob/main/DQS_MRSic.mp4
- (4) https://github.com/allen0chen/thesis/blob/main/DQS_travelingWave.mp4
- (5) https://github.com/allen0chen/thesis/blob/main/DQS_front.mp4

Bibliography

- [1] D. M. AMBROSE, G. SIMPSON, J. WRIGHT, AND D. G. YANG, *Ill-posedness of degenerate dispersive equations*, *Nonlinearity*, 25 (2012), pp. 1965–2072.
- [2] V. ARNOLD, *Geometric methods in the theory of ordinary differential equations*, Springer-Verlag, (1983).
- [3] T. BUCKMASTER, S. SHKOLLER, AND V. VICOL, *Shock formation and vorticity creation for 3d euler*, *Communications on Pure and Applied Mathematics*, 76 (2022), pp. 1965–2072.
- [4] R. CAMASSA AND D. D. HOLM, *An integrable shallow water equation with peaked solitons*, *Physics Review*, 71 (1993).
- [5] K. CARLOS E., P. GUSTAVO, AND V. LUIS, *The cauchy problem for quasi-linear schrödinger equations*, *Nonlinearity*, 158 (2004), pp. 343–388.
- [6] D. CHRISTODOULOU, *The euler equations of compressible fluid flow*, *American Mathematical Society*, 4 (2007), pp. 581–602.
- [7] C. M. DAFERMOS, *Hyperbolic Conservation Laws in Continuum Physics*, Springer Nature, 2010.
- [8] J. M. DELORT, *Private communications*.
- [9] G. A. EL AND M. A. HOEFER, *Dispersive shock waves and modulation theory*, *Physica D* 333, (2016).
- [10] L. C. EVANS, *Partial Differential Equations*, American Mathematical Society, 1998.
- [11] J. FRITZ, *Formation of singularities in one-dimensional nonlinear wave propagation*, *Communications on Pure and Applied Mathematics*, XXVII (1974), pp. 377–405.
- [12] P. GERMAIN, *Space-time resonances*, *Journées équations aux dérivées partielles*, 8 (2010).
- [13] P. GERMAIN, B. HARROP-GRIFFITHS, AND J. L. MARZUOLA, *Existence and uniqueness of solutions for a quasi-linear kdv equation with degenerate dispersion*, *math.AP*, (2018).
- [14] ———, *Compactons and their variational properties for degenerate kdv and nls in dimension 1*, *Quart. Appl. Math.*, 78 (2020), pp. 1–32.
- [15] P. GERMAIN, N. MASMOUDI, AND J. SHATAH, *Global solutions for 3d quadratic schrödinger equations*, *International Mathematics Research Notices*, 2009 (2009), pp. 414 – 432.
- [16] ———, *Global solutions for 2d quadratic schrödinger equations*, *International Mathematics Research Notices*, 97 (2012), pp. 505–543.
- [17] ———, *Global solutions for the gravity water waves equation in dimension 3*, *Annals of Mathematics*, 175 (2012), pp. 691–754.

- [18] J. GLIMM, *Solutions in the large for nonlinear hyperbolic systems of equations*, Communications on Pure and Applied Mathematics, XVIII (1965), pp. 697–715.
- [19] J. GLIMM AND P. D. LAX, *Decay of solutions of systems of nonlinear hyperbolic conservation laws*, Providence : American Mathematical Society, 1970.
- [20] B. HARROP-GRIFFITHS AND J. L. MAEZUOLA, *Local well-posedness for a quasilinear schrodinger equation with degenerate dispersion*, math.AP, (2020).
- [21] H. HOLDEN AND X. RAYNAUD, *Global conservative solutions of the camassa–holm equation—a lagrangian point of view*, Communications in Partial Differential Equations, 32 (2007), pp. 1511–1549.
- [22] J. HUNTER AND M. IFRIM, *Enhanced life span of smooth solutions of a burgers–hilbert equation*, SIAM Journal on Mathematical Analysis, (2011).
- [23] J. HUNTER, M. IFRIM, D. TATARU, AND T. K. WONG, *Long time solutions for a burgers–hilbert equation via a modified energy method*, Proceedings of the American Mathematical Society, (2015).
- [24] J. HUNTER AND E. SMOTHERS, *On the resonant reflection of weak, nonlinear sound waves off an entropy wave*, Studies in Applied Mathematics, (2018).
- [25] J. K. HUNTER, *Private communications*.
- [26] J. K. HUNTER AND M. IFRIM, *A quasi-linear schrödinger equation for large amplitude inertial oscillations in a rotating shallow fluid*, IMA Journal of Applied Mathematics, 78 (2013), pp. 777–796.
- [27] M. IFRIM AND D. TATARU, *Local well-posedness for quasilinear problems: A primer*, American Mathematical Society, 60 (2023), pp. 167–194.
- [28] I.-J. JEONG AND S.-J. OH, *Strong ill-posedness for degenerate dispersive equations in sobolev spaces*, Preprint, (2020).
- [29] ———, *Illposedness for dispersive equations: Degenerate dispersion and takeuchi–mizohata condition*, arXiv:2308.15408, (2023).
- [30] T. KATO, *The cauchy problem for quasi-linear symmetric hyperbolic systems*, Archive for Rational Mechanics and Analysis, 58 (1975), p. 181–205.
- [31] P. D. LAX, *Development of singularities of solutions of nonlinear hyperbolic partial differential equations*, Journal of Mathematical Physics, 5 (1964), pp. 611–613.
- [32] ———, *Hyberbolic Systems of Conservation Laws and the Mathematical Theory of Shock Waves*, CBMS-NSF Regional Conference Series in Applied Mathematics, 1973.
- [33] F. LINARES AND G. PONCE, *Introduction to Nonlinear Dispersive Equations*, Springer New York, NY, 2015.
- [34] T.-P. LIU, *Development of singularities in the nonlinear waves for quasi-linear hyperbolic partial differential equations*, Journal of Differential Equations, 33 (1974), pp. 92–111.
- [35] A. MAJDA, R. ROSALES, AND M. SCHONBEK, *A canonical system of integrodifferential equations arising in resonant nonlinear acoustics*, Studies in Applied Mathematics, (1988).

- [36] J. L. MARZUOLA, J. METCALFE, AND D. TATARU, *Quasilinear schrödinger equations iii: Large data and short time*, Rational Mechanics and Analysis, 242 (2021), pp. 1119–1175.
- [37] I. NEAL, C. RICKARD, S. SHKOLLER, AND V. VICOL, *A new type of stable shock formation in gas dynamics*, Communications on Pure and Applied Analysis, (2023).
- [38] R. L. PEGO, *Some explicit resonating waves in weakly nonlinear gas dynamics*, Studies in Applied Mathematics, 79 (1988), pp. 263–270.
- [39] R. RAMANI, *Private communications*.
- [40] Y. RUOXUAN, *Shock formation of the burgers–hilbert equation*, SIAM Journal on Mathematical Analysis, 53 (2021), pp. 5756–5802.
- [41] S. SCHOCHET, *Resonant nonlinear geometric optics for weak solutions of conservation laws*, Journal of Differential Equations, 113 (1994), pp. 473–504.
- [42] J. SHATAH, *Normal forms and quadratic nonlinear klein-gordon nonlinearities*, Comm. Pure Appl. Math. 38, (1985).
- [43] S. SHKOLLER AND V. VICOL, *The geometry of maximal development and shock formation for the euler equations in multiple space dimensions*, Inventiones mathematicae, 32 (2024), pp. 1511–1549.
- [44] C.-W. SHU, *High order weighted essentially nonoscillatory schemes for convection dominated problems*, SIAM Review, 51 (2009), pp. 82–126.
- [45] ———, *Essentially non-oscillatory and weighted essentially non-oscillatory schemes for hyperbolic conservation laws*, NTRS - NASA, (2013).
- [46] ———, *Essentially non-oscillatory and weighted essentially non-oscillatory schemes*, Acta Numerica, 29 (2020), pp. 701–762.
- [47] G. SIMPSON, M. SPIEGELMAN, AND M. I. WEINSTEIN¹, *Degenerate dispersive equations arising in the study of magma dynamics*, London Mathematical Society, (2006).
- [48] E. SMOTHER, *Self-similar solutions and local wavefront analysis of a degenerate schrödinger equation arising from nonlinear acoustics*, Dissertation, University of California, Davis, (2018).
- [49] J. TAKEUCHI, *A necessary condition on the well-posedness of the cauchy problem for a certain class of evolution equations*, Iron and Steel Technical College, (1974).
- [50] M. E. TAYLOR, *Partial Differential Equations III: Nonlinear Equations*, Springer Science Business Media, 2010.
- [51] B. TEMPLE AND R. YOUNG, *Time-periodic solutions of the compressible euler equations and the nonlinear theory of sound*, arXiv:2406.00200 [math.AP] preprint.
- [52] T. R. WAGONMAKER, *Analytic solutions and resonant solutions of hyperbolic partial differential equations*, Dissertation, University of Michigan, (1994).
- [53] G. WHITHAM, *Linear and Nonlinear Waves*, John Wiley Sons, 1974.